Philipps-Universität Marburg

On the growth performance of two competing species in an Andean pasture of southern Ecuador - monitoring and simulations

kumulative Dissertation
zur Erlangung des Doktorgrades
der Naturwissenschaften
(Dr. rer. nat.)

dem Fachbereich Geographie
der Philipps-Universität Marburg

vorgelegt von
Brenner Stefan Gomes Silva
Master (M.Sc.) und Bachelor (B.Sc.)
aus Itajubá - Minas Gerais – Brasilien

Marburg / Lahn 2013

Vom Fachbereich Geographie

der Philipps-Universität Marburg als Dissertation

am 15. Januar 2013 angenommen.

Prüfungskommission:

Prof. Dr. Jörg Bendix (Erstgutachter)

Prof. Dr. Georg Miehe (Zweitgutachter)

Prof. Dr. Christian Opp

Tag der mündlichen Prüfung: 13. Februar 2013

Preface

This endeavour began with the acceptance for grants to pursue the PhD starting in 2008. After working with remote sensing in Brazil, I've realized I should learn how ecosystem processes take place, to go deeper in what I was used to observe. In my PhD-research I investigated primary productivity and the environment on which it depends. I could contribute to the understanding of a farming problem in a mountain ecosystem, like the place I grew up. By this way, I went back to my academic roots to put in practice programming lessons, now at the department of Geography. I changed my area of expertise to learn plant physiology, to be able to give dynamics to the synoptic, but also static view of mapping. I've learned climatology and experimented with state-of-the-art instrumentation, but also with a cost-effective camera-balloon system. And so, I could scratch the understanding one needs to put all pieces together in a vegetation model. Now, it is my pleasure to make this work available and I would like to give my gratitude to those who shared with me this story.

I am in deep gratitude to my advisor Jörg Bendix, who gave me this opportunity and all assistance I needed. I thank my colleagues at the Laboratory for Climatology and Remote Sensing and at the University of Marburg for sharing knowledge, coffee and milk. Thanks to R. Rollenbeck for electronic lessons. Thanks to E. Beck and K. Roos for help and discussions. Thanks to D. Dörnemann for photosynthesis lessons. I thank B. Kühne-Bialozyt, S. Haese, C. Philippi for the support. I thank F. Schraag, D. Kanwischer, T. Nauss, A. Obregon, A. Bendix and their Families for their friendship. I thank all colleagues at the research station in Ecuador for their help.

I thank the Conselho Nacional de Desenvolvimento Científico e Tecnológico (CNPq) for grants (GDE290033/2007-1). I thank the Deutscher Akademischer Austauschdienst (DAAD) for the German course, without I could easily get lost. I thank the Deutsche Forschungsgemeinschaft (DFG) for supporting the Research Unity 816 - "Biodiversity and Sustainable Management of a Megadiverse Mountain Ecosystem in South Ecuador" (especially BE 473/38-1) - the scope of infrastructure and scientific exchange of this work. I thank the University of Marburg, for the support and the atmosphere. Thanks also to the mentors and developers of the Community Land Model, for the construction.

This work is to my family Adauto, Rita, Thiago, Carla, Cristian always in mind.

This work is to Mariana, with love, for my greatest moments.

Marburg, January 2013. Brenner Silva

Contents

List of Figures v
List of Tables xi
List of Acronyms xiii
List of Symbols xv

1. Introduction 1

1.1 Study area 3
1.2 Aims and hypotheses 5
1.3 Structure of the thesis 6
1.4 Model development and setup 8
1.5 Experimental plot design and monitoring setup of the thesis 12
1.5.1 Forcing meteorology 13
1.5.2 Ground observations for parameterization and validation 14
1.5.3 Remote sensing for monitoring and validation 14
1.6 Global relevance of the thesis: The induced invasion of bracken .. 16

2. Model parameterization to simulate PAR absorption potential 23

2.1 Introduction 24
2.2 Materials and methods 26
2.2.1 Study area and data 26
2.2.2 Radiation scheme 27
2.2.3 Decomposition of global radiation data 29
2.2.4 Field observations of plant and soil parameters 31
2.3 Results 33
2.3.1 Derived plant and soil traits 33
2.3.2 Simulated PAR absorption capability 36
2.4 Discussion 42

3. Simulating canopy photosynthesis 51

3.1 Introduction 52
3.2 Methods 55
3.2.1 Study site and experimental design 56
3.2.2 The canopy photosynthesis model 56
3.2.3 Species- and site-specific model parameterization 64
3.2.4 Model setup 71
3.3 Results 72
3.3.1 Assimilation parameter validation 72

3.3.2 Model run with realistic meteorological forcing 74
3.4 Discussion 77
3.5 Conclusions 79

4. Climate Change and its Impact on Current and Future Vegetation Dynamics and Carbon Cycling 89

4.1 Introduction 90
4.2 Methods 91
4.2.1 The SoBraCoMo Model 91
4.2.2 The FORMIND Model 91
4.3 Results and Discussion 93
4.3.1 Biomass Production and Competition on the Pastures 93
4.3.2 Forest Dynamics after Natural Disturbance 97
4.4 Conclusion 99

5. Low-altitude, cost-effective aerial photography of two competing grassland species 103

5.1 Introduction 104
5.2 Study area, data, and methods 106
5.2.1 Study area 106
5.3 Balloon photos and ancillary data 108
5.3.1 Ground control points and elevation model 109
5.3.2 Leaf area index data 110
5.3.3 Image processing 110
5.3.4 Contrast balancing 111
5.3.5 Geometric rectification 112
5.3.6 Enhancement 114
5.3.7 Segmentation 114
5.3.8 Attributes calculation 114
5.3.9 Classification 115
5.3.10 Conversion of FPC to LAI 115
5.4 Validation 116
5.4.1 Validation of classification: 116
5.4.2 Validation of LAI maps 117
5.5 Results 117
5.5.1 Image acquisition 117
5.5.2 Geometric processing 118
5.5.3 Relationship between brightness and reflectance 118
5.5.4 Segmentation and classification 120

5.5.5 Validation of classification 121
5.5.6 Maps of vegetation development 122
5.5.7 Conversion of FPC to LAI 124
5.5.8 Validation of LAI data 124
5.6 Discussion 126
5.7 Conclusion 127
6. Summary and outlook 133
6.1 Summary 133
6.2 Outlook 136
Executive Summary 139
Zusammenfassung 141
Curriculum Vitae 143

List of Figures

Figure 1-1. Location of the Rio San Francisco basin in Ecuador (a) and the Ecological Burnplot in the valley (b). 4

Figure 1-2. Conceptual design and outline of this work. Related chapters of the thesis are indicated in brackets. 7

Figure 1-3. Relation of knowledge gained with a model and model complexity. The solid-line curve represents a small or poor-quality dataset in comparison with the broken-line curve. The arrow inside the plot represents the enhancement from a starting point – a local application inheriting concepts from a global model – to a model with proper data, parameters and new variables, which can be applied in a plot up to a regional scale (Adapted from Joergensen 2001). 9

Figure 1-4. Model scheme for diagnostic runs, including field data and meteorologic forcing, particular sub-modules and the main vegetation state variables. 10

Figure 1-5. General experimental setup for field measurements and monitoring of post-fire canopy recovery. 13

Figure 1-6. Spectral signatures at leaf (LAI = 1) and canopy levels (LAI > 1) collected in the field (a); sum of chlorophyll a and b from pigment analysis (pigment analysis were done under supervision of PD D. Dörnemann); and leaf cross-section of bracken and *Setaria* sun leaves (c) (cross-sections by N.König, scale by I. Voss, and notations by B. Silva). 15

Figure 1-7. Distribution map of (colour circles) bracken fern species (Der et al. 2009) and bibliography review of bracken fern observations with geographical reference (black points). Grey areas indicate possible bracken occurrence detected by a land-use remote sensing product (Ellis and Ramankutty 2008). 17

Figure 2-1. The research area showing fractional cover by southern bracken as derived from Landsat TM data with the probability guided spectral unmixing technique (Göttlicher et al. 2009); BS experimental bracken site and micrometeorological station, ECSF Estación Científica San Francisco, ECSF met Meteorological station of the Estación, TS1 and Cerro met are meteorological stations located at 2,660 and 3,180 m asl, respectively. Grey

shades indicate different bracken coverage per pixel, white means bracken-free pixel. 25

Figure 2-2. (a) Average diurnal course of global and derived diffuse radiation at ECSF met station (1998–2005). (b) The diffuse fraction from six decomposition functions is also shown as a function of the clearness index (bottom). For abbreviations, see text. 32

Figure 2-3. Partitioning into reflectance (albedo), transmittance and absorptance of spectral radiation incident on *Setaria sphacelata*, *Pteridium arachnoideum* (as an average of three representative samples, LAI=1) and bare soil. The traced line represents the division between visible (PAR) and near infra red (>700 nm). 35

Figure 2-4. Sunlit and shaded leaf fractions of bracken and *Setaria* for solar elevations between 5 and 85° (solar elevation=90°-solar zenith). 36

Figure 2-5. Leaf area index of sunlit and shaded leaves of bracken and *Setaria* as depending on the solar zenith angle (solar elevation=90°-solar zenith). 37

Figure 2-6. (a) Leaf area indices of sunlit and shaded portions of the leaves of bracken and *Setaria* in the course of a day with regard to the average leaf–sun geometry of the study area. (b) Annual average of the diurnal course of irradiance at the ECSF meteorological station (1998–2005; Bendix et al. 2008a), sum of absorbed direct and diffuse PAR by sunlit and shaded leaves of bracken and *Setaria* plotted on the left ordinate axis and typical solar elevation in degrees on the right ordinate axis. 38

Figure 2-7. PAR absorption of southern bracken and *Setaria* for (left) a sunny day (5 December 2007) and (right) a typical overcast day (5 January 2008). Radiation data for model initialization are taken from the micrometeorological station at the bracken experimental site. 39

Figure 2-8. Different PAR components absorbed by the sunlit canopy of bracken (left) and *Setaria* (right) on the sunny day, 5 December 2007, based on the radiative transfer scheme. 40

Figure 2-9. Frequency and intensity of the daily irradiance maximum between 1200 and 1300 hours for the ECSF meteorological station (1998–2005) and total daily PAR absorption by bracken and *Setaria*, respectively, based on the relative diurnal course of radiation from 5 December 2007. 41

Figure 3-1. Location of the study site and design of the experimental plot (Burnplot). 56

Figure 3-2. Conceptual model used to calculate potential biomass production as a factor of leaf photosynthesis and plant respiration (leaves and roots). Shade acclimation is considered in calculating leaf photosynthesis and respiration as denoted by sunlit or shade-leaf. 57

Figure 3-3. Photosynthetic light (a, left) and CO_2 response (b, right), showing the average of measurements (closed circles for sunlit and open circles for shade) at each given incident PAR radiation or intercellular CO_2. Solid lines show model results after fitting to data. Dashed curves show a quadratic fitting to the measured data. In the light response curve (a) the initial increase for *Setaria* sunlit (left line) and shade (right line) are plotted as solid lines. In the CO_2 response curve (b), the model framework distinguishes between C3 and C4 pathways. Thus, a piecewise fitting is applied to bracken (refer to text; solid black lines), while a linear fitting is used for *Setaria* (solid grey lines). The zero line at y-axis is shown in all figures as a reference for respiration (=negative net photosynthesis). 66

Figure 3-4. Effect of leaf temperature on net photosynthesis (assimilation minus respiration) at saturating radiation of bracken and *Setaria* adjusted to the data of maximum net photosynthesis (points). The frequency of leaf temperatures is displayed as grey bars (right y-axis). 68

Figure 3-5. Clay and sand profiles in soils of bracken infested pastures with measurements (dots) and average profile (lines) for the eight soil layers (between the vertical lines) used in the model. 69

Figure 3-6. Distribution functions (solid lines) based on averages of belowground biomass data (dots). Maximum and minimum values for each biomass sample are depicted as deviation bars from the averages (n = 9 for each species). 71

Figure 3-7. Daily measurements of net photosynthesis (in grey) and simulation results (in black) for bracken (a) and *Setaria* (c), including the difference of sums for each diurnal run. Measurements vs. simulations are shown on the right for bracken (b) and for *Setaria* (d) including the coefficient of determination. 73

Figure 3-8. Daily means of canopy gross assimilation (positive bars) and total respiration (negative bars) for bracken (black bars) and *Setaria* (grey bars) throughout the year 2008. Main climatic variables are displayed in lines: (top)

daily mean of incoming shortwave radiation, (middle) leaf temperature and (bottom) soil temperatures (black: −15 cm; grey: −50 cm) and soil water content at −20 cm. With exception of soil temperature lines are superimposed by a moving average (time lag of one month) shown in grey. 74

Figure 3-9. Relationship of daily gross assimilation to total global solar radiation observed over the year for bracken (in black) and *Setaria* (in grey).... 76

Figure 3-10. Relationship between daily canopy net photosynthesis and average temperature observed over the year for bracken (in black) and *Setaria* (in grey). 76

Figure 3-11. Dry matter production of bracken (in black) and *Setaria* grass (in grey) calculated over the year 2008. The bars (bottom) show the difference between the biomass increments of *Setaria* and bracken (*Setaria* minus bracken). 77

Figure 4-1. Temperature dependency of photosynthesis in Southern Bracken (*Pteridium arachnoideum*) C3-plant) and *Setaria sphacelata* (C4-plant). Measurements (a): Southern Bracken (white bars) and *Setaria* (grey bars) were cultivated at 20 °C, and net CO_2 assimilation was determined at different leaf temperatures at 1200 µmol quanta m^{-2} s^{-1}. (b): Southern Bracken (white bars) and *Setaria* (grey bars) were cultivated at 10, 20, and 30 °C, respectively, at 500 µmol quanta m^{-2} s^{-1}, and CO_2 assimilation was measured at the growth temperatures. (c): Amount of RubisCO protein in leaves of bracken and *Setaria* which were grown under 10, 20, and 30 °C, respectively. The relative amounts of the protein were determined by rocket immuno-electrophoresis of leaf extracts. Simulations (d): Scatter plot of canopy net CO_2 assimilation with daily means of leaf temperature in the year 2008. (e): Canopy net CO_2 assimilation depending on leaf temperature. 94

Figure 4-2. Modelled influence of increasing temperatures on *Setaria* and bracken for future years. (a) Air temperature of the research site (at 2 m height) according to the IPCC-SRES A1B scenario (average and standard deviation of 10 models) and (b) resulting changes (= difference be-tween scenario – present day values) of gross photosynthesis (GPP), (c) respiration (sum of maintenance and growth respiration), as well as (d) dry matter production for Southern Bracken and the pasture grass *Setaria*. 96

Figure 4-3. Simulated impact of landslides on the forest. (a): Visualisation of the forest model (area 1 ha) with recent landslide disturbance (cf. Dislich and Huth 2012, Fig. 1). (b): Photograph of the RBSF forest with several visible traces of landslides. (c): Simulated accumulation of above-ground tree

biomass after landslide disturbance from different plant functional types (PFT). (d): Aboveground tree biomass under different landslide frequencies (current landslide frequency is 0.02 ha^{-1} $year^{-1}$). All simulation runs apply a reduced growth rate of trees on landslide-disturbed areas due to nutrient limitation. The functional types of the tree-species are classified as: fast-growing pioneer species (PFT 1 and 2, green), mid-successional species (PFT 3 and 4, blue), slow growing species (PFT 5, 6 and 7, orange and red). 98

Figure 5-1. Site location. 107

Figure 5-2. Experimental setup. 107

Figure 5-3. Main processing workflow. The numbers in brackets refer to the following sections. 111

Figure 5-4. Acquisition geometry for flight 27-10-2010. 113

Figure 5-5. Reflectance of green leaves in red (R), green (G), blue (B) and near infrared (N) channels by (a) field spectroscopy, (b) camera digital values measured in the field spectroscopy setup, and (c) camera digital values in the image mosaic of 27-10-2010. 119

Figure 5-6. Aerial image mosaic (a) before and (b) after enhancement and (c) after segmentation. In (c), objects resulting from four consecutive segmentation steps are shown. In (d) the classified segments are plotted as overlay on the NIR image (bracken fern is in red, *Setaria* in blue). 121

Figure 5-7. Time-series of five dates for the experimental plot. From left to right: time sequence corresponding to balloon flights. From top to bottom: image mosaics, cover maps, and foliage projective cover for *Setaria* (blue) and bracken (red). Areas of ground LAI measurements are depicted in the bottom left FPC maps. 123

Figure 5-8. Relationship between ground FPC and LAI data; and conversion function calculated for bracken and *Setaria* foliages. 124

Figure 5-9. Comparison of LAI in time (left, (a) and (c)) and in dynamic range between ground measurement and LAI derived from balloon photography (right, (b) and (d)). Open circles are interpolated values. 125

Figure 6-1. Palm-tree detection using LiDAR data and the method developed for bracken and *Setaria* classification. 138

List of Tables

Table 1-1. Parameters table required in the corresponding modules..... 11

Table 1-2. Meteorological forcing variables. 11

Table 2-1. Leaf area index (LAI) and mean tilt angle (MTA) of 24 representative measurements of *Setaria sphacelata* and bracken (*Pteridium arachnoideum*) on the experimental site..... 33

Table 2-2. Integrated optical traits (PAR) of *Setaria sphacelata*, bracken (*Pteridium arachnoideum*) and bare soil. (Source: field observations with Handy- Spec)..... 34

Table 3-1. Meteorological sensors at the pasture site..... 55

Table 3-2. Physiological and morphological plant parameters..... 61

Table 5-1. Summary of image and ancillary data. The date of the flight is shown in the leftmost column. “MAB” is the number of months post-burn. “Mode” is the camera mode (VIS: visible; NIR: near-infrared). “Shots” is the number of images captured per flight. “Tiles” refers to the selected image-tiles from shots. Leaf area index (Ground LAI) measurements (n=40 per date and species) are shown by date and “MAB”. A summary of the DGPS survey is shown in the rightmost column..... 109

Table 5-2. Summary of acquisition, post-hoc geometry (maximum roll , maximum pitch, and mean height) and spatial accuracy (root mean square error after geo-rectification) for the VIS and NIR aerial image-tiles..... 117

Table 5-3. Area under the ROC curve for the classification of each mosaic/date..... 122

List of Acronyms

asl	Above sea level
AUC	Area under the ROC curve
BRT	Boosted Regression Trees
CLM	Community Land Model
CRT	Canopy radiation transfer
DGVM	Dynamic Global Vegetation Model
ECSF	Estación Científica San Francisco
FPC	Foliage projective cover
GPP	Gross primary productivity
IPCC	Intergovernmental Panel on Climate Change
LAI	Leaf area index
LARS	Low altitude remote sensing
LiDAR	Light Detection and Ranging
MTA	Mean tilt angle
NIR	Near infrared
PAR	Photosynthetic Active Radiation [300-700 nm]
RBSF	Reserva Biológica San Francisco
RMSE	Root mean square error
ROC	Receiver Operating Characteristic
RuBisCO	Ribulose-1,5-bisphosphate carboxylase/oxygenase
RUE	Radiation use efficiency
SoBraCoMo	Southern Bracken Competition Model
SRES	Special Report Emissions Scenarios
SVAT	Soil Vegetation Atmosphere Transfer
VIS	Visible

List of Symbols

A	Gross CO_2 assimilation
$Anet$	Net CO_2 assimilation
b	Image blue channel
BCO_2	Assimilated CO_2 to biomass conversion factor
Ci	Intercellular CO_2 partial pressure
e	Enhanced image
E_a	Activation energy
f	False alarm rate
g	Image green channel
G	Gap fraction in light transmittance
$G(\mu)$	Average leaf projection
h	Hit rate
h	Difference between iteration steps
H_d	Deactivation energy
I_0	Incoming radiation at the earth surface
I_0	Incident global radiation above the canopy
I_{b0}	Direct radiation
I_{d0}	Diffuse radiation
I_{PAR}	PAR radiation
f_{PAR}	Fraction of absorbed PAR
I_{TOA}	Radiation at the top of the atmosphere
k	Diffuse fraction of radiation
K	Diffuse fraction of solar radiation
k'	Diffuse fraction of radiation modified by solar geometry
k'	Diffuse fraction of radiation modified by solar geometry
Kc , Ko	Michaelis constants for CO2 and O_2
Kt	Clearness index
kt	Atmospheric clearness index
m	True negative

m	Efficiency of the CO_2 concentration in C4-plants
N	False negative
p	True positive
q	False positive
Q_{10}	Increase in enzyme kinetics with 10°C temperature
r	Image red channel
Rd_{sha}	Dark respiration of sunlit leaves
Rd_{ssun}	Dark respiration of shade-adapted leaves
Rm_{root}	Maintenance respiration of roots and rhizomes
si	Cut-off digital value
$Vm_{sun,sha}$	Maximum carboxylation rate of sunlit/shaded leaves
Wc	Photosynthesis limitation by CO_2
We	Photosynthesis limitation by export rate
Wi	Photosynthesis limitation by light
x	Canopy depth
α	Radiation absorption by leaf
α	Absorbed photon flux
β	Plant wilting factor
Γ'	Compensation point for CO_2
ΔS	Entropy factor
μ	Cosine of the solar zenith
ρ	Leaf reflectance
τ	Leaf transmittance
φ	Quantum yield
ϕ_1, ϕ_2	Coefficients from the Ross-Goudriaan function
χ	Leaf angle distribution
Ω	Leaf scattering coefficient

Chapter 1

1. Introduction

There is now a global consensus that anthropogenic environmental change poses a severe threat to ecosystem services and biodiversity. Climate and land-use change are considered to be the major triggers of ecosystem deterioration and biodiversity loss (Pereira et al. 2012; Sala et al. 2000). In the tropics, this detrimental process is almost entirely due to intervention in areas of high biodiversity, which will continue into the foreseeable future. The tropical Andes appear at the top of flora and fauna biodiversity and endemism rankings worldwide (Myers et al. 2000), while at the same time suffering the highest deforestation rate (per area) in South America (Brooks et al. 2002). In the southern Ecuadorian Andes, slash and burn clearing of the natural mountain forest to gain pasture land (Goettlicher et al. 2009) implies the loss of current climate regulation services (Fries et al. 2009; Fries et al. 2012), with negative consequences especially for species vulnerable to climate change, such as epiphytes (Noeske et al. 2008) that characterize the mountain forest and the sub-páramo.

On the anthropogenic side, pasture areas have proven to be an unsustainable land use option, because they are susceptible to invasive species that outcompete pasture grass. Previous studies investigated the infestation of pasture areas by the aggressive bracken fern - *Pteridium arachnoideum* (Kaulf.) Maxon. This invasion often causes farmers to abandon gained pasture and to deforest new tracts of land (Hartig and Beck 2003; Knoke et al. 2009; Roos et al. 2010). Recurrent burning is the common management practice for the rejuvenation of pasture, especially of the pasture grass *Setaria sphacelata* (Schumach.) Stapf & C.E. Hubb., yet researchers also believe that fire promotes bracken invasion. In general, the mechanisms and dynamics of bracken fern's competitive strength have been poorly understood. Thus, knowledge must be gained to develop bracken control measures and thus to support sustainable land use practises while also protecting the natural forest.

Both exogenous and endogenous factors (recurrent pasture burning and plant response to environmental factors, respectively), as well as direct plant competition, have been hypothesized to promote bracken fern growth, spatial occurrence and invasive strength. The following aspects might account for bracken fern's competitive success over pasture grass: (i) bracken fern develops a huge stock of reserve material (rhizomes) able to produce new

fronds; (ii) rhizomes grow deep in the soil, meaning that fire cannot damage them, but might instead very well supply heat that stimulates the re-growth of new fronds from the rhizomes; (iii) bracken fern is resilient and more productive under local climate conditions; and (iv) a closed fern canopy casts shadows on the grass beneath it, thus significantly reducing its vitality and biomass production.

While (i)-(ii) can and has been investigated by specific field studies (Hartig and Beck 2003; Roos et al. 2010), the analysis of (iii-iv) requires numerical model experiments.

To date several types of models are used to simulate vegetation dynamics and its interaction with climate. Equilibrium biogeography models are based on the adaptation of vegetation to demographic and environmental variation (Schurr et al. 2012). Terrestrial biogeochemistry models describe biogeochemical and physical processes involving energy and water exchange on large spatial scales (Bonan 2008; Bonan et al. 2003). So-called forest gap models are based on tree individuals and successional processes in homogeneous forest patches (Perry and Millington 2008). The more recent Dynamic Vegetation Model (DVM) is a concept used to integrate all existing vegetation model families and can be applied either to predict primary productivity or to investigate the impact of the terrestrial ecosystem on water, carbon and nutrients cycles (Fisher et al. 2010).

Different concepts can be chosen to implement a DVM and generally fall into two classes. The first one is based on empirical regressions between productivity and incoming radiation. This is a more simplistic approach in which productivity is calculated by multiplying the existent green area by the radiation use efficiency. Also no representation of canopy structure is required (the "big-leaf" assumption) and the biochemistry of photosynthesis is implicit in the productivity data used to estimate the radiation use efficiency. This kind of model has been extensively used, especially for global applications (Roderick et al. 2001). The second class comprises mechanistic models which highly depend on a proper representation of canopy structure and biochemical processes (Randerson et al. 2009). The latter is the state of the art of DVM's and has impelled new developments from local to global applications. However, these models require accurate data on photosynthesis and well understood radiation transfer in the canopy (Chen et al. 2008).

To simulate the growth of bracken fern there are only a few approaches known in the literature. They utilize concepts either of biogeography models (Birnie et al. 2000) or empirically-based models (Pakeman et al. 1994). Furthermore, hitherto conducted model experiments have focused on

"northern bracken" (Blackburn and Pitman 1999) where the growth cycle is characterized by strong seasonal variations.

In summary, there are two clear gaps in the knowledge and technology regarding the ecology of southern bracken: (i) A knowledge gap on growth dynamics of southern bracken under global environmental change (non-sustainable land use practises and climate change) and (ii) a technology gap regarding sophisticated species-specific DVM adaptations and validation tools, applicable to analysing growth dynamics of southern bracken and its competitor grasses, forced by realistic present and future climate/environmental states.

Regarding the technology gap for modelling southern bracken growth, the DVM concept has the advantage of modularity (e.g. soil processes are in a different module than biochemistry, though coupled). It encompasses the concept of an average parameterized individual, also called Plant Functional Type (PFT), and a hierarchical structure to comprise two PFTs sharing the same soil substrate and atmosphere.

Fortunately, the novel community earth system model (CESM) includes the Community Land Model and Dynamic Global Vegetation Model (CLM-DGVM) which implement the DVM concept for simulation of plant growth and competition (for light or water) at global scale (Bonan et al. 2003; Dai et al. 2004; Randerson et al. 2009). However, default model setups are only available for global applications and cannot be applied to two distinct species. Hence, a species-specific DVM adaptation applicable to the problem of southern bracken invasion requires:

1. A proper parameterization of the species of interest, replacing the PFT's of the currently available model
2. A proper parameterization of the local environment with in-situ observations
3. Realistic environmental forcing of the model
4. Validation of the adapted model with field observations

1.1 Study area

The study area is located in the Rio San Francisco Valley in the south-eastern Ecuadorian Andes between the two provincial capitals Loja and Zamora (Figure 1-1). Figure 1-1a gives a global perspective of areas with no bracken occurrence and which are instead characterized mainly by rainforest, high elevations, and arid areas (Ellis and Ramankutty 2008). Complementary white

areas indicate possible bracken occurrence. Solid lines indicate elevations (2 and 4 km a.s.l) of the Andean Cordillera, while dashed lines show political divisions. Figure 1-1b shows the boundary of the Rio San Francisco basin over a true-colour composite satellite image (Quickbird satellite). The basin is part of the biodiversity hotspot of the Ecuadorian Andes, where especially the pristine and partly protected mountain forest harbours a vast range of species (Barthlott et al. 2007; Bendix and Beck 2009; Liede-Schumann and Breckle 2008). The deeply incised valley (between 1800 to 3200 m asl height) is characterized by high cloud frequency (>70%). The eastern slopes of the Cordillera are on the windward side of almost constant easterly winds during the year (>85% of all days), which bring in moist Amazon air masses, causing forced convection, condensation and cloud formation. An average annual rainfall of 2180 mm is observed at the "Estación Científica San Francisco" (ECSF) research station (1960 m asl); the rainfall increases to more than 6700 mm at the crest level (including moist deposition of cloud water). Coordinates of the ECSF are given in Figure 1-1b.

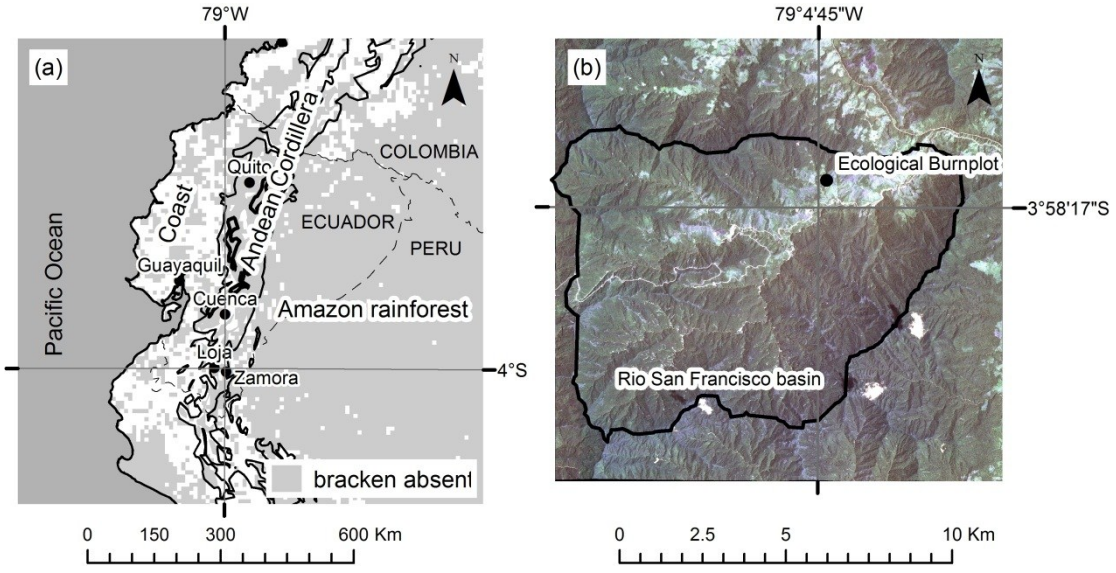

Figure 1-1. Location of the Rio San Francisco basin in Ecuador (a) and the Ecological Burnplot in the valley (b).

The natural vegetation of the valley is generally characterized by evergreen mountain rainforest with vegetation subtypes along the altitudinal gradient (Homeier et al. 2010). The position of the timberline is around 2700 m asl; above this altitude, shrubs, herbs and bryophytes become dominant, forming a belt of sub-páramo vegetation (Homeier et al. 2008). Below 2200 m asl, 48% of the natural mountain forest has been cleared by slash and burn activities mainly to gain pastureland (Göttlicher et al. 2009). About 40% of the

pastures are heavily infested by a terrible weed, the southern bracken fern, which causes farmers to abandon their pastures within a decade or less, after which they (usually illegally) cut down sections of the remnants of natural forest (Hartig and Beck 2003).

For more information on the study area and the specific design of the experimental plot used for this thesis, the reader may refer to section 1.5 and the individual chapters of the thesis.

1.2 Aims and hypotheses

Two guiding scientific issues are the basis of the current thesis:

- To understand the response of two competing species (bracken fern and *Setaria* pasture) to current and future climate conditions in a valley of the south-eastern Ecuadorian Andes.

- To understand the particular post-fire canopy recovery of both species by monitoring an ecological experimental burning in the study area.

Three main hypotheses will be tested with the thesis:

H1: Under current climate conditions, net-productivity of the bracken fern is higher than that of the pasture grass *Setaria*.

H2: Growth performance of the pasture grass *Setaria* will be favoured by global warming.

H3: Bracken growth is stimulated by recurrent burning.

To address these scientific issues and hypotheses, a sequence of working packages was designed, which will be described in more detail in the following chapters. The specific aims of the working packages are:

(a) to recode and extend the existing dynamic vegetation model (CLM-DGVM) and adapt it to a new model – the Southern Bracken Competition Model – for species-specific simulations using a single-point dataset for testing bracken fern and pasture grass *Setaria* individuals (see chapters 2 and 3 respectively).
(b) to derive eco-physiological information from field surveys for the species-specific parameterization using an average of the model individual traits of bracken fern and pasture grass (see chapter 3).

(c) to conduct diagnostic simulations of potential growth for assessing the competitive strength of both species under future warming scenarios (see chapter 4).
(d) to monitor and analyse the effect of burning on the initial succession of the two competing species (bracken fern and pasture grass *Setaria*) (see chapter 5).

These working packages should enable future grid-based simulations on the plot scale using simultaneous monitoring and meteorological data, thus testing a model for direct competition for light (see chapter 6).

In a first step, single-point model runs were used to test the hypotheses H1 and H2. It was expected to realistically simulate the particular response of the bracken fern and pasture grass *Setaria* using meteorological forcing in very high temporal resolution (10 minutes time-step). In this case, the validation strategy for single-point runs of the extended model is a direct comparison of productivity values between model, field surveys and literature values. Testing H3 required monitoring, in particular ground measurements (e.g. biomass and leaf-area) and the exploitation of remotely-sensed spatial data for the identification of species cover before and after burning. These data were usable for two purposes: (i) to analyse canopy recovery after a fire and (ii) to validate model runs using a grid-based dataset.

1.3 Structure of the thesis

The general design of the current thesis combines modelling and monitoring activities (Figure 1-2). Model development consists of the sequential programming, parameterization and validation of different required modules, each module requiring extensive coding and derivation of specific parameters from field data. Three modules were developed for the Southern Bracken Competition Model (SoBraCoMo): (i) a module describing the transfer of solar radiation within the canopy (see chapter 2); (ii) a module for calculating species-specific photosynthesis (see chapter 3); and (iii) a module for calculating biomass under the future climate scenario (see chapter 4).

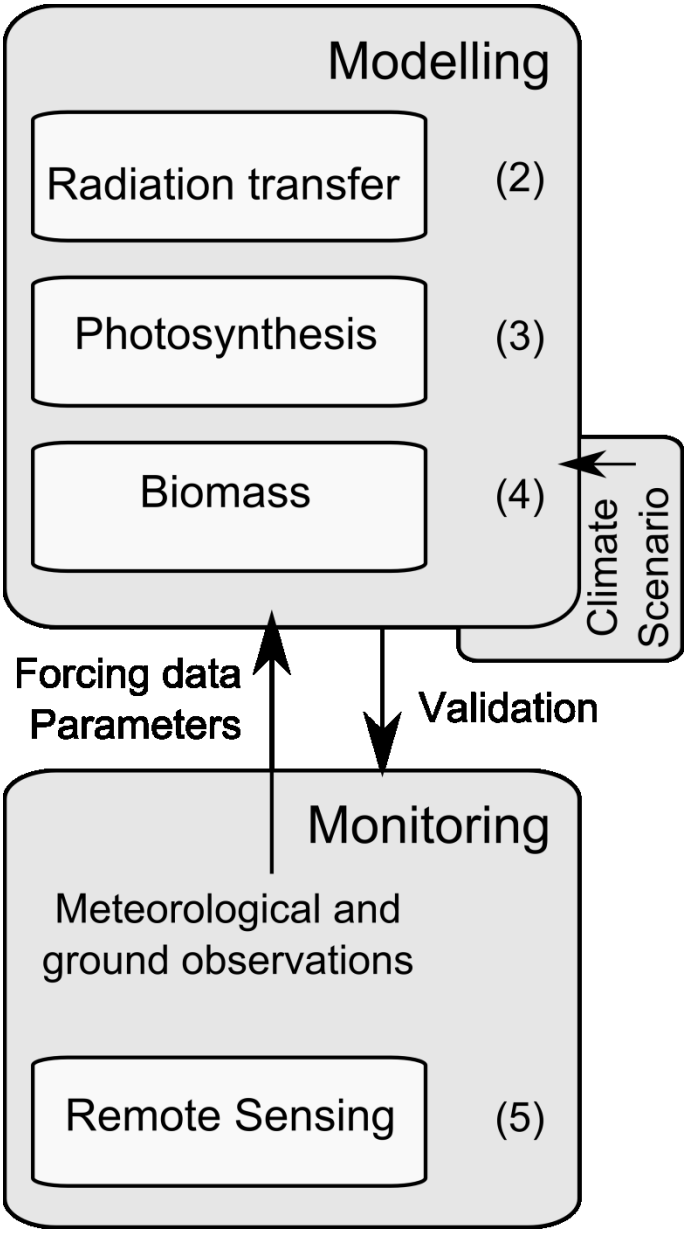

Figure 1-2. Conceptual design and outline of this work. Related chapters of the thesis are indicated in brackets.

Simultaneously, field surveys and continuous monitoring activities of environmental variables were conducted over the research period in the study area to supply model the development with data. These data are needed for (i) realistic environmental forcing (realistic atmospheric and soil conditions) and (ii) validation of model variables (e.g. leaf area and biomass) using ground observations and remote-sensing. Accordingly, the arrows between modelling and monitoring boxes represent methods developed for handling data (e.g. storage, input, conversion, and scaling).

1.4 Model development and setup

The development of the new species-specific DVM Southern Bracken Competition Model (SoBraCoMo) is based on the theory that the most appropriate model setup optimizes the relation between knowledge gain and model complexity (Joergensen 2001). Figure 1-2 shows that the simplest models tend to increase knowledge gain with complexity in the beginning. At a certain level, a trade-off between complexity and knowledge arises due to the uncertainty caused by adding too many new variables. Considering a model on the solid curve, forcing/parameterization data quality and quantity enhance the model-based knowledge of the system. In the present work, the available global model (CLM-DGVM) is the starting point which lies on the solid curve (Figure 1-3) at an intermediate level of complexity. However, if directly applied to the local scale, the model-based knowledge would decrease considerably due to the absence of the required complexity supplied by adequate species- and area-specific parameters. At the point of end development, after reconstruction and additional formulations, proper parameterization and realistic forcing simulations are expected to deliver a better knowledge at plot scale. This representation (Figure 1-2) offers a conceptual basis for potential improvement in vegetation modelling. A validation of this improvement is beyond the scope of this work.

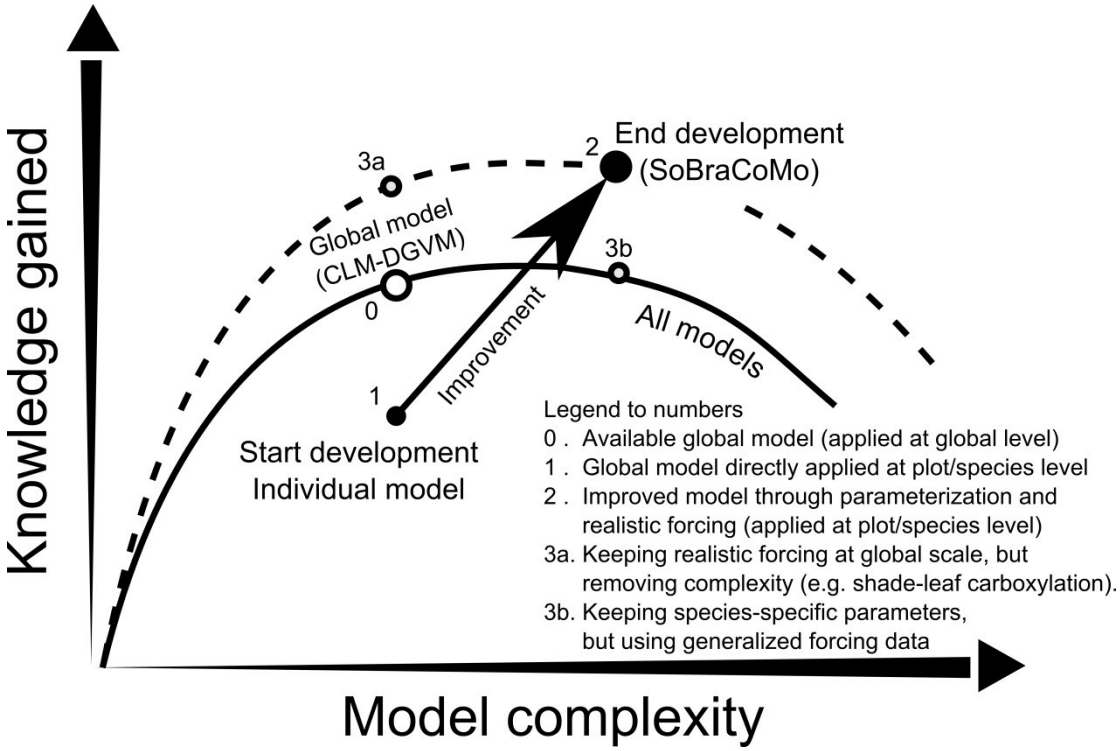

Figure 1-3. Relation of knowledge gained with a model and model complexity. The solid-line curve represents a small or poor-quality dataset in comparison with the broken-line curve. The arrow inside the plot represents the enhancement from a starting point – a local application inheriting concepts from a global model – to a model with proper data, parameters and new variables, which can be applied in a plot up to a regional scale (Adapted from Joergensen 2001).

As stressed in Figure 1-2 and 1-4, model development was conducted via modules. The **first module** determines the species-specific absorption of solar radiation. Here incoming radiation was partitioned into diffuse and direct fractions, and formulations were made to estimate the shaded and sunlit leaf area (Dai et al. 2004). For parameterization and validation, a specifically designed pyranometer was used to derive site-dependent coefficients for solar radiation partitioning into direct, diffuse, and PAR components. These coefficients can then be applied to standard pyranometer sensors which commonly measure global radiation. Here, a new formulation with proper parameters was added to the model (see chapter 2 and 3).

In the **second biochemistry module**, formulations for C3 (bracken) and C4 (*Setaria*) photosynthetic pathways were combined to consider the photosynthetic response of different plant species to the local environment. This advance has been already incorporated in the CLM-DGVM base model, as well as in formulations based on leaf nitrogen (Thornton and Zimmermann

2007). In this work, the same nitrogen effects within the canopy were considered by adding the corresponding new formulations for carboxylation rate for shade-adapted leaves (see chapter 3). This improvement can be considered an alternative method with a focus on the available field instrumentation (porometery).

The current SoBraCoMo is implemented as shown in Figure 1-4. The elements of the schematic in Figure 1-4 were cumulatively constructed for diagnostic runs (chapters 2-4). Prognostic simulations are beyond the scope of this thesis. The required list of parameters for diagnostic simulations is shown in Table 1 and atmospheric and soil forcing data in Table 2.

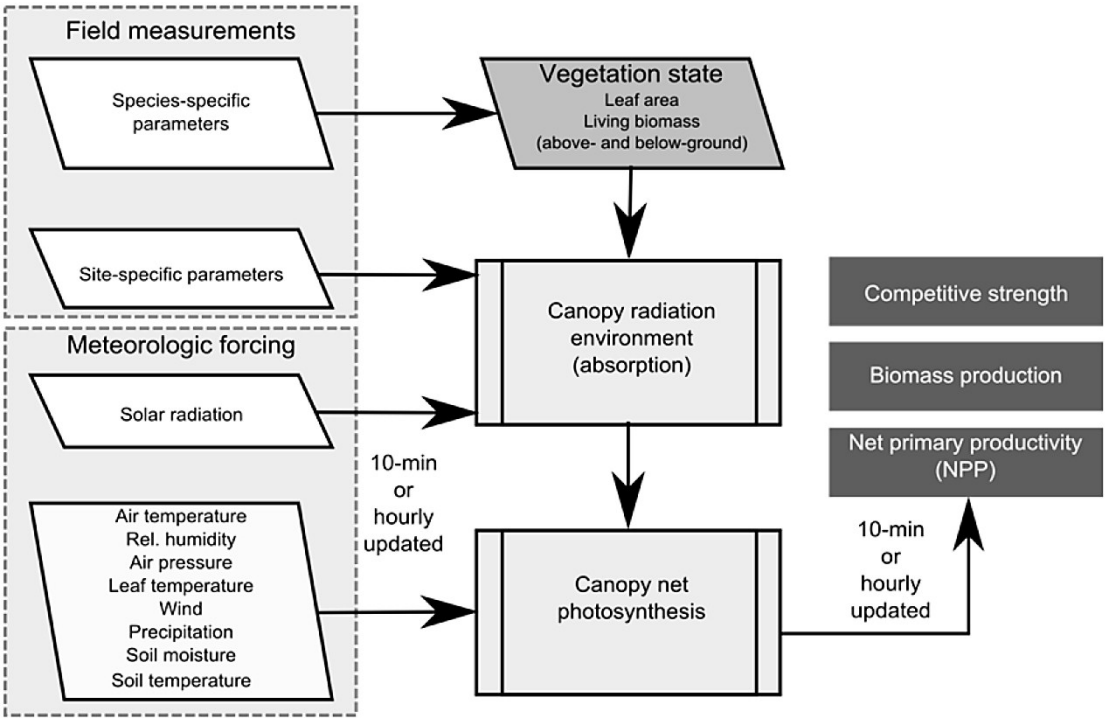

Figure 1-4. Model scheme for diagnostic runs, including field data and meteorologic forcing, particular sub-modules and the main vegetation state variables.

Table 1-1. Parameters table required in the corresponding modules.

Module	Parameter	Unit	Use
(i) Radiation transfer	Diffuse to global radiation coefficients	-	Partition of global radiation
	Leaf Angle	°	CRT
	Leaf area index	$m^2\ m^{-2}$	CRT and photosynthesis
	Spectral traits	%	CRT and photosynthesis
(ii) Canopy net photosynthesis	Carboxylation rate	$\mu mol\ m^{-2}\ s^{-1}\ ppm^{-1}$	GPP
	Quantum efficiency	$\mu mol\ \mu mol^{-1}$	GPP
	Temperature coefficients	$J\ mol^{-1}\ K^{-1}$; $kJ\ mol^{-1}$	GPP and Respiration
	Roots C:N ratio	$gC\ g^{-1}N$	Root respiration
	Roots distribution	-	Water uptake
	Soil texture (clay and sand)	%	Water available per depth

Table 1-2. Meteorological forcing variables.

Meteorological forcing
Solar radiation (PAR, direct and diffuse)
Air temperature and humidity
Air temperature and humidity at canopy height
Leaf temperature
Soil temperature
Soil water
Precipitation
Air pressure

1.5 Experimental plot design and monitoring setup of the thesis

To properly parameterize, force and validate the developed model, an experimental plot with sophisticated instrumentation was established in the pasture area (Figure 5). The experimental plot has dimensions of 50 x 20 m on the ground and is located at 2109 m asl. Almost 70% of the area is covered predominantly by the pasture grass *Setaria* planted in rows, while the other 30% is covered by bracken fern. The area was fenced in 2007 and then burned twice (October 2008 and November 2009) to monitor canopy recovery after a fire.

The operation of the established plot warrants:

1. continuous atmospheric forcing and further parameterization data
2. data of other environmental conditions, e.g. soil moisture (parameterization/forcing)
3. the feasibility of field studies for obtaining parameterization data, e.g. field spectrometry
4. the opportunity to conduct ecological experiments, e.g. the simulation of pasture management by recurrent burning
5. the application of low altitude remote sensing (LARS) technology to monitor vegetation development before and after burning which can be used for spatio-temporal validation of a grid-based SoBraCoMo simulation.

The experimental and monitoring setup is illustrated in Figure 5. In general, monitoring activities included meteorology (see chapter 3), balloon-borne aerial photography (see chapter 5), field spectroscopy, and ground observations of canopy traits.

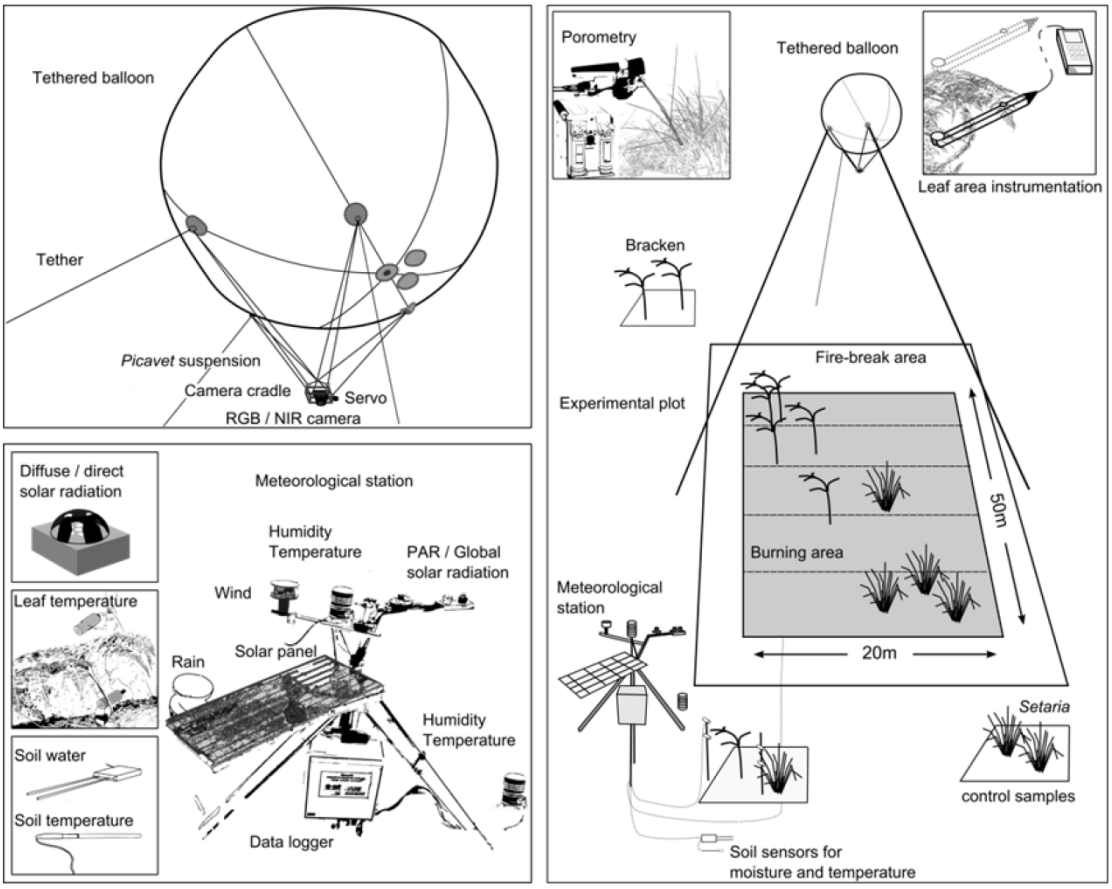

Figure 1-5. General experimental setup for field measurements and monitoring of post-fire canopy recovery.

1.5.1 Forcing meteorology

An automatic meteorological station was specifically designed to consider conditions at canopy level, in root depth, and at leaf surface (temperature, humidity, and wetness) for *Setaria* and bracken. In contrast to the common practice at global scale, the exact measurements of leaves are more accurate than by alternatively deriving estimates based on the energy balance equation as done in the original CLM-DGVM model. Thus, these measurements substitute the respective CLM modules in the SoBraCoMo. Realistic forcing at the canopy and in the rooted soil layers provide an enhanced data set for calculating gas and water exchange between leaf and atmosphere, as well as for root respiration and water limitations in the soil.

1.5.2 Ground observations for parameterization and validation

Ground observations include in situ measurements and laboratory experiments on soil and plant physiology with samples collected at the study site. In this thesis, state of the art techniques were combined to measure net photosynthesis, canopy traits (including biomass), and soil properties for either a single characterization or continuous measurements. Laboratory experiments (e.g. photosynthetic response in shade, plant and soil carbon and nitrogen) and field campaigns at the plot and within the valley complete the investigations to support both model parameterization and remote sensing.

1.5.3 Remote sensing for monitoring and validation

Low altitude remote sensing, or LARS (Aber et al. 2010), was used to observe the spatio-temporal development of bracken and *Setaria* species cover before and after burning. Furthermore, the data are intended to be used for later validation of a spatial representation of SoBraCoMo (chapter 6). However, to observe vegetation development after pasture management in LARS data, proper classification and calibration methodology had to be developed. An appropriate camera system was selected which was (i) applicable to LARS in higher altitudes (low weight system), (ii) cost effective and (iii) able to discriminate between the optical signals of the two species. (For detailed descriptions the reader may refer to chapter 5).

Fortunately, the camera used was able to distinguish between the two plants due to their spectral differences in visible and near infrared ranges (Figure 1-3a). For leaf area index (LAI) equals one, the bracken's lower reflection in the visible range is due to higher pigmentation – a considerably higher amount of chlorophyll a and b – as observed in leaf extracts (Figure 1-3b). The bracken's higher reflectance in the near infrared range is due to thicker leaves, while the higher absorption in the visible range of radiation is due to well-distributed pigments within the mesophyll (avoiding the so-called "clumping effect"). In *Setaria* leaves, palisade cells are more solid and pigments are concentrated within the mesophyll, in the bundle sheath cells (Figure 1-3c). Consequently, the leaf structure of green bracken fronds leads to optimization of photosynthetic active radiation (PAR) absorption and a pronounced red edge, which means a potential segmentation by optical remote sensing. For LAI higher than one, or at the canopy level, the bracken's higher reflectance in the near infrared range holds (Figure 1-3a), but *Setaria* absorbs more in the visible range. One reason is the leaf clumping, which is higher in *Setaria* canopies at moderate LAI (between 1 and 3) and completely

excludes reflection from the background (soil and stones) or from non-green parts of the plants.

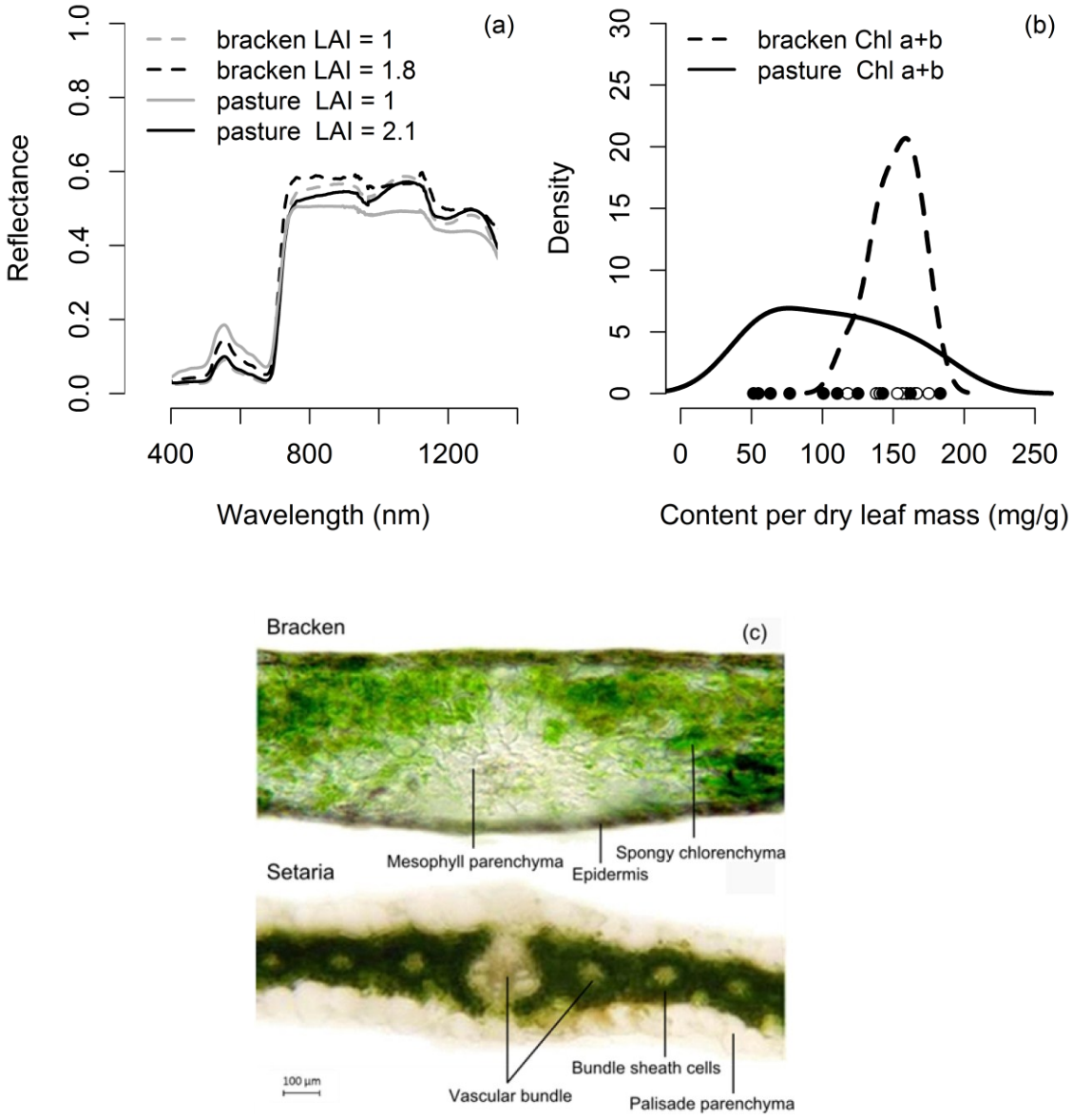

Figure 1-6. Spectral signatures at leaf (LAI = 1) and canopy levels (LAI > 1) collected in the field (a); sum of chlorophyll a and b from pigment analysis (pigment analysis were done under supervision of PD D. Dörnemann); and leaf cross-section of bracken and *Setaria* sun leaves (c) (cross-sections by N.König, scale by I. Voss, and notations by B. Silva).

This clear spectral difference at the leaf and canopy level allowed the use of a cost-effective two-camera system based on standard digital sensors: (i) a standard VIS and (ii) a modified NIR camera. Balloon-borne photography was used to obtain species-specific plant cover (chapter 5). Combined with ground

measurements, the plant cover was also used to provide conversion coefficients for projected cover to leaf area.

1.6 Global relevance of the thesis: The induced invasion of bracken

Although the current study focuses on a small subset area of the eastern Andes, the infestation of ecosystems by bracken is a global problem. This is illustrated in Figure 1-7, which shows the global distribution of the genus *Pteridium* (Der et al. 2009) through a distribution map of locations where "bracken fern" was investigated. As part of this thesis, a bibliography survey (n = 251) reveals that much attention has been given to the "northern complex" (21% of all publications are related to the European *P. aquilinum*). All bracken bioregions outside the "northern complex" comprise less than 5% of publications. To cite a few studies, the invasive strength of bracken is well known in Great Britain, where significant reductions (up to -71 %) in pasture production have been reported (Thomson and Smith 1990). More recent research developed and tested bracken control techniques in Europe (Stewart et al. 2007). The problem of bracken invasion has also occurred in the US, in south-eastern Australia and New Zealand, where bracken is also connected with wildfires (McGlone et al. 2005). The recent increase in publications in Southern Brazil is exclusively related to bracken toxicity, which is a recognized problem for all ruminants (Lucena et al. 2011). Despite bracken offering a few possible and site-dependent ecological advantages, e.g. erosion prevention (McGlone et al. 2005), the literature overwhelmingly points to the detrimental role of bracken on pasture and cultivated land.

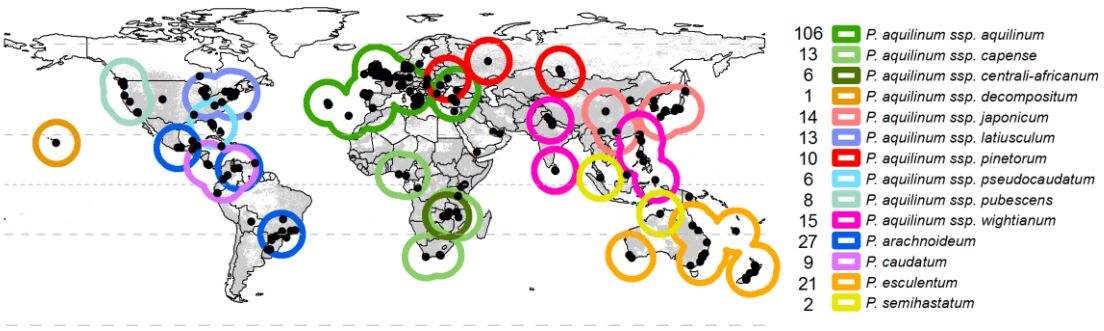

Figure 1-7. Distribution map of (colour circles) bracken fern species (Der et al. 2009) and bibliography review of bracken fern observations with geographical reference (black points). Grey areas indicate possible bracken occurrence detected by a land-use remote sensing product (Ellis and Ramankutty 2008).

Bibliography

Aber, J.S., Marzolff, I., & Ries, J. (2010). Small-Format Aerial Photography: Principles, techniques and geoscience applications. Amsterdam: Elsevier

Barthlott, W., Hostert, A., Kier, G., Koper, W., Kreft, H., Mutke, J., Rafiqpoor, M.D., & Sommer, J.H. (2007). Geographic patterns of vascular plant diversity at continental to global scales. Erdkunde, 61

Bendix, J., & Beck, E. (2009). Spatial aspects of ecosystem research in a biodiversity hot spot of southern ecuador - an introduction. Erdkunde, 63

Bendix, J., Silva, B., Roos, K., Göttlicher, D.O., Rollenbeck, R., Nauss, T., & Beck, E. (2010). Model parameterization to simulate and compare the PAR absorption potential of two competing plant species. International journal of biometeorology, 54, 283-295

Birnie, R.V., Miller, D.R., Horne, P.L., Leadbeater, S., & Macdonald, A. (2000). The potential distribution and impact of bracken in upland Scotland: An assessment using a GIS-based niche model. Annals of Botany, 85

Blackburn, G.A., & Pitman, J.I. (1999). Biophysical controls on the directional spectral reflectance properties of bracken (*Pteridium aquilinum*) canopies: Results of a field experiment. International Journal of Remote Sensing, 20, 2265-2282

Bonan, G. (2008). Ecological Climatology. (2 ed.). Cambridge: Cambridge University Press

Bonan, G.B., Levis, S., Sitch, S., Vertenstein, M., & Oleson, K.W. (2003). A dynamic global vegetation model for use with climate models: concepts and description of simulated vegetation dynamics. Global Change Biology, 9

Brooks, T.M., Mittermeier, R.A., Mittermeier, C.G., da Fonseca, G.A.B., Rylands, A.B., Konstant, W.R., Flick, P., Pilgrim, J., Oldfield, S., Magin, G., & Hilton-Taylor, C. (2002). Habitat loss and extinction in the hotspots of biodiversity. Conservation Biology, 16

Chen, Q., Baldocchi, D., Gong, P., & Dawson, T. (2008). Modeling radiation and photosynthesis of a heterogeneous savanna woodland landscape with a hierarchy of model complexities. Agricultural and Forest Meteorology, 148, 1005-1020

Dai, Y.J., Dickinson, R.E., & Wang, Y.P. (2004). A two-big-leaf model for canopy temperature, photosynthesis, and stomatal conductance. Journal of Climate, 17

Der, J.P., Thomson, J.A., Stratford, J.K., & Wolf, P.G. (2009). Global chloroplast phylogeny and biogeography of bracken (*pteridium*; *dennstaedtiaceae*). American Journal of Botany, 96

Ellis, E.C., & Ramankutty, N. (2008). Putting people in the map: anthropogenic biomes of the world. Frontiers in Ecology and the Environment, 6

Fisher, R., McDowell, N., Purves, D., Moorcroft, P., Sitch, S., Cox, P., Huntingford, C., Meir, P., & Woodward, F.I. (2010). Assessing uncertainties in a second-generation dynamic vegetation model caused by ecological scale limitations. New Phytologist, 187, 666-681

Fries, A., Rollenbeck, R., Goettlicher, D., Nauss, T., Homeier, J., Peters, T., & Bendix, J. (2009). Thermal structure of a megadiverse andean mountain ecosystem in southern ecuador and its regionalization. Erdkunde, 63

Fries, A., Rollenbeck, R., Nauss, T., Peters, T., & Bendix, J. (2012). Near surface air humidity in a megadiverse Andean mountain ecosystem of southern Ecuador and its regionalization. Agricultural and Forest Meteorology, 152

Goettlicher, D., Obregon, A., Homeier, J., Rollenbeck, R., Nauss, T., & Bendix, J. (2009). Land-cover classification in the Andes of southern Ecuador using Landsat ETM plus data as a basis for SVAT modelling. International Journal of Remote Sensing, 30

Göttlicher, D., Obregón, A., Homeier, J., Rollenbeck, R., Nauss, T., & Bendix, J. (2009). Land-cover classification in the Andes of southern Ecuador using Landsat ETM+ data as a basis for SVAT modelling. International Journal of Remote Sensing, 30, 1867-1886

Hartig, K., & Beck, A. (2003). The bracken fern (*Pteridium arachnoideum* (Kaulf.) Maxon) dilemma in the andes of southern Ecuador. Ecotropica, 9

Homeier, J., Breckle, S.-W., Günter, S., Rollenbeck, R.T., & Leuschner, C. (2010). - Tree Diversity, Forest Structure and Productivity along Altitudinal and Topographical Gradients in a Species-Rich Ecuadorian Montane Rain Forest, - 42, - 148

Homeier, J., Werner, F.A., Gradstein, S.R., Breckle, S.-W., & Richter, M. (2008). Potential vegetation and floristic composition of Andean forests in South Ecuador, with a focus on the RBSF. In E. Beck, J. Bendix, I. Kottke, F. Makeschin, & R. Mosandl (Eds.), Gradients in a tropical mountain ecosystem of Ecuador (pp. 87–100). Berlin - Heidelberg: Springer

Joergensen, S.E. (2001). Fundamentals of ecological modelling. (3 ed.). Amsterdam: Elsevier

Knoke, T., Calvas, B., Aguirre, N., Roman-Cuesta, R.M., Guenter, S., Stimm, B., Weber, M., & Mosandl, R. (2009). Can tropical farmers reconcile subsistence needs with forest conservation? Frontiers in Ecology and the Environment, 7

Liede-Schumann, S., & Breckle, S.-W. (2008). Provisional checklists of flora and fauna of the San Francisco valley and its surroundings. Ecotropical Monographs, 4

Lucena, R.B., Rissi, D.R., Kommers, G.D., Pierezan, F., Oliveira-Filho, J.C., Macedo, J.T.S.A., Flores, M.M., & Barros, C.S.L. (2011). A Retrospective Study of 586 Tumours in Brazilian Cattle. Journal of Comparative Pathology, 145

McGlone, M.S., Wilmshurst, J.M., & Leach, H.M. (2005). An ecological and historical review of bracken (Pteridium esculentum) in New Zealand, and its cultural significance. New Zealand Journal of Ecology, 29

Myers, N., Mittermeier, R.A., Mittermeier, C.G., da Fonseca, G.A.B., & Kent, J. (2000). Biodiversity hotspots for conservation priorities. Nature, 403

Noeske, N.M., Hilt, N., Werner, F.A., Brehm, G., Fiedler, K., Sipman, H.J.M., & Gradstein, S.R. (2008). Disturbance effects on diversity of epiphytes and moths in a montane forest in Ecuador. Basic and Applied Ecology, 9

Pakeman, R.J., Marrs, R.H., & Jacob, P.J. (1994). A model of bracken (Pteridium-aquilinum) growth and the effects of control strategies and changing climate. Journal of Applied Ecology, 31

Pereira, H.M., Navarro, L.M., & Martins, I.S. (2012). Global Biodiversity Change: The Bad, the Good, and the Unknown. Annual Review of Environment and Resources, Vol 37, 37

Perry, G.L.W., & Millington, J.D.A. (2008). Spatial modelling of succession-disturbance dynamics in forest ecosystems: Concepts and examples. Perspectives in Plant Ecology Evolution and Systematics, 9, 191-210

Randerson, J.T., Hoffman, F.M., Thornton, P.E., Mahowald, N.M., Lindsay, K., Lee, Y.H., Nevison, C.D., Doney, S.C., Bonan, G., Stockli, R., Covey, C., Running, S.W., & Fung, I.Y. (2009). Systematic assessment of terrestrial biogeochemistry in coupled climate-carbon models. Global Change Biology, 15, 2462-2484

Roderick, M.L., Farquhar, G.D., Berry, S.L., & Noble, I.R. (2001). On the direct effect of clouds and atmospheric particles on the productivity and structure of vegetation. Oecologia, 129, 21-30

Roos, K., Rollenbeck, R., Peters, T., Bendix, J., & Beck, E. (2010). Growth of Tropical Bracken (*Pteridium arachnoideum*): Response to Weather Variations and Burning. Invasive Plant Science and Management, 3

Sala, O., Chapin, F., Armesto, J., Berlow, E., Bloomfield, J., Dirzo, R., Huber-Sanwald, E., Huenneke, L., Jackson, R., Kinzig, A., Leemans, R., Lodge, D., Mooney, H., Oesterheld, M., Poff, N., Sykes, M., Walker, B., Walker, M., & Wall, D. (2000). Biodiversity - Global biodiversity scenarios for the year 2100. Science, 287, 1770-1774

Schurr, F.M., Pagel, J., Cabral, J.S., Groeneveld, J., Bykova, O., O'Hara, R.B., Hartig, F., Kissling, W.D., Linder, H.P., Midgley, G.F., Schroder, B., Singer, A., & Zimmermann, N.E. (2012). How to understand species' niches and range dynamics: a demographic research agenda for biogeography. Journal of Biogeography, 39, 2146-2162

Stewart, G.B., Pullin, A.S., & Tyler, C. (2007). The effectiveness of asulam for bracken (*Pteridium aquilinum*) control in the united kingdom: A meta-analysis. Environmental Management, 40

Thomson, J.A., & Smith, R.T. (1990). Bracken biology and management. (40 ed.). University of Sydney: Australian institute of agricultural science

Thornton, P.E., & Zimmermann, N.E. (2007). An improved canopy integration scheme for a land surface model with prognostic canopy structure. Journal of Climate, 20

Chapter 2

2. Model parameterization to simulate PAR absorption potential

This chapter has been published as: Bendix, J., Silva, B., Roos, K., Göttlicher, D., Rollenbeck, R., Nauß, T., Beck, E., 2010. Model parameterization to simulate and compare the PAR absorption potential of two competing plant species. **International Journal of Biometeorology, Volume 54, Pages. 283–295**, 25. November 2009.

with kind permission from Springer Science and Business Media and the International Journal of Biometeorology.

Abstract

Mountain pastures dominated by the pasture grass *Setaria sphacelata* in the Andes of southern Ecuador are heavily infested by southern bracken (*Pteridium arachnoideum*), a major problem for pasture management. Field observations suggest that bracken might outcompete the grass due to its competitive strength with regard to the absorption of photosynthetically active radiation (PAR). To understand the PAR absorption potential of both species, the aims of the current paper are to (1) parameterize a radiation scheme of a two-big-leaf model by deriving structural (LAI, leaf angle parameter) and optical (leaf albedo, transmittance) plant traits for average individuals from field surveys, (2) to initialize the properly parameterized radiation scheme with realistic global irradiation conditions of the Rio San Francisco Valley in the Andes of southern Ecuador, and (3) to compare the PAR absorption capabilities of both species under typical local weather conditions. Field data show that bracken reveals a slightly higher average leaf area index (LAI) and more horizontally oriented leaves in comparison to *Setaria*. Spectrometer measurements reveal that bracken and *Setaria* are characterized by a similar average leaf absorptance. Simulations with the average diurnal course of incoming solar radiation (1998–2005) and the mean leaf–sun geometry reveal that PAR absorption is fairly equal for both species.

However, the comparison of typical clear and overcast days show that two parameters, (1) the relation of incoming diffuse and direct irradiance, and (2) the leaf–sun geometry play a major role for PAR absorption in the two-big-leaf approach: Under cloudy sky conditions (mainly diffuse irradiance), PAR absorption is slightly higher for *Setaria* while under clear sky conditions (mainly direct irradiance), the average bracken individual is characterized by a higher PAR absorption potential. (~74 MJ m^{-2} $year^{-1}$). The latter situation which occurs if the maximum daily irradiance exceeds 615 W m^{-2} is mainly due to the nearly orthogonal incidence of the direct solar beam onto the horizontally oriented frond area which implies a high amount of direct PAR absorption during the noon maximum of direct irradiance. Such situations of solar irradiance favoring a higher PAR absorptance of bracken occur in ~36% of the observation period (1998–2005). By considering the annual course of PAR irradiance in the San Francisco Valley, the clear advantage of bracken on clear days (36% of all days) is completely compensated by the slight but more frequent advantage of *Setaria* under overcast conditions (64% of all days). This means that neither bracken nor *Setaria* show a distinct advantage in PAR absorption capability under the current climatic conditions of the study area.

2.1 Introduction

The Ecuadorian Andes are one of the major hot spots of vascular plant diversity worldwide (Barthlott et al. 2007). At the same time, the natural forests in Ecuador suffer from the highest deforestation rate (1.2% per year) in Latin America (FAO 2001). In the eastern Cordillera, large areas of tropical forest have been cleared by slash and burn for gaining pastureland. On slopes of moderate inclination, the Sorghum-like tillering *Setaria sphacelata* is grown in monocultures. Our previous studies on *Setaria* pastures have shown that the current mode of pasture management favors the growth of an extremely aggressive weed, the tropical bracken fern *Pteridium arachnoideum* (Hartig and Beck 2003). This process is particularly prominent in the lower parts of the Rio San Francisco valley <2,400 m asl (Figure 2-1) where large areas (~68%) of former pastures have been abandoned due to bracken infestation and the concomitant supersession of the pasture grass (Beck et al. 2008a; Göttlicher et al. 2009). Unfortunately, the loss of pasture usability boosts the land use pressure on the remaining natural forest, threatening its unique biodiversity.

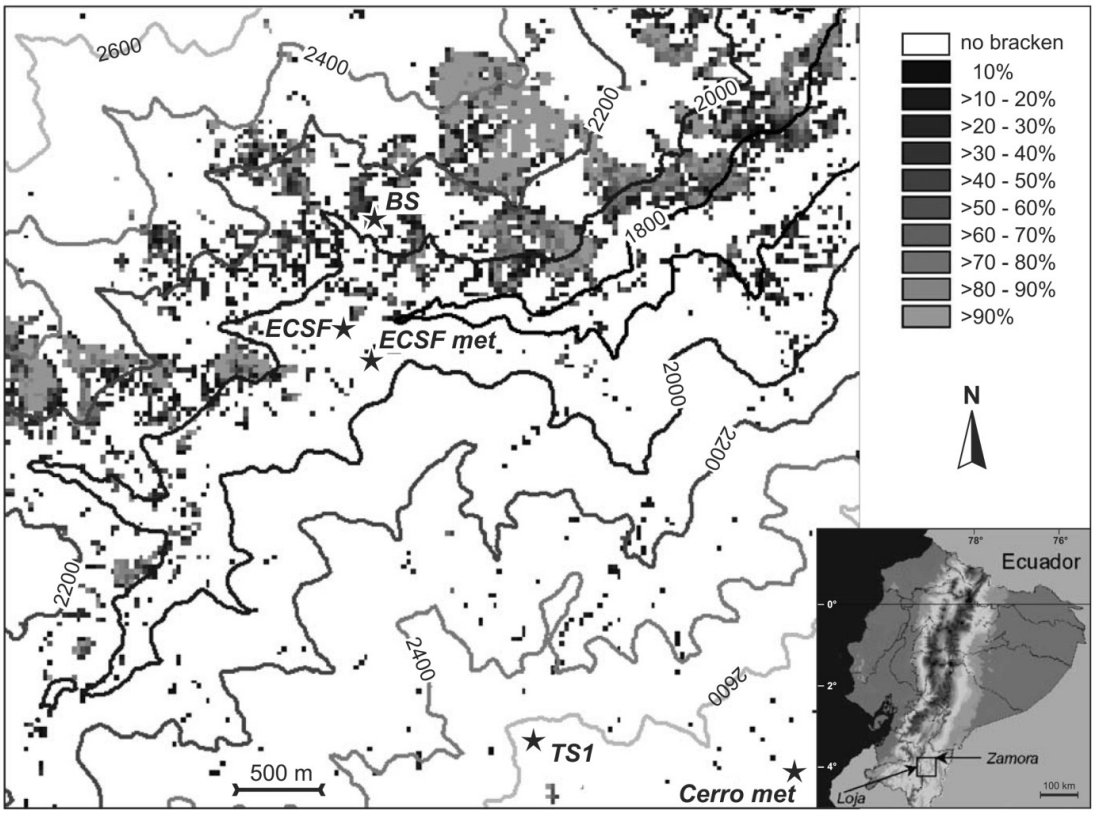

Figure 2-1. The research area showing fractional cover by southern bracken as derived from Landsat TM data with the probability guided spectral unmixing technique (Göttlicher et al. 2009); BS experimental bracken site and micrometeorological station, ECSF Estación Científica San Francisco, ECSF met Meteorological station of the Estación, TS1 and Cerro met are meteorological stations located at 2,660 and 3,180 m asl, respectively. Grey shades indicate different bracken coverage per pixel, white means bracken-free pixel.

Consequently, bracken should be effectively controlled to retain pasture productivity, but to date, the reason for its competitive strength is not well understood. Some investigations suggest that spreading and growth of bracken seems to be stimulated by burning (e.g., Page 1986; Cruz et al. 2009). Other studies on bracken in England and Mexico (Marrs et al. 2000a, b; Schneider 2004) point out that bracken fronds cast shadow on underlying plants, thus outcompeting understorey vegetation like grass tufts. Field observations in the study area show that bracken accelerates growth after burning which suggests that the shading of the pasture grass by the fast emerging fronds seems to boost the dominance of bracken after recurrent burning (Hartig and Beck 2003). However, final evidence is still lacking. Numerical simulation models encompassing radiative transfer approaches

(e.g., Pronk et al. 2007) might help to unveil the importance of frond shadow for the competitive strength of bracken in the study area. For spatial applications, grid-cell based two-big-leaf models have been proven to be computationally efficient (Wang and Leuning 1998) with good accuracy compared to more complex multilayer models (Zhang et al. 2001). The first research question in order to estimate the competitive strength of species with regard to radiation available for plant growth is if the two competing species reveal different PAR (photosynthetically active radiation) absorption potentials. Consequently, the main objective of the current paper is to compare the PAR absorption potential of the two competing plant species, *Setaria sphacelata* and *Pteridium arachnoideum*, as the basis for future research on growth competition modeling using a numerical vegetation growth model. The comparison is conducted by applying the radiation scheme of a state of the art grid-based two-bigleaf model (Dai et al. 2004; Thornton and Zimmermann 2007). Because the model is normally operated with default parameters for broad groups of plant functional types (broadleaf trees, grass, etc.), a proper parameterization with structural and optical plant traits is required to adapt the scheme to the competing species (e.g., Larocque 2002; Wang et al. 2006b; Boulain et al. 2007). With regard to structural plant traits, Lappi and Stenberg (1998), for instance, stressed that simulation of PAR interception/ absorption is highly dependent on the relation of leaf orientation and solar geometry.

Thus, the second goal of the current study is to adapt the radiation scheme to the two species of interest by providing the required structural and optical plant traits based on extensive field surveys. The properly parameterized scheme is then used to simulate the PAR absorption capabilities of both species under the varying and realistic illumination conditions of the study area in the Andes of southern Ecuador.

2.2 Materials and methods

2.2.1 Study area and data

The current investigation is part of a multidisciplinary ecological research project. The study area comprises parts of the deeply incised valley of the Rio San Francisco in the eastern range of the South Ecuadorian Andes in the vicinity of the research station Estación Científica San Francisco (ECSF, 3°58′18″S, 79°4′45″W, alt. 1,860 m asl; Figure 2-1). The station is situated between the provincial capitals of Loja in the inner-Andean basin west of the main cordillera and Zamora in the foothills of the eastern Andes. The core

area displayed in Figure 2-1 encompasses an altitudinal gradient from 1,800 to 3,200 m asl. A detailed description is given in Bendix et al. (2006a) and Beck et al. (2008b). The climate of the Rio San Francisco valley is perhumid (Richter 2003; Bendix et al. 2008a, b). Important for the radiation conditions is the high cloud frequency over the entire year, especially at higher altitudes (Bendix et al. 2006b, 2008c). While the north-facing slopes of the valley are covered by a species-rich natural mountain forest (Brehm et al. 2008), the south-facing slopes have been cleared by slash and burn for the acquisition of pasture land where large portions of the lower terrain between 1,800 and 2,500 m are already infested or completely overgrown by bracken (Figure 2-1).

Long-term meteorological data for the current study were available from the ECSF meteorological station located at 1,960 m asl (ECSF met in Figure 2-1), the altitudinal level of the bracken-infested pastures. At this station, global radiation has been measured since 1998. Monthly means of global radiation from 1998–2005 as presented in Bendix et al. (2008a) were used in this study. Additionally, an experimental site (BS in Figure 2-1) consisting of ten 10×10 m plots with different fractions of bracken and *Setaria* was established in 2007 in the vicinity of the main meteorological station (ECSF met). The site encompasses a micrometeorological station that measures global radiation at 5-min temporal resolution. Global radiation at both stations was measured with the Kipp & Zonen CM3 pyranometer for the entire solar spectrum (spectral range 305–2,800 nm).

2.2.2 Radiation scheme

To calculate PAR absorption by bracken and *Setaria*, the radiation scheme of the two-big-leaf approach of Dai et al. (2004) was applied. Generally, big-leaf approaches describe the water and gas exchange of vegetation in a simple way where the canopy is treated as one layer with a single physiological and aerodynamic resistance to water /CO_2 transfer. A big-leaf model generally encompasses (1) a radiation scheme as discussed in this study, (2) a leaf model accounting for the interaction of conductance and photosynthesis and the response of stomata to water vapour pressure deficit and available soil water, and (3) a parameterization of radiative conductance to solute the leaf energy balance equation (Wang and Leuning 1998). The two-big-leaf extension separates the whole canopy leaf area into sunlit and shaded leaf portions and the canopy-average PAR values are estimated for each leaf portion, which needs the application of radiative transfer calculations between the sunlit and shaded leaf fraction and the underlying soil (Zhang et al. 2001). Species are represented in a two-big-leaf model as a single plant with one sunlit and one shaded leaf. Average traits (e.g., leaf albedo) that are

representative for the species are assigned to the model plant. It is presupposed that the sunlit leaf receives both diffuse and direct radiation while the shaded leaf receives diffuse light only.

The photon transport among the atmosphere, the sunlit and shaded leaf area, and the ground is calculated by using the two-stream approximation with single scattering and uniform leaf orientation as presented in Dickinson (1983) and Sellers (1985). This module is the central part of the radiation scheme of Dai et al. (2004) which was used in the current study. With regard to canopy albedo, Myneni et al. (1992) showed that the accuracy of similar 1D radiative transfer schemes is adequate in comparison to more complex and computational expensive 3D approaches. Also, the prediction of PAR provided reasonable values when compared with a more complex multi-layer model (Zhang et al. 2001).

The numerical solutions and all relevant equations of the radiation scheme used in this study are already published in Dai et al. (2004) and will not be repeated here in detail. In the current study, the scheme is initialized by global radiation data at hand so that the decomposition for the direct, diffuse and PAR fraction is necessary.

On the plant level, the study focused on an average individual of bracken and the pasture grass Setaria. PAR absorption of the two species is strongly dependent on their functional traits that have to be derived from field observations to parameterize the radiation scheme properly. The first plant trait (or model parameter) of importance is the average leaf angle because it determines the leaf orientation to the sun and thus radiation absorption. In the radiation scheme, the average leaf projection $G(\mu)$ is used which is derived from (Dai et al. 2004):

$$G(\mu) = \phi_1 + \phi_2 \cdot \mu \,;\; \phi_1 = (0.5 - 0.633 \cdot \chi - 0.33 \cdot \chi^2) \;;\; \phi_2 = 0.877 \cdot (1 - 2 \cdot \phi_1) \quad (1)$$

where μ is the cosine of the solar zenith angle, ϕ_1 and ϕ_2 are coefficients from the Ross-Goudriaan function (see Sellers 1985) and χ represents the leaf angle distribution (1= horizontal, −1=vertical, 0=spherical leaf angle distribution) that have to be measured for representative individuals of bracken and *Setaria* in the experimental plots. It is obvious that the leaf orientation in relation to the solar angle determines drop shadow on shaded leaves and thus, the sunlit and shaded fractions of leaf area (see Dai et al. 2004).

The second important trait is the spectral leaf albedo because it determines the proportion of solar radiation remaining available for absorption and transmission. For instance, the direct incident beam radiation

absorbed by leaves at canopy depth (x) per unit leaf area index LAI (excluding scattering) is calculated in the scheme as (Dai et al. 2004):

$$I_{lb} = (1-\omega)\cdot kb\cdot \exp(-kb\cdot xLAI)\cdot I_{b0} \quad (2)$$

where I_{b0} is the incident direct beam radiation above the canopy, k_b the direct beam extinction (see Dai et al. 2004) and the leaf scattering coefficient ω is:

$$\omega = \alpha + \tau \quad (3)$$

with α is the spectral leaf albedo (second parameter) and τ the spectral leaf transmittance as the third important functional trait, determining the transmission of radiation to the shaded leaf area fraction and the underlying bare soil. Consequently, both optical parameters have to be derived from field measurements of representative individuals of bracken and *Setaria*. Equation (2) also uses the leaf area index that is available for PAR absorption. Thus, also the average leaf area index is a model parameter that has to be derived from field observations.

On the soil level, soil spectral albedo has to be measured because it determines the backscattered direct and diffuse radiation fractions in direction of the green phytoelements which are generally available for PAR absorption, increasing with soil albedo (Nouvellon et al. 2000).

2.2.3 Decomposition of global radiation data

The two-big-leaf scheme requires the diffuse and direct fractions of solar radiation as input. Because only global radiation was measured at the meteorological stations, we used an empirical decomposition function to partition incident solar radiation in its diffuse and direct fractions. Generally, such functions are based on the diffuse fraction of radiation (k') and the clearness index (kt). The clearness index (kt) is the ratio of incoming radiation at the earth surface (I_0) to the radiation at the top of the atmosphere on a horizontal surface (I_{TOA}).

$$kt = I_0 / I_{TOA} \quad (4)$$

Diffuse I_{d0} and direct I_{b0} radiation incident above the canopy is then derived by:

$$I_{d0} = I_0 \cdot k \quad (5)$$

$$I_{b0} = I_0 \cdot (1 - k) \tag{6}$$

where I_0 is the incident global radiation above the canopy. Empirical radiation decomposition functions are generally more or less site dependent. To find the most appropriate function for the San Francisco valley, six published functions are examined. Erbs et al. (1982) used data sets from U.S. locations to formulate a piecewise regression function that has been widely and successfully used in other parts of the world (Elminir 2007). A modified version of Erbs function was recently proposed by Wang et al. (2006a). Two versions of a function of Boland et al. (2001, 2008) for Australia yields lower fractions of diffuse radiation at a high clearness index, which could principally apply to situations in high elevations in the absence of clouds. A function taking annual seasonality into account was determined for southeast Brazil by Oliveira et al. (2002). Maduekwe and Chendo (1994) presented a numerical solution with solar elevation as a second predictor for the diffuse fraction. Figure 2-2a shows the long-term averaged (1998–2005) daily course of diffuse radiation calculated from the long-term incident global radiation at the ECSF meteorological station. The diffuse fraction as a function of the clearness index is also displayed (Figure 2-2b). The data show that the fraction of diffuse radiation in the study area is generally high. In the early morning and late afternoon hours, almost the only radiation present is diffuse, while around noon, direct irradiance accounts for approximately one third. The dominance of diffuse radiation is mainly due to the overall high cloudiness of ~80% over the day and the year in the San Francisco valley (Bendix et al. 2006b, 2008c).

The function of Boland et al. (2001) (BSL), with the solar apparent time as predictor (BSLa at 0800 and BSLb at 1700 hours in Figure 2-2b), results in relatively strong deviations in the afternoon. Oliveira's function (OESM), which summarizes the winter (OESMa) and summer (OESMb) regressions, gives the lowest diffuse radiation fraction. The other four decomposition functions which comprise Boland et al. (2008) (BRB) and Erbs et al. (1982) (EKD) give more or less identical daily courses. The difference between the mean of these functions and Oliveira's solution varies between −1 and +22% of the global radiation. For the current study, we used the modified Erbs' function (EKD2) because it considers the increase of diffuse radiation on lower solar elevation (see Figure 2-2b where EKD2 is calculated for a solar elevation of 15°). The diffuse fraction k' is calculated in a two-step procedure as follows:

$$k' = \begin{cases} 1 - 0.09 \cdot kt & 0 \le kt \le 0.22 \\ 0.9511 - 0.1604 \cdot kt + 4.388 \cdot kt^2 - 16.638 \cdot kt^3 + 12.336 \cdot kt^4 & 0.22 < kt \le 0.8 \\ 0.165 & 0.8 \le kt \le 1 \end{cases} \quad (7)$$

$$k = \frac{k'}{(1 - k').\mu + k'} \quad (8)$$

where k' is the diffuse fraction of radiation modified due to solar geometry with the cosine of solar zenith angle μ.

To obtain the PAR fraction from global radiation, a conversion factor of 0.48 is generally multiplied by I_0, but Zhang et al. (2000) and Lee and Hernández-Andrés (2005) showed that the PAR fraction varies particularly in the presence of clouds. A slight increase of the PAR fraction from clear to cloudy sky due to larger forward scattering was observed by Papaioannou et al. (1993) and Roderick et al. (2001). Tsubo and Walker (2005) considered clouds by applying the clearness index as predictor for the PAR fraction. Consequently, this function addresses best the high cloud frequency in the San Francisco valley and is therefore used in the current study:

$$I_{PAR} = (0.121 \cdot kt^2 - 0.334 \cdot kt + 0.613) \cdot I_0 \quad (9)$$

2.2.4 Field observations of plant and soil parameters

The two required structural plant parameters, the leaf area index and the leaf to ground angles, were measured with a LICOR LAI-2000 plant canopy analyzer. Leaf area index and leaf angles were taken for representative *Setaria* and bracken individuals. A total of 24 measurements for each species were conducted between October 2007 and March 2008 on the experimental site (BS in Figure 2-1). Canopy leaf angle was determined as mean tilt angle (MTA) (see Peri et al. 2003) that, however, is in good agreement with directly derived mean leaf angles (Antunes et al. 2001). Mean tilt angle orientation of measured foliage is converted to the leaf angle parameter χ (Eq. 1) by:

$$\chi = \cos(MTA) - \sin(MTA) \quad (10)$$

The two optical plant traits (leaf albedo and transmission) and soil albedo were measured with the field spectrometer Tec5 HandySpec Field 14 during late 2007 and early 2008. The instrument encompasses a Zeiss MMS 1 NIR enhanced (310–1,100 nm, dλ=3.3 nm) and a Zeiss Plangitter PGS NIR 1.7 (960–1,690 nm, dλ=1.5 nm) sensor. For reflection measurements, fresh leaves

of representative individuals were collected and inserted in a wooden frame to normalize the measurements to a leaf area index of 1. Average values were calculated from three measurements of each species. Topsoil samples were taken from the experimental bracken site, representing the soil under bracken and grass. Spectral integration of the data was conducted for PAR (<700 nm) and NIR (≥700 nm).

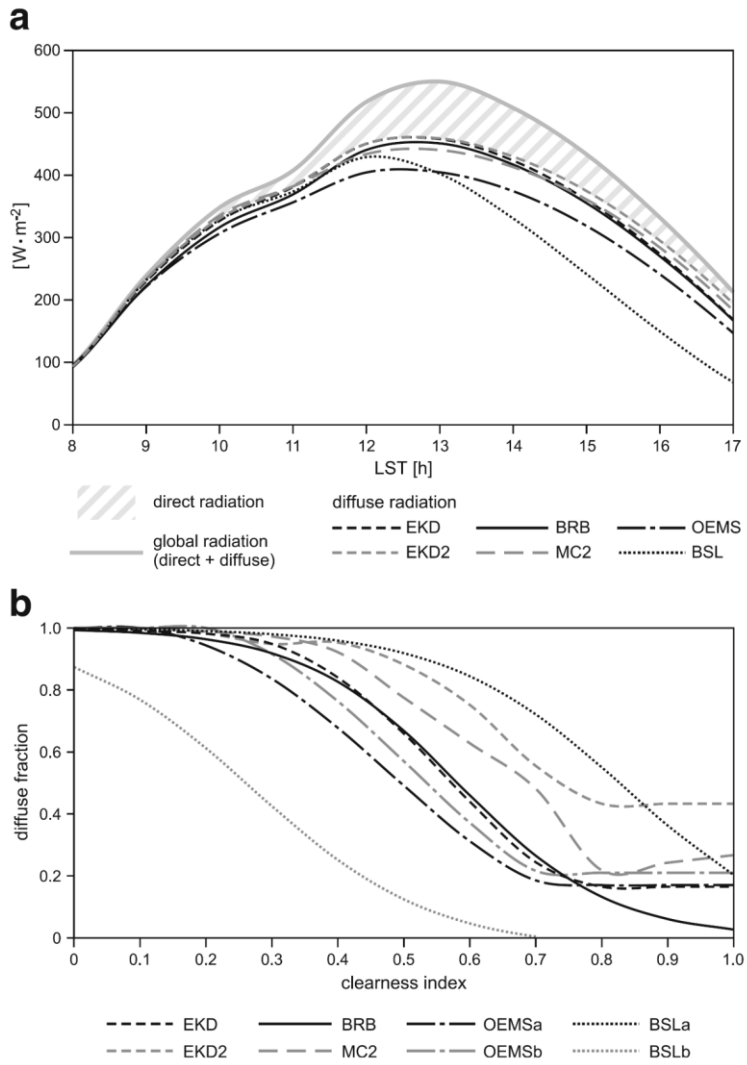

Figure 2-2. (a) Average diurnal course of global and derived diffuse radiation at ECSF met station (1998–2005). (b) The diffuse fraction from six decomposition functions is also shown as a function of the clearness index (bottom). For abbreviations, see text.

2.3 Results

2.3.1 Derived plant and soil traits

The observed values of LAI and χ for representative individuals of *Setaria* and bracken are presented in Table 2-1. They show that LAI and χ (indicated by the mean tilt angle) differ between the samples and thus, the observation situation. However, the principle of the two-big-leaf approach only permits one average individual per species. Thus, the plants selected in the field survey which are presented in Table 2-1 are chosen to properly represent an average individual. The calculated average structural plant traits are then assigned to the average *Setaria* and bracken individual used by the radiation scheme which is applied in the next subsection. The same holds for the optical traits presented in Table 2-2.

Table 2-1. Leaf area index (LAI) and mean tilt angle (MTA) of 24 representative measurements of *Setaria sphacelata* and bracken (*Pteridium arachnoideum*) on the experimental site

	Setaria		Bracken	
Sample	LAI (m^2 m^{-2})	MTA (deg.)	LAI (m^2 m^{-2})	MTA (deg.)
1	1.31	58	1.38	8
2	1.79	73	1.51	40
3	1.32	62	1.65	49
4	1.75	60	1.41	0
5	1.38	61	1.88	8
6	1.76	54	1.40	31
7	1.99	57	2.17	28
8	3.84	45	2.24	46
9	2.42	59	2.87	0
10	3.20	59	3.21	36
11	2.76	42	2.85	0
12	3.95	45	4.76	40
13	1.54	76	3.53	40
14	1.50	76	4.08	42
15	2.42	63	2.23	40
16	3.00	65	2.60	0
17	2.71	59	5.27	41
18	2.04	62	3.97	40
19	1.52	75	2.65	13
20	1.72	63	3.27	37
21	4.34	51	4.88	0
22	3.41	57	3.95	36
23	2.76	60	3.24	0

24	3.11	53	3.50	0
Average	2.40	59.79	2.94	23.96
1 σ	0.90	9.14	1.15	18.87
Average χ		-0.37		0.48

Table 2-2. Integrated optical traits (PAR) of *Setaria sphacelata*, bracken (*Pteridium arachnoideum*) and bare soil. (Source: field observations with Handy- Spec)

	Setaria	Bracken	Bare soil
Reflectance (%) PAR (400 – 700 nm)	11.7	7.4	10.7
Transmittance (%) PAR (400 – 700 nm)	1.5	3.7	-
Absorptance (%) PAR (400 – 700 nm)	86.8	88.9	89.3

With regard to the field data of structural plant traits presented in Table 2-1, the average leaf are index of bracken (2.94) is higher than that of *Setaria* (2.4). The standard deviation reveals that the LAI of bracken is characterized by a slightly higher variation in comparison to *Setaria*. Additionally, Table 2-1 points to a clear difference in leaf angle orientation towards more vertical leaves for the *Setaria* tufts and more horizontally oriented leaf blades for bracken where the span of leaf angles is generally higher for bracken than for *Setaria*. The grass reveals a mean leaf angle of ~59° and an average leaf angle distribution parameter of $\chi = -0.37$ which clearly confirms the more vertical orientation of the grass stalks. MTA values and the low standard deviation show that the angular distribution of *Setaria* culms is almost unimodal. With regard to bracken, MTA seems to points to a bimodal distribution. Bracken fronds are composed of a long vertical petiole and a nearly triangular tripinnate lamina. Emerging fronds, whose laminas are still unfolded, have not been included in the study. Unfolding of the leaf blade starts when it turns from a vertical position into an angle between 40 and 50°. During further unfolding of the lamina, the leaf blade approaches a more horizontal orientation (MTA of 0 – 8°). Because an average fern canopy consists of young and mature leaves, the average individual of the two-big-leaf approach must consider both representations which is warranted by the mean leaf angle parameter of χ=0.48.

The albedo data gathered during our field surveys show that both plant species exhibit a marked red edge spectrum of green vegetation with a slightly enhanced reflectance in the green waveband (Figure 2-3).

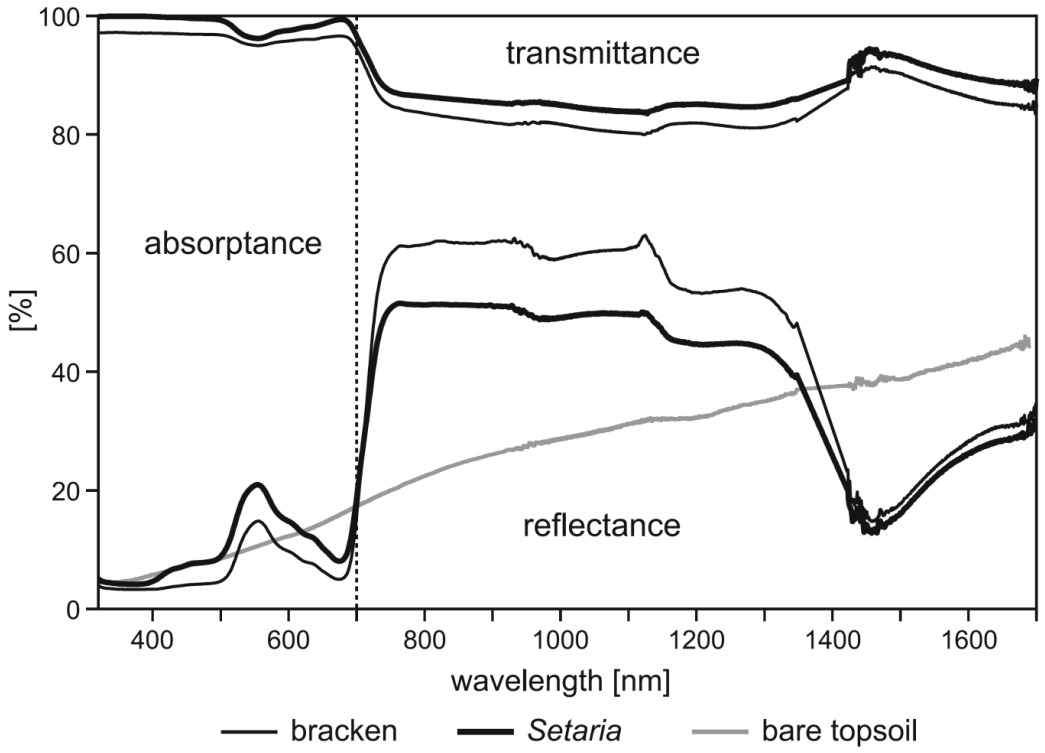

Figure 2-3. Partitioning into reflectance (albedo), transmittance and absorptance of spectral radiation incident on *Setaria sphacelata*, *Pteridium arachnoideum* (as an average of three representative samples, LAI=1) and bare soil. The traced line represents the division between visible (PAR) and near infra red (>700 nm).

In contrast, the topsoil reveals the typical, almost linear increase of reflectance towards the near infrared. Bracken contrasts with *Setaria* by a lower reflectance in the PAR and a higher reflectance in the NIR. Transmittance of bracken fronds is slightly higher than that of *Setaria* over the whole spectrum. The integrated optical traits for the PAR spectral range (300–700 nm) as derived from the measurements of the field spectrometer for both species (*Setaria* and bracken) are presented in Table 2-2. Average integrated PAR reflectance of *Setaria* (11.7%) is higher than bracken PAR albedo (7.4%). At the same time, integrated PAR transmittance of *Setaria* (1.5%) is lower in comparison to bracken (3.7%), resulting in a slightly higher absorptance of 2.1% for bracken which might potentially favor bracken with regard to photosynthesis.

2.3.2 Simulated PAR absorption capability

The first quantity that determines the PAR absorption capacity is the species-specific leaf–sun geometry which is mainly influenced by the average leaf angle parameter from

Table 2-1. Figure 2-4 demonstrates the changing illumination situation for the average individuals of *Setaria* and bracken depending on solar elevation in relation to leaf orientation. The sunlit and shaded leaf fractions of bracken with its more horizontally oriented fronds run inversely to *Setaria* with its more upright leaves. At higher solar elevations (>28°) around noon (i.e., at solar zenith lower than 62°) bracken shows a smaller sunlit leaf fraction in comparison to *Setaria* because the sunlit bracken frond casts shadow on the underlying frond area due to the horizontal frond orientation. In contrast, shadowing around noon is clearly reduced in case of the vertically oriented leaves of *Setaria*. The situation changes in times of lower sun elevation (morning, evening) when cast shadow is preferentially caused by vertically oriented leaves. Then, bracken is favored in receiving direct radiation.

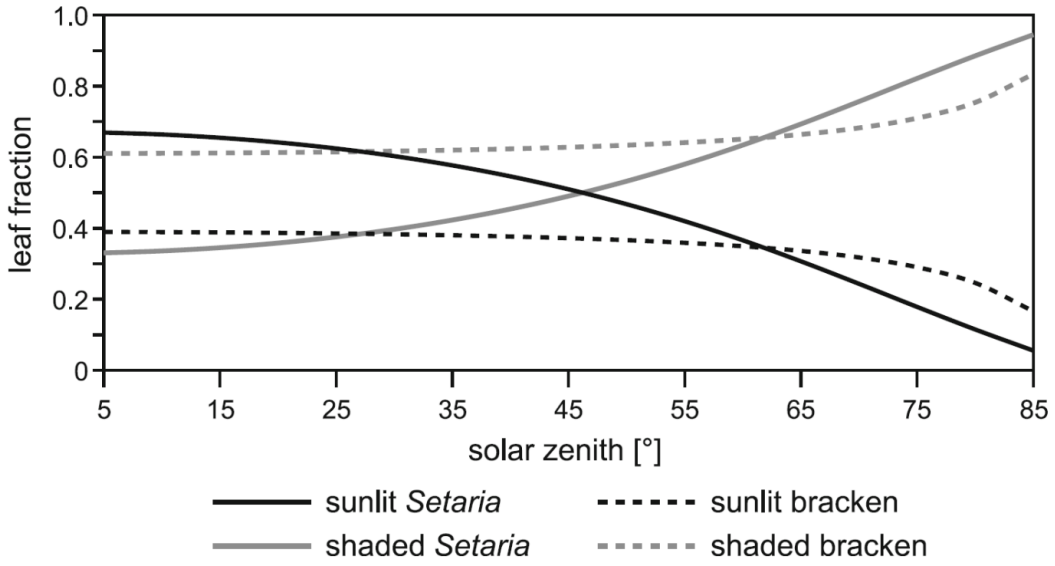

Figure 2-4. Sunlit and shaded leaf fractions of bracken and *Setaria* for solar elevations between 5 and 85° (solar elevation=90°-solar zenith).

However, the sunlit and shaded leaf fraction must be scaled by the species-specific leaf area index (Table 2-1) of the average individuals to complete the view on leaf–sun geometry effects on PAR absorption potential. By doing so, *Setaria* sunlit leaf area exceeds that of bracken at solar zenith angles <55° (Figure 2-5). The shift of the inversion point of the sunlit leaf

fraction (see Figure 2-4: 62° solar zenith angle) is an effect of the slightly greater LAI of the average bracken individual. This also explains the fact that the shaded leaf area of bracken exceeds the shaded leaf area of *Setaria* at all solar elevations.

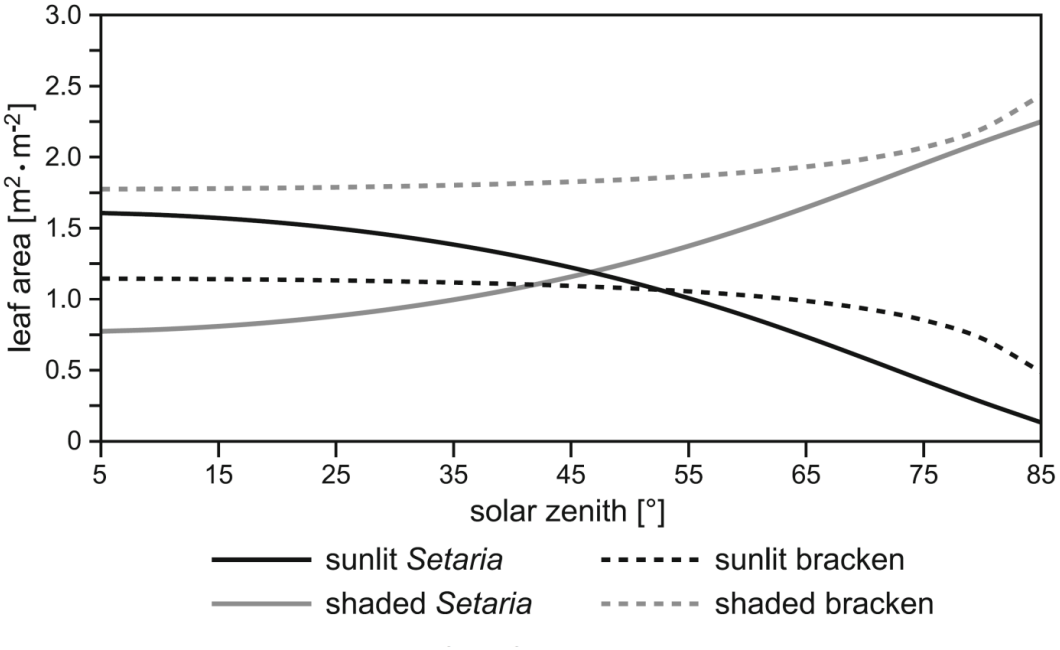

Figure 2-5. Leaf area index ($m^2 \cdot m^{-2}$) of sunlit and shaded leaves of bracken and *Setaria* as depending on the solar zenith angle (solar elevation=90°-solar zenith).

Summarizing Figure 2-4 and Figure 2-5 could suggest that *Setaria* receives more direct radiation around noon in comparison to bracken. However, the amount of PAR absorption is not only a function of sunlit and shaded leaf area but is strongly dependent on (1) the resulting angle of incidence on the leaves for direct beam radiation, (2) the relation of direct/ diffuse irradiance at the top of the canopy, and (3) the optical leaf traits. With regard to (1), a more perpendicular angle of incidence would be reached at low sun elevations for *Setaria* with its vertically oriented leaves when the sunlit leaf area is clearly reduced. In contrast, bracken shows the highest sunlit leaf area around noon when the solar rays are shining nearly perpendicular onto the horizontally oriented canopy fronds.

To address all governing factors (1–3) under realistic environmental conditions of the Rio San Francisco valley, a simulation was conducted which was initialized with the longterm averaged diurnal course of global irradiance (1998 – 2005) at the ECSF meteorological station (Figure 2-1). The decomposition of global radiation was conducted by applying Eqs. 4–9. The

results depicted in Figure 2-6b clearly reveal that PAR absorption of bracken (4.2 MJ m^{-2} day^{-1}) is fairly equal to PAR absorption of *Setaria* (4.5 MJ m^{-2} day^{-1}. Integrated over the day, the difference (ΔPAR) amounts to just 0.3 MJ m^{-2} day^{-1}. At first glance, this result is unexpected because considerable differences in sunlit and shaded leaf area of the two species exist (Figure 2-6a).

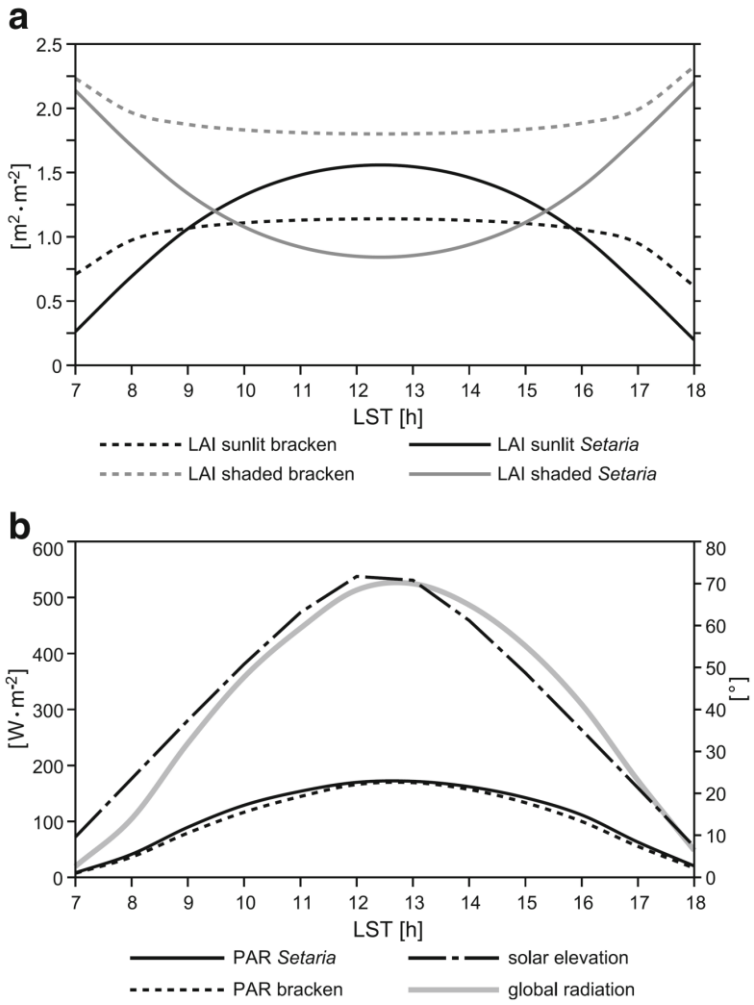

Figure 2-6. (a) Leaf area indices ($m^2 \cdot m^{-2}$) of sunlit and shaded portions of the leaves of bracken and *Setaria* in the course of a day with regard to the average leaf–sun geometry of the study area. (b) Annual average of the diurnal course of irradiance at the ECSF meteorological station (1998–2005; Bendix et al. 2008a), sum of absorbed direct and diffuse PAR by sunlit and shaded leaves of bracken and *Setaria* plotted on the left ordinate axis and typical solar elevation in degrees on the right ordinate axis.

This effect is most likely the result of the predominantly diffuse solar radiation available in the San Francisco valley due to the high cloudiness. The

reason is that the available direct radiation at an inclined surface (leaf), following Lambert's law, depends on the incident angle of the light beam as a combination of leaf angle and position of the sun, but this angular dependence is not applicable to isotropically distributed diffuse radiation. Consequently, the species-specific differences in sunlit and shaded leaf area are not as crucial as they should be under clear sky conditions. As a result, bracken can compensate for the lower fraction of sunlit frond area by its slightly higher absorption coefficient and the total LAI exceeding that of *Setaria* (Table 2-1 and Table 2-2). Thus, the total radiation surplus of *Setaria* yields not more than 0.3 MJ m^{-2} day^{-1} (4.2 MJ m^{-2} day^{-1} bracken, 4.5 MJ m^{-2} day^{-1} *Setaria*) in comparison to bracken over an average day in the Rio San Francisco valley.

To unravel the role of diffuse radiation on the PAR absorption potential, simulations were conducted for a typical sunny (5 December 2007) and cloudy (5 January 2008) day (Figure 2-7).

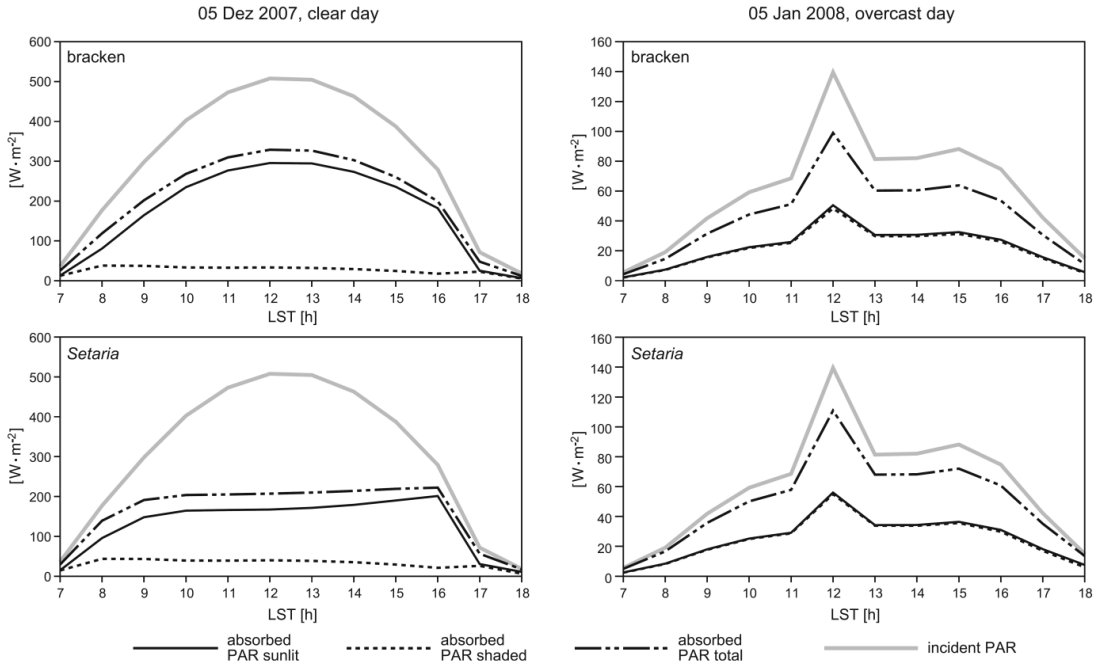

Figure 2-7. PAR absorption of southern bracken and *Setaria* for (left) a sunny day (5 December 2007) and (right) a typical overcast day (5 January 2008). Radiation data for model initialization are taken from the micrometeorological station at the bracken experimental site.

The cloudy day with dominating diffuse irradiance reveals that *Setaria* has a slightly higher PAR absorption over the day (2.1 MJ m^{-2} day^{-1}) that exceeds that of bracken by 9.5% (or 0.2 MJ m^{-2} day^{-1}) (Figure 2-7, right). However, it is striking that this potential growth advantage of *Setaria* is

abolished during a sunny day with a great portion of direct solar irradiance around noon (Figure 2-7, left). On such a day, bracken absorbs 8.5 MJ m^{-2} day^{-1}, which is 16.4% (or 1.2 MJ m^{-2} day^{-1}) more than total PAR absorption by *Setaria*. The reason of this inversion is illustrated in Figure 2-8.

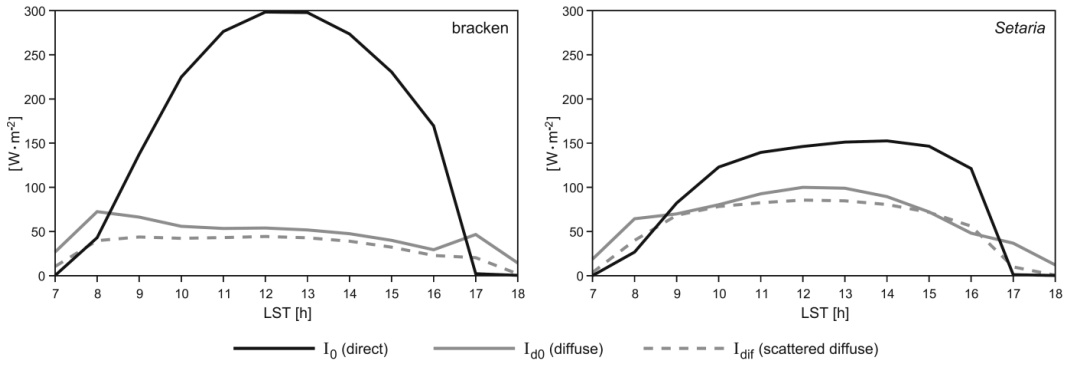

Figure 2-8. Different PAR components absorbed by the sunlit canopy of bracken (left) and *Setaria* (right) on the sunny day, 5 December 2007, based on the radiative transfer scheme.

On sunny days, the major gain of PAR absorption by bracken as compared to *Setaria* is achieved by the absorption of incident direct beam radiation (I_0 direct) only. Here, the geometric configuration mentioned earlier takes effect. Fairly perpendicular incidence of the direct solar beam around noon (sun elevations 60–80°) onto nearly horizontally oriented bracken fronds provides the markedly higher direct radiation gain as compared to the nearly vertically oriented *Setaria* leaves. Even if PAR absorption of diffuse solar radiation (I_{d0}) and scattered diffuse radiation (I_{dif}) is higher for *Setaria* on the sunny day, this cannot compensate for the higher gain of direct beam PAR absorption by bracken fronds.

To test the PAR absorptance for different sunny and cloudy weather situations potentially occurring in the San Francisco valley, the ideal relative diurnal course of irradiance as measured on 5 December 2007 was taken and applied to incrementally increased daily radiation maxima ranging from 100 to 1,000 W m^{-2} (with an increment of 100 W m^{-2}). Ten simulations were conducted with the radiation scheme based on the synthetically generated irradiation data. The decomposition of the generated diurnal data of global radiation by using Eqs. 4–9 leads to an increase of the direct radiation fraction with increasing radiation maximum. Consequently, a maximum of 100 W m^{-2} is mainly characterized by diffuse irradiance, a maximum of 1,000 W m^{-2} by a greater portion of direct solar irradiance. Figure 2-9 shows clear species-specific distinction of PAR absorption capabilities due to varying radiation composition. Above a daily radiation maximum of about 615 W m^{-2} where

direct radiation dominates, bracken absorbs clearly more direct PAR, as illustrated in Figure 2-8 (direct PAR I_0). The surplus of bracken PAR absorption is continuously increasing with increasing daily radiation maximum. Below the inversion point, *Setaria* shows a slight but nearly constant advantage in PAR absorption in comparison to bracken. In a next step, the hourly radiation data at the ECSF meteorological station from 1998–2005 were evaluated to derive the frequency of daily radiation maxima in the valley. Figure 2-9 reveals that illumination situations favoring *Setaria* PAR absorption occur on 64% of all days, while a third of all days with more direct radiation support the higher PAR absorption potential of bracken.

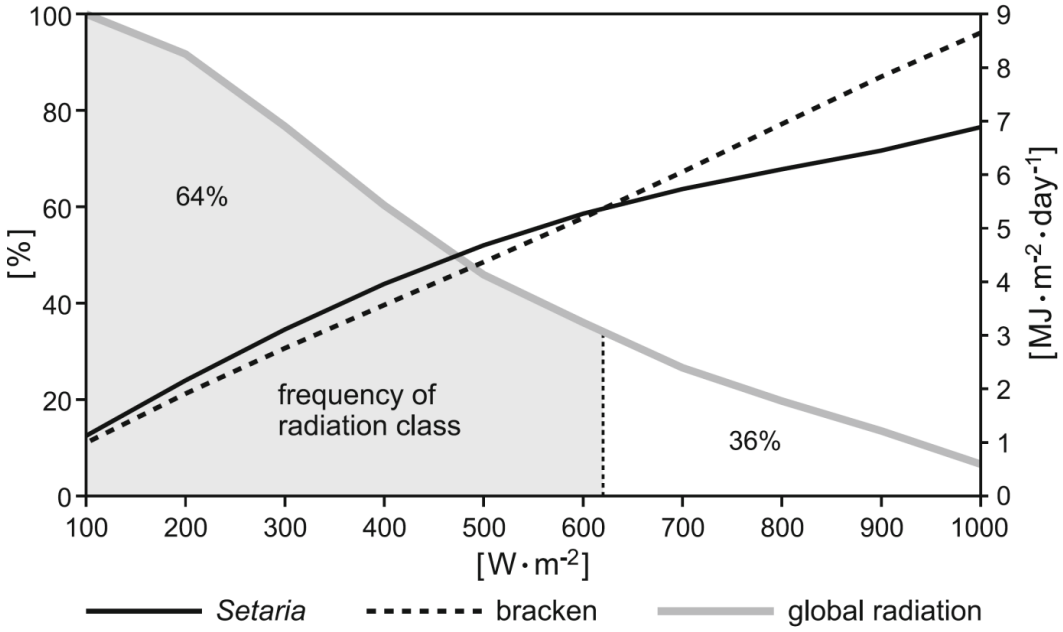

Figure 2-9. Frequency and intensity of the daily irradiance maximum between 1200 and 1300 hours for the ECSF meteorological station (1998–2005) and total daily PAR absorption by bracken and *Setaria*, respectively, based on the relative diurnal course of radiation from 5 December 2007.

By summing up the daily PAR absorption based on the synthetically generated data over all days of the year, while considering the frequency distribution of the radiation classes in Figure 2-9, yields no clear advantage of one of the both species. *Setaria* absorbs 1,533 MJ m^{-2} $year^{-1}$ PAR while bracken reaches almost the same annual PAR absorption capacity of 1,530 MJ m^{-2} $year^{-1}$.

2.4 Discussion

The current paper focuses on a comparison of the PAR radiation absorption capabilities of two competing species, the pasture grass *Setaria sphacelata* and an aggressive weed, the southern bracken (*Pteridium arachnoideum*), in the anthropogenic pasture system of a tropical mountain biodiversity hotspot in the eastern Andes of southern Ecuador. The work relies on a numerical two-big-leaf radiation scheme specifically parameterized with field surveys of plant functional traits, encompassing structural and optical parameters of both species. The samples selected during the field studies to derived plant functional traits were chosen to properly represent an average individual of both species under different growth situations (elevation, slope angle and aspect). The resulting structural and optical plant parameters are in good agreement with measured values for similar species or model defaults of comparable plant functional types (as, e.g., functional group of tropical C4 grasses). The average LAI of *Setaria*, for instance, coincides quite well with default values used for climate modeling of tropical C4 grasslands with land surface models (e.g., Buermann et al. 2001). The average LAI of southern bracken is lower than the maximum values for a fully developed canopy of northern bracken (P. aquilinum) in England (LAI ~4 in late July; Blackburn and Pitman 1999; Pitman 2000). Leaf angle values for *Setaria* were similar to those reported by other studies of grasslands (e.g., Miller-Goodman et al. 1999; Peri et al. 2003). The average leaf angle distribution parameter for *Setaria* (χ=−0.37) is in the same order of the default value (χ= −0.3) supplied by a comparable radiation scheme for C4 grassland (Oleson et al. 2004).

With regard to the optical traits, reflection measurements of bracken canopies in England (400–1,100 nm; Blackburn and Pitman 1999; *Pteridium aquilinum*) confirm the shape of the reflection curve, however with a slightly lower reflectance over the whole spectrum compared to the southern bracken. At the same time, transmittance in the visible and near infrared spectrum of bracken fronds in England (Pitman 2000) is somewhat higher in comparison to the southern bracken. Average measured PAR reflectance of *Setaria* is in almost perfect agreement with default values for C4 grasslands (11%) provided by different studies (e.g., Fisch et al. 1995) and the CLM SVAT model that uses a similar radiation scheme as described in this study (Oleson et al. 2004). Even if the overall good coincidence indicates that the gathered field samples represent an average individual under average growth conditions in the study area, it should be stressed that plant parameters used in numerical models might even change with spatial resolution. This complicates the comparison of measured plant traits and respective published model parameters. By applying the parameterized radiation scheme, it is

proven that the average individuals of bracken and *Setaria* have similar PAR absorption potentials under the typical radiation conditions of the Rio San Francisco valley. Comparable similarities were also found on the landscape level by other studies (e.g., Asner et al. 1998). The most important parameter for the determination of the fraction of absorbed PAR (f_{PAR}) in this study where the leaf area index of the *Setaria* and bracken average individuals is differing moderately (ΔLAI=0.54 m^2 m^{-2}) is the leaf–sun geometry (and thus, the leaf angle) in combination with the fractionation of the radiation components (direct, diffuse). Bracken has a higher PAR absorption potential under clear sky conditions because the leaf angle distribution favors PAR consumption during hours of high solar elevation. Similar directional effects are described for short grass ecosystem by Nouvellon et al. (2000). However, by scaling up to the landscape level, other authors stress that leaf area is the main decisive variable accounting for 60–80% of f_{PAR} variations while individually contributing canopy-level factors explain only a smaller proportion of f_{PAR} variations (Asner and Wessman 1997; Mwanamwenge et al. 1997; Asner et al. 1998).

With regard to the current state of the radiation scheme, the main uncertainty remains the decomposition of global radiation to its direct, diffuse, and PAR fractions. Comprehensive field observation of all radiation parameters is needed to derive a local decomposition function which can be implemented in the radiation scheme, replacing the currently used average decomposition functions (based on Eqs. 7–9). However, to derive local functions, several years (at least one) of diffuse radiation and PAR measurements are necessary. Most recently, respective sensors are installed and a preliminary comparison with 1 month of data and the results of the average functions used in this paper is conducted. With respect to diffuse radiation, 46% of values differ less than 10% of the calculated radiation where best results were reached for clear and completely overcast days. Generally, the average decomposition function (based on Eqs. 7–8) underestimates the observed values. With regard of PAR decomposition (based on Eq. 9), a slight overestimation by the function has been proven (+12% on average). In most situations, this counterbalances the underestimation of the composition function for diffuse radiation so that the final calculation for incoming PAR radiation provides reasonable data for the radiation scheme. Nevertheless, locally derived decomposition functions replacing Eqs. 7–9 will be implemented when sufficient data have been gathered.

The results of the simulations gained with the parameterized radiation scheme reveal that neither bracken nor *Setaria* exhibit a clear advantage in PAR absorption capability under the current climatic conditions of the study area. This means that, at first glance, PAR absorption seems not to be the

reason for bracken invasion. Another reason could be that the bracken plants have more biological growth power, e.g., due to the well-developed rhizome system which make them grow faster to get more PAR, water and nutrients. However, it must be stressed that radiation absorption is just the initial factor of plant growth. The transfer of absorbed PAR to biomass depends on the radiation use efficiency (RUE) that can exhibit great species-specific variations, particularly under water and nutrient stress (for bracken, refer, e.g., to Bray 1991 and Pakeman et al. 1994; for tropical C4 grass, to Kiniry et al. 1999 and Marques da Silva and Arrabaça 2004; for PAR absorption under fertilization, to Ostrowska et al. 2008). While water is not a limiting factor in the perhumid environment of the Rio San Francisco valley, nutrient deficiency (P, N) occurs (Makeschin et al. 2008). These effects will be tested in future research by using a photosynthesis module driven by the radiation scheme presented in this paper.

Acknowledgements

The authors gratefully acknowledge funding of the work by the German Research Foundation (DFG) in the scope of the DFG-Research Unit RU816 'Biodiversity and Sustainable Management of a Megadiverse Mountain Ecosystem in South Ecuador', subprojects C3.1, B3.1 and Z1.1. We further would like to thank Prof. Dr. Michael Richter (University of Erlangen-Nürnberg) for providing the data of the ECSF meteorological station that he collected in his subproject B1.4. B. Silva gratefully appreciates granting by the Brazilian Council of Technological and Scientific Development (CNPq). The authors thank three anonymous reviewers for their valuable comments, which helped to improve the paper.

Bibliography

Antunes MAH, Walter-Shea EA, Mesarch MA (2001) Test of an extended mathematical approach to calculate maize leaf area index and leaf angle distribution. Agr For Meteorol 108:45–53

Asner GP, Wessman CA (1997) Scaling PAR absorption from the leaf to landscape level in spatially heterogeneous ecosystems. Ecol Model 103:81–97

Asner GP, Wessman CA, Archer S (1998) Scale dependence of absorption of photosynthetically active radiation in terrestrial ecosystems. Ecol Appl 8:1003–1021

Barthlott W, Hostert A, Kier G, Koper W, Kreft H, Mutke J, Rafiqpoor MD, Sommer J (2007) Geographic patterns of vascular plant diversity at continental to global scales. Erdkunde 61:305–315

Beck E, Hartig K, Roos K (2008a) Forest clearing by slash and burn. In: Beck E, Bendix J, Kottke I, Makeschin F, Mosandl R (eds) Gradients in a tropical mountain ecosystem of Ecuador. Springer, Berlin, pp 371–374

Beck E, Makeschin F, Haubrich F, Richter M, Bendix J, Valerezo C (2008b) The ecosystem (Reserva Biologíca San Francisco). In: Beck E, Bendix J, Kottke I, Makeschin F, Mosandl R (eds) Gradients in a tropical mountain ecosystem of Ecuador. Springer, Berlin, pp 1–13

Bendix J, Homeier J, Cueva Ortiz E, Emck P, Breckle S-W, Richter M, Beck E (2006a) Seasonality of weather and tree phenology in a tropical evergreen mountain rain forest. Int J Biometeorol 50:370–384

Bendix J, Rollenbeck R, Göttlicher D, Cermak J (2006b) Cloud occurrence and cloud properties in Ecuador. Climate Res 30:133–147

Bendix J, Rollenbeck R, Fabian P, Emck P, Richter M, Beck E (2008a) Temporal heterogeneities - climate variability. In: Beck E, Bendix J, Kottke I, Makeschin F, Mosandl R (eds) Gradients in a tropical mountain ecosystem of Ecuador. Springer, Berlin, pp 281–290

Bendix J, Rollenbeck R, Göttlicher D, Nauß T, Fabian P (2008b) Seasonality and diurnal pattern of very low clouds in a deeply incised valley of the eastern tropical Andes (South Ecuador) as observed by a cost-effective WebCam system. Meteorol Appl 15:281–291

Bendix J, Rollenbeck R, Richter M, Fabian P, Emck P (2008c) Gradual changes along the altitudinal gradients - the climate. In: Beck E, Bendix J, Kottke I, Makeschin F, Mosandl R (eds) Gradients in a tropical mountain ecosystem of Ecuador. Springer, Berlin, pp 63–73

Blackburn GA, Pitman JI (1999) Biophysical controls on the directional spectral reflectance properties of bracken (*Pteridium aquilinum*) canopies: results of a field experiment. Int J Remote Sens 20:2265–2282

Boland J, Scott L, Luther M (2001) Modelling the diffuse fraction of global solar radiation on a horizontal surface. Environmetrics 12:103–116

Boland JW, Ridley B, Brown B (2008) Models of diffuse solar radiation. Renew Energy 33:575–584

Boulain N, Simoni G, Gignoux J (2007) Changing scale in ecological modelling: a bottom up approach with an individual based vegetation model. Ecol Model 203:257–269

Bray JR (1991) Growth, biomass, and productivity of a bracken (Pteridium esculentum) infested pasture in Marlborough Sounds, New Zealand. N Z J Bot 29:169–176

Brehm G, Homeier J, Fiedler K, Kottke I, Illig J, Nöske NM, Werne FA, Breckle SW (2008) Mountain rain forest in southern Ecuador as a hotspot of biodiversity - limited knowledge and diverging pattern. In: Beck E, Bendix J, Kottke I, Makeschin F, Mosandl R (eds) Gradients in a tropical mountain ecosystem of Ecuador. Springer, Berlin, pp 15–23

Buermann W, Dong J, Zeng X, Myneni RB, Dickinson RE (2001) Evaluation of the utility of satellite-based vegetation leaf area index data for climate simulations. J Climate 14:3536–3550

Cruz DR, Reyes ES, Sánchez JS (2009) Effects of meteorological factors on airborne bracken (*Pteridium aquilinum* (L.) Kuhn.) spores in Salamanca (middle-west Spain). Int J Biometeorol doi:10.1007/s00484-009-0208-5

Dai Y, Dickinson RE, Wang Y-P (2004) A two-big-leaf model for canopy temperature, photosynthesis, and stomatal conductance. J Climate 17:2281–2299

Dickinson RE (1983) Land surface processes and climate surface albedos and energy-balance. Adv Geophys 25:305–353

Elminir HK (2007) Experimental and theoretical investigation of diffuse solar radiation: data and models quality tested for Egyptian sites. Energy 32:73–82

Erbs DG, Klein SA, Duffie JA (1982) Estimation of the diffuseradiation fraction for hourly, daily and monthly-average global radiation. Sol Energy 28:293–302

FAO - Food and Agriculture Organisation (2001) Global forest resources assessment 2000 main report, FAO Forestry Paper 140. Rome, Italy

Fisch G, Wright IR, Bastable HG (1995) Albedo of a tropical grass: a case study of pre- and post-burning. Int J Climatol 14:103–107

Göttlicher D, Obregón A, Homeier J, Rollenbeck R, Nauß T, Bendix J (2009) Land cover classification in the Andes of southern Ecuador using Landsat ETM+data as a basis for SVAT modelling. Int J Remote Sens 30:1867–1886

Hartig K, Beck E (2003) The bracken fern (*Pteridium aquilinum*) dilemma in the Andes of South Ecuador. Ecotropica 9:3–13

Kiniry JR, Tischler CR, Van Esbroeck GA (1999) Radiation use efficiency and leaf CO_2 exchange for diverse C4 grasses. Biomass Bioenergy 17:95–112

Lappi J, Stenberg P (1998) Joint effect of angular distribution of radiation and spatial pattern of trees on radiation interception. Ecol Model 112:45–51

Larocque GR (2002) Coupling a detailed photosynthetic model with foliage distribution and light attenuation functions to compute daily gross photosynthesis in sugar maple (Acer saccharum Marsh.) stands. Ecol Model 148:213–232

Lee R, Hernández-Andrés J (2005) Colors of the daytime overcast sky. Appl Optics 44:5712–5722

Maduekwe AAL, Chendo MAC (1994) Atmospheric turbidity and the diffuse irradiance in Lagos, Nigeria, 1994. ICTP Internal report IC/IR/94/141, Trieste, Italy

Makeschin F, Haubrich F, Abiy M, Burneo JI, Klinger T (2008) Pasture management and natural soil generation. In: Beck E, Bendix J, Kottke I, Makeschin F, Mosandl R (eds) Gradients in a tropical mountain ecosystem of Ecuador. Springer, Berlin, pp 397–408

Marques da Silva J, Arrabaça MC (2004) Photosynthesis in the waterstressed C4 grass *Setaria sphacelata* is mainly limited by stomata with both rapidly and slowly imposed water deficits. Physiol Plant 121:409–420

Marrs RH, Le Duc MG, Mitchell RJ, Goddard D, Paterson S, Pakeman RJ (2000a) The ecology of bracken: Its role in succession and implications for control. Ann Bot (Suppl B) 85:3–15

Marrs RH, Johnson SW, Le Duc MG (2000b) Control of bracken and restoration of heathland. VI. The response of bracken fronds to 18 years of continued bracken control or 6 years of control followed by recovery. J App Ecol 35:479–490

Miller-Goodman MS, Moser LE, Waller SS, Brummer JE, Reece PE (1999) Canopy analysis as a technique to characterize defoliation intensity on Sandhills range. J Range Manage 52:357–362

Mwanamwenge J, Siddique KHM, Sedgley RH (1997) Canopy development and light absorption of grain legume species in a short season Mediterranean-type environment. J Agron Crop Sci 179:1–7

Myneni BB, Asrar G, Hall FG (1992) A three-dimensional radiative transfer method for optical remote sensing of vegetated land surfaces. Remote Sens Environ 41:105–121

Nouvellon Y, Begue A, Susan Moran SM, Seen DL, Rambal S, Luquet D, Chehbouni G, Inoue Y (2000) PAR extinction in shortgrass ecosystems: effects of clumping, sky conditions and soil albedo. Agric For Meteorol 105:21–41

Oleson KW, Dai Y, Bonan G, Bosilovich M, Dickinson R, Dirmeyer P, Hoffman F, Houser P, Levis S, Niu G-Y, Thornton P, Vertenstein M, Yang Z-L, Zeng X (2004) Technical description of the Community Land Model (CLM). NCAR Technical Note NCR/TN-461+STR., Boulder, USA

Oliveira AP, Escobedo JF, Machado AJ, Soares J (2002) Correlation models of diffuse solar-radiation applied to the city of Sao Paulo, Brazil. Appl Energ 71:59–73

Ostrowska D, Pietkiewicz S, Cieslinski M, Kucinska K, Gozdowski D (2008) Biomass accumulation and absorption of photosynthetic active radiation by rapeseed plants depending on sulphur fertilization. World J Agricult Sci 4:133–136

Page CN (1986) The strategies of bracken as a permanent ecological opportunist. In: Smith RT, Taylor JA (eds) Bracken: ecology, land use and control technology. Parthenon, Carnforth, UK, pp 173–181

Pakeman RJ, Marrs RH, Jacob PJ (1994) A model of bracken (*Pteridium aquilinum*) growth and the effect of control strategies and changing climate. J Appl Ecol 31:145–154

Papaioannou G, Papanikolaou N, Retalis D (1993) Relationships of photosynthetically active radiation and shortwave irradiance. Theor Appl Climatol 48:23–27

Peri PL, Moot DJ, McNeil DL (2003) A canopy photosynthesis model to predict the dry matter production of cocksfoot pastures under varying temperature, nitrogen and water regimes. Grass Forage Sci 58:416–430

Pitman JI (2000) Absorption of photosynthetically active radiation, radiation use efficiency and spectral reflectance of bracken [*Pteridium aquilinum* (L.) Kuhn] canopies. Ann Bot 85:101–111

Pronk TE, During HJ, Schieving F (2007) Coexistence by temporal partitioning of the available light in plants with different height and leaf investments. Ecol Model 204:349–358

Richter M (2003) Using plant functional types and soil temperatures for eco-climatic interpretation in southern Ecuador. Erdkunde 57:161– 181

Roderick ML, Farquhar GD, Berry SL, Noble IR (2001) On the direct effect of clouds and atmospheric particles on the productivity and structure of vegetation. Oecologia 129:21–30

Schneider LC (2004) Bracken fern invasion in southern Yucatán: a case for land-change science. Geogr Rev 94:229–241 Sellers PJ (1985) Canopy reflectance, photosynthesis and transpiration. Int J Remote Sens 6:1335–1372

Thornton PE, Zimmermann NE (2007) An improved canopy integration scheme for a land surface model with prognostic canopy structure. J Climate 20:3902–3923

Tsubo M, Walker S (2005) Relationships between photosynthetically active radiation and clearness index at Bloemfontein, South Africa. Theor Appl Climatol 80:17–25

Wang Y-P, Leuning R (1998) A two-leaf model for canopy conductance, photosynthesis and partitioning of available energy I: model description and comparison with a multi-layered model. Agr For Meteorol 91:89–111

Wang Q, Tenhunen J, Schmidt M, Kolcun O, Droesler M, Reichstein M (2006a) Estimation of total, direct and diffuse PAR under clear skies in complex alpine terrain of the National Park Berchtesgaden, Germany. Ecol Model 196:149–162

Wang X, Guo Y, Li B, Wang X, Ma Y (2006b) Evaluating a three dimensional model of diffuse photosynthetically active radiation in maize canopies. Int J Biometeorol 50:349–357

Zhang X, Zhang Y, Zhoub Y (2000) Measuring and modelling photosynthetically active radiation in Tibet Plateau during April-October. Agr For Meteorol 102:207–212

Zhang L, Moran MD, Brook JR (2001) A comparison of models to estimate in-canopy photosynthetically active radiation and their influence on canopy stomatal resistance. Atmos Environ 35:4463– 4470

Chapter 3

3. Simulating canopy photosynthesis

This chapter has been published as: Silva BSG, Roos K, Voss I, König N, Rollenbeck R, Scheibe R, Beck E, Bendix J (2012) Simulating canopy photosynthesis for two competing species of an anthropogenic grassland community in the Andes of southern Ecuador. **Ecological Modelling, vol.239, pp. 14-26**., 14. February 2012.
Reprinted with permission.

Abstract

Tropical mountain forest in the Andes of southeastern Ecuador is regularly destroyed to gain pasture land by cultivating the C4 grass *Setaria sphacelata*. After recurrent burning of the pastures, the grass is partly outcompeted by the C3 southern bracken (*Pteridium arachnoideum*). This competition represents the problematic of pasture degradation and increasing deforestation, due to the necessity of new pasture land. Because no information on the growth potential of both species in the Andes of Ecuador is available, a growth simulation model has been improved and properly parameterized with field observations. The measured species- and site-specific physiological and edaphic parameters are presented in this paper, as well as the model validation with field observations of leaf CO_2 assimilation. The validation showed deviations of simulated from observed leaf net assimilation lower than 5% of the observed values. The validated model was run with a fully realistic meteorological forcing of the year 2008 (10 min time step). The main result points to slightly higher growth potential of *Setaria* with 5879 g m^{-2} a^{-1}, based on an annual CO_2 net assimilation rate of 217 mol CO_2 m^{-2} a^{-1}. The calculated growth potential of bracken was 5554 g m^{-2} a^{-1}, based on the CO_2 net assimilation of 197 mol CO_2 m^{-2} a^{-1}. In addition, it was shown that decreasing incoming solar radiation and low temperature are favourable weather conditions for bracken in contrary to the pasture grass *Setaria*.

3.1 Introduction

Large areas of tropical mountain forest in the Rio San Francisco Valley (eastern Andes of South Ecuador) have been cleared by slash-and-burn to gain pasture land. After the pasture grass (*Setaria sphacelata*) has been manually planted, the current management strategy of recurrently burning the pastures for rejuvenation favours the growth of the tropical bracken fern *Pteridium arachnoideum*, an extremely aggressive weed (Hartig and Beck, 2003 and Bendix and Beck, 2009). Satellite observations have shown that, particularly in the lower parts of the Rio San Francisco valley (<2400 m above sea level), large areas (~68%) of former pastures have been abandoned due to the infestation by bracken that outcompetes the pasture grass (Beck et al., 2008 and Göttlicher et al., 2009). The reason for the competitive strength of bracken is not yet understood. Some investigations in other regions concluded that the spreading and growth of bracken is stimulated by burning (Page, 1986, Cruz et al., 2009 and Roos et al., 2010). Other studies in England and Mexico (Marrs et al., 2000a, Marrs et al., 2000b and Schneider, 2004) assumed that bracken is able to compete for light more successfully. To test the latter hypothesis, it is of fundamental interest to compare the photosynthesis potential of the C3 plant bracken and the C4 plant *Setaria* (da Silva and Arrabaça, 2004) under realistic environmental conditions by applying a process model for canopy photosynthesis.

Numerical models to simulate photosynthesis have been developed for more than 20 years. They are capable to calculate the photosynthesis of single species (leaf and canopy level) and/or plant types grouped by ecosystem functions under varying environmental conditions and on various spatio–temporal scales (e.g. Farquhar et al., 1980 and Farquhar et al., 2001). With regard to model architectures, two-big-leaf models have been shown to compute net canopy photosynthesis quite accurately (Wang and Leuning, 1998), performing as well as more complex multilayer models (Zhang et al., 2001). However, to compare canopy photosynthesis and related processes (as e.g. evapotranspiration) of specific species in a certain area, species-specific as well as abiotic site-specific model parameters have to be adapted and provided by respective field surveys to reach a high and realistic model accuracy (Oltchev et al., 2002 and Groenendijk et al., 2011).

Consequently, the aim of the current paper is to adapt a two-big-leaf canopy photosynthesis process model for the two competing plants species, the pasture grass S. *sphacelata* [(Schumach.) Stapf & C.E. Hubb.ex Chipp.] and the weed *P. arachnoideum* [(Kaulf.) Maxon] (the so-called Southern Bracken). Major effort has to be made to (i) properly parameterize and improve the model with special reference to the species-specific differences as e.g. related

to the C3 and C4 photosynthetic pathways. The second main point (ii) is to force the model with on-site weather observations to properly compare the potential of canopy photosynthesis of both species in the course of a year under realistic meteorological conditions.

(i) With regard to time-invariant site-specific parameters required for a proper simulation of canopy photosynthesis, soil texture in the root zone is crucial because its relation to the wilting point, affecting photosynthesis via soil moisture and evapotranspiration particularly during drier periods (Franks et al., 1997, Montaldo et al., 2003 and Olioso et al., 2005). For biotic parameters, non-adapted physiological properties revealed for instance an overestimation of 50% in simulated fluxes related to canopy photosynthesis (Oltchev et al., 2002). A species- and site specific rooting zone depth and root fraction is especially important for model accuracy during drier conditions when soil water limits evapotranspiration (Feddes and Raats, 2004). Species-specific photosynthesis parameters have been proven to be most sensitive regarding simulation accuracy (White et al., 2000 and Knorr and Heimann, 2001). Luo et al. (2001) and Bendix et al. (2010) demonstrated that species-specific leaf area index (LAI), leaf optical properties and orientation in relation to site-specific solar geometry are important parameters for the proper simulation of absorption of photosynthetic active radiation (PAR). The availability of species-specific light response curves measured in situ in the field (Pachepsky and Acock, 1996) and the consideration of realistic below-ground plant parts (as e.g. species-specific root to shoot ratio) is highlighted in several studies as crucial for a high simulation accuracy (Fourcaud et al., 2008). Further important factors are the varying influence of temperature on the effectivity of RuBisCO of different species (Leuning, 1997, Leuning, 2002 and Medlyn et al., 2002), the apparent quantum yield and the Q10, a parameter for the exponential increase of kinetic parameters and respiration (and thus, important for net photosynthesis) on changing temperature (e.g. Dang et al., 1998). With regard to simulation accuracy, Müller et al. (2009) and Vuichard et al. (2010) revealed that an accuracy >80% for photosynthetic parameters (as inter alia carboxylation) can be tolerated to reach an overall accuracy of about 5%. With regard to parameter estimation in the field, Lenz et al. (2010) emphasized the importance of avoiding artefacts from data collection under extreme environmental situations (drought stress, etc.).

(ii) With reference to realistic model forcing, high-resolution and time-variant atmospheric data are of focal importance (Montaldo et al., 2003). Knorr and Heimann (2001) and Olioso et al. (2005) stressed that models require continuous (at least hourly) meteorological input to capture all weather variations affecting photosynthesis and flux calculations. Forcing

with realistic PAR-radiation values and other elements of the radiation balance is a fundamental basis of realistic simulations of canopy photosynthesis and related fluxes (e.g. Lynch et al., 2001). Particularly the differentiation between sunlit and shade leaves and thus, the influence of radiation partitioning into its direct and diffuse components, provided better model accuracy (Mercado et al., 2006). In addition, photosynthesis is strongly regulated by temperature which plays a key role in the succession of C3 and C4 species (Ehleringer and Monson, 1993 and Harnos et al., 2006). Furthermore, photosynthesis is closely related to rainfall and the availability of soil moisture, particularly in dry areas and during dry spells (Shena et al., 2005, Bonan and Levis, 2006 and Thum et al., 2007). Thus, model accuracy is highly sensitive to abiotic factors, especially to incoming radiation, temperature and moisture parameters, which have to be provided as realistic as possible.

Despite of all these findings regarding parameter sensitivity and realistic model forcing, the major shortcoming of the most simulation studies on canopy photosynthesis is that they still (at least partly) rely on default, not species- and site-specific biotic and abiotic parameters. This is mainly due to the time- and cost-expensive parameter determination in the field which additionally presupposes multidisciplinary knowledge in all relevant field methods. Secondly, in the most cases, no actual site-specific meteorological data in high temporal resolution is at hand so that simulation results are frequently based on remotely measured meteorological information or even on relatively insecure outputs of weather models. Even if basic variables as e.g. air temperature and rainfall are measured at site, derived meteorological quantities in "two-big-leaf models" relevant for canopy photosynthesis as stratification stability and related fluxes (vapour, etc.), which in turn affect leaf and soil temperature, impose high insecurities which could be mitigated by replacing them as effectively as possible by site-specific measurements as well. The current study strives for overcoming these limitations by benefiting from an interdisciplinary research effort which provides all required species- and site-specific above- and below ground parameters relevant for model accuracy for the two competing species (refer to details in Section 3.2.3, Table 3-2). Furthermore, the properly parameterized model is fully forced with meteorological on-site measurements (refer to details in Section 3.2.4, Table 3-1) which includes also sensors for normally model-derived (and thus uncertain) parameters as e.g. temperature of sunlit and shade leaves, but also for improving radiation partitioning (Section 3.2.2.1). The expected benefit is an accurate species- and site-specific canopy photosynthesis model which is indispensable to assess the real competitive strength of both antagonists with regard of their growth potential.

Table 3-1. Meteorological sensors at the pasture site.

Variable	Sensor	Instrumentation
Global radiation	Pyranometer; CNR1 Kipp & Zonen, Inc.	Sensors set at 2 meters height
Air temperature and relative humidity	Thermometer and hygrometer; MP100A Rotronic, AG	Two coupled sensors, one at 2 m and one at 50 cm canopy height
Barometric pressure	Barometer; CS100 Campbell, Inc.	Single sensor
Leaf temperature	Infrared thermocouple; IRTS-P Apogee, Inc.	Four sensors, sunlit and shaded for *Setaria* and bracken
Wind speed	Ultrasonic anemometer; Windsonic, Gill Inc.	Sensor at two meters height
Precipitation	Rain gauge; ARG100 Campbell, Inc.	Tipping bucket gauge on the ground
Soil water content	TDR reflectometer; CS616 Campbell, Inc.	Sensor at 20 cm depth
Soil temperature	Thermocouple; TCAV Campbell, Inc.	Three sensors profile at 10, 20 and 50 cm depth

3.2 Methods

The following section is dedicated to depict the methodology of the paper. It is structured as follows: after a brief introduction to the study site and the experimental design, Section 3.2.2 presents the model description, Section 3.2.3 the description of the required model parameters and corresponding measurements, and Section 3.2.4 the model setup.

3.2.1 Study site and experimental design

The study area in the Rio San Francisco Valley is described in Bendix and Beck (2009). The climate of the area is perhumid but characterized by a slightly drier season from September to March and the main rainy season from April to August (Richter, 2003, Bendix et al., 2008a and Bendix et al., 2008b). Solar radiation is reduced over the whole year due to the high cloud frequency, in particular during the main rainy season (Bendix et al., 2006 and Bendix et al., 2008c). Air temperature is higher and daily extremes are more pronounced during months with less precipitation. An experimental site in the pasture was established close to the research station (Estación Científica de San Francisco, ECSF, latitude: 3°58′18″S, longitude: 79°4′45″W, altitude: 1860 m asl) at an altitude of 2109 m asl, consisting of ten 10 × 10 m plots (burnplot) with differing proportions of bracken and *Setaria* (Figure 3-1). The site was equipped with a micro-meteorological station measuring all required meteorological input variables (Table 3-1).

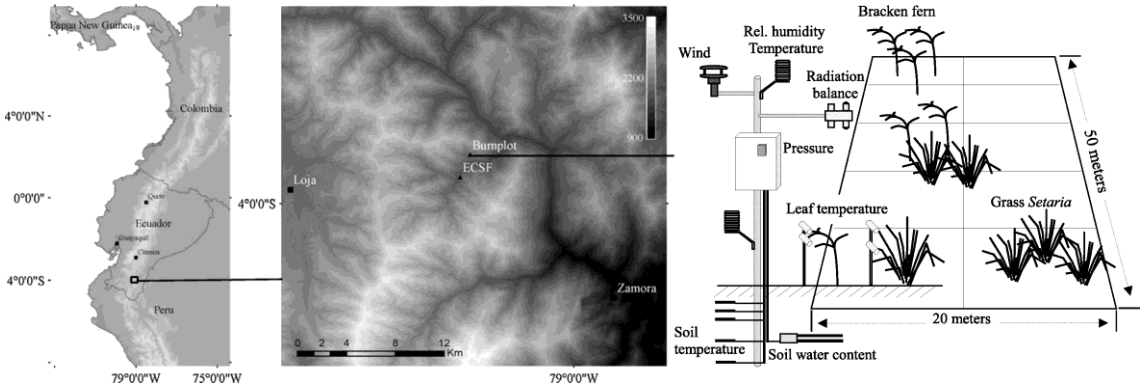

Figure 3-1. Location of the study site and design of the experimental plot (Burnplot).

In addition to the operational meteorological station, a radiation sensor for diffuse radiation (BF3 Delta-T, Inc.) was installed and operated for one year to derive a site-specific radiation decomposition function applicable to the long-term observations of global radiation in the study area.

3.2.2 The canopy photosynthesis model

The canopy photosynthesis model used in this study was based on the two-big leaf approach (Dai et al., 2004). The conceptual sketch of the adapted and improved model is shown in Figure 3-2. Its general components are: (i) a radiation module, including radiation partitioning and canopy radiation, (ii) a canopy photosynthesis module, (iii) a respiration module for leaves and roots,

and (iv) a module for conversion of net assimilated CO_2 into dry biomass (Figure 3-2, centre).

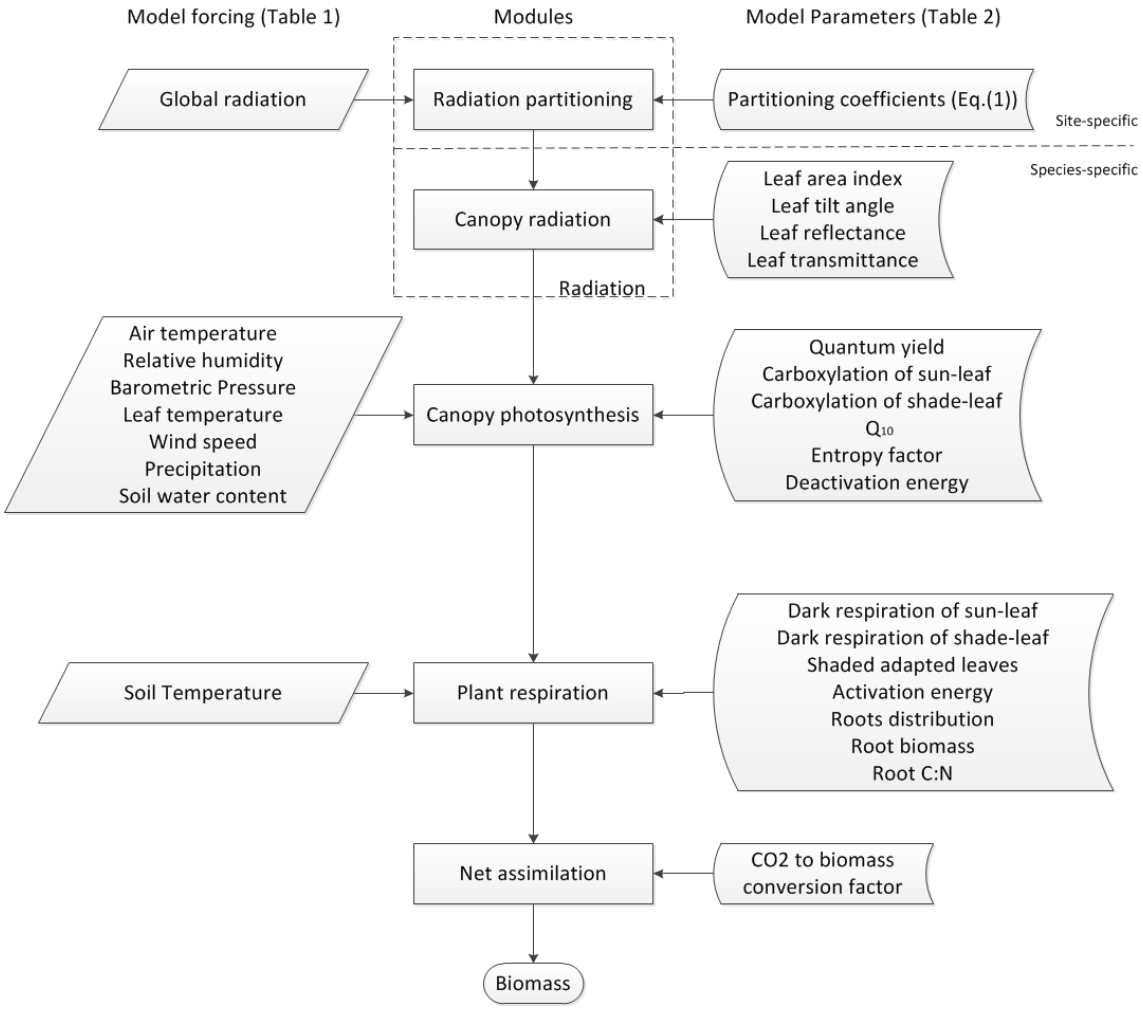

Figure 3-2. Conceptual model used to calculate potential biomass production as a factor of leaf photosynthesis and plant respiration (leaves and roots). Shade acclimation is considered in calculating leaf photosynthesis and respiration as denoted by sunlit or shade-leaf.

3.2.2.1 The radiation module

The basics of the radiation module are described in detail in Bendix et al. (2010). Regarding solar incoming radiation, the module requires the partitioning of the global radiation into its direct (I_{b0}) and diffuse components (I_{d0}), which is site-specific.

$$I_{d0} = I_0 \cdot k'; I_{b0} = I_0 \cdot (1 - k') \quad (1)$$

where I_0 is the incident global radiation above the canopy and k' the diffuse fraction of radiation modified due to solar geometry with the cosine of solar zenith angle μ.

$$k' = \frac{k}{(1-k) \cdot \mu + k} \quad (2)$$

with the at-site observed diffuse radiation fraction k. An empirical formulation for calculating k is given in Section 3.2.3.1.

3.2.2.2 The photosynthesis module

In the photosynthesis module, a framework based on Farquhar et al. (1980) was used for the C3 bracken. The equations from Collatz et al., 1991 and Collatz et al., 1992 were applied to the C4 grass *Setaria*. A detailed description of the most model equations is given in the cited papers and should not be repeated here. Here we present basic equations of photosynthesis necessary to understand the model and its parameterization. Where mentioned, small improvements are proposed to the original formulation. In our model, gross photosynthesis (A) is either limited by light, by CO_2 or by the export rate of photosynthates, with:

$$A = \min(Wi, Wc, We) \quad (3)$$

where A is set to the minimum of the three photosynthesis functions for light (Wi), CO_2 (Wc) and export rate of photosynthates (We), calculated as follows:

$$Wi = \varphi \cdot \alpha \cdot \frac{(C_i - \Gamma')}{(C_i + 2\Gamma')} \quad \text{, for bracken (C3 type)} \quad (4.1)$$

$$Wi = \varphi \cdot \alpha \quad \text{, for } \textit{Setaria} \text{ (C4 type)} \quad (4.2)$$

$$Wc = Vm_{sun,sha} \cdot \frac{C_i - \Gamma'}{C_i + K_c \cdot (1 + O/K_o)} \quad \text{, for bracken (C3 type)} \quad (4.3)$$

$$Wc = Vm_{sun,sha} \cdot m \cdot \frac{C_i}{P_a} \quad \text{, for } \textit{Setaria} \text{ (C4 type)} \quad (4.4)$$

$$We = \frac{Vm_{sun,sha}}{2} \quad \text{, for bracken and } \textit{Setaria} \text{ (C3 and C4 types)} \quad (4.5)$$

The first function (*Wi*) represents the limitation due to light, assuming no loss of the absorbed photon flux (α, μmol quanta m^{-2} s^{-1}). For the C3 plant, the relationship of the compensation point for CO_2 (Γ') to the intercellular CO_2 partial pressure (*Ci*) represents the loss due to photorespiration. For the C4 plant, photosynthesis is given by a direct relationship to quantum yield (φ, μmol CO_2 μmol $quanta^{-1}$). The second function (*Wc*) represents the limitation due to carboxylation efficiency. For the C3 plant, photorespiration is positively related to the leaf internal CO_2:O_2 ratio, and the RuBisCO activity is expressed in terms of Γ' and the Michaelis constants *Kc* and *Ko* (Long and Bernacchi, 2003). For the C4 plant, a low ratio of *Ci* to air pressure (Pa) leads to CO_2 leakage from the leaf, which limits photosynthesis. The efficiency of the CO_2 concentrating mechanism in the C4 photosynthetic pathway is given by the parameter m. The third function (*We*) represents the limitation due to the export rate of photosynthate (triose phosphate from Calvin cycle) to the heterotrophic tissues of the plant. Operation to capacity is assumed by setting the parameter e to 0.5 for C3 and 1 for C4-type. The parameters quantum yield (φ) and maximum carboxylation rate ($Vm_{sun,sha}$) are explained in more detail in Section 3.2.3.2.

Different from previous works, carboxylation limitations (Eqs. (4.3) and (4.4)) are brought together to facilitate the understanding of the photosynthesis model. As a consequence, and the export rate limitation (Eq. (4.5)) is expressed by a single function for C3 and C4-type. Other improvements are (i) to differ between sunlit and shade-adapted leaves regarding the maximum carboxylation rate ($Vm_{sun,sha}$ equals Vm_{sun} or Vm_{sha}) and (ii) to parameterize the model with gas-exchange measurements. In addition *Ci* depends on photosynthesis and on the atmospheric mole fraction of CO_2,

which in this work was considered constant at 354.2 ppm after measurements at the study site in 2008. The constant mole fraction of 209,000 ppm is used to calculate the partial pressure of oxygen (O).

The maximum carboxylation rate $Vm_{sun,sha}$ in Eqs. (4.3), (4.4) and (4.5) depends on enzymatic activity which is significantly affected by leaf temperature. So $Vm_{sun,sha}$ is calculated by multiplying $Vm_{sun,sha}$ estimated at 25 °C (Section 3.2.3.2) by a temperature function for carboxylation $g_v(T_l)$:

$$g_v(T_l) = Q_{10}^{\left(\frac{T_l - 25}{10}\right)} \cdot \left(1 + \exp\left(\frac{-Hd + \Delta s \cdot T_l}{R \cdot T_l}\right)\right)^{-1} \quad (5)$$

where Q_{10} is the proportional change by a variation of 10 °C in temperature. T_l is the leaf temperature in Kelvin. R is the universal gas constant (8.3145 J K^{-1} mol^{-1}). Temperature regulation is not considered to differ from sunlit to shade leaves. The estimation of activation energy (E_a), entropy factor (Δ_s), and deactivation energy (H_d) is given in Section 3.2.3.2.

Leaf photosynthesis ceases by insufficient soil water. So the leaf gross photosynthesis (Eq. (3)) is multiplied by the plant wilting factor (β) in $A = \min(Wc,Wi,We)\cdot\beta$ and β is given by:

$$\beta = \sum_j fB_{root,j} \cdot \left(\frac{-\Psi_{sat,j} \cdot \left(\frac{\Theta_j}{\Theta_{sat,j}}\right)^{-C_j} - \Omega_c}{\Omega_o - \Omega_c} \right) \quad (6)$$

where $fB_{root,j}$ is the fraction of root biomass for each soil layer j (Section 3.2.3.3, Eq. (17)). Θ_j is the soil water content (Section 3.2.3.2, Eq. (13)). Ω_o = −275,000 mm and Ω_c = −74,000 mm are the soil water potentials at maximum and minimum plant transpiration, respectively. The variables $\Theta_{sat,j}$, $\Psi_{sat,j}$ and C_j are functions of soil texture (Section 3.2.3.2, Eqs. (14), (15) and (16)) and β ranges from 0 for completely dry soils to 1 for water-logged soils.

3.2.2.3 The leaf and root respiration module

To calculate the net photosynthesis, A is subtracted by the maintenance respiration of leaves (Rd_{sun} and Rd_{sha}) and roots (Rm_{root}) and by the construction respiration, which according to Ryan (1991) corresponds to 25% of assimilation less maintenance respiration. So net photosynthesis is given by:

$$A_{net}=0.75\cdot(A\cdot\beta-(Rd_{sun}+Rd_{sha}+Rm_{root})) \quad (7)$$

Construction respiration is assumed to include ion-uptake costs and to be species-independent. In the leaf respiration module, maintenance respiration is calculated separately for shade and sunlit leaves. Similarly to the determination of the maximum carboxylation rate $Vm_{sun,sha}$ (Section 3.2.2.2), the effect of temperature on respiration was given by multiplying the estimated respiration at 25 °C (Rd0sun,sha) by the temperature function, $g_r(T_l)$, as follows:

$$\begin{aligned} Rd_{sun} &= Rd_{0sun}\cdot g_r(T_l)\cdot LAI_{sun} \\ Rd_{sha} &= Rd_{0sha}\cdot g_r(T_l)\cdot LAI_{sha} \end{aligned} \quad (8)$$

where Rd_{0sun} and Rd_{0sha} are estimates of dark respiration rates derived from measurements of sunlit and shade leaves at 25 °C leaf temperature (Table 3-2). For respiration, the leaf area indices LAI_{sun} and LAI_{sha} are complementary values of the total LAI (Table 3-2), i.e. LAI_{sun} + LAI_{sha} = LAI. In this work the fraction of shade adapted leaves was set to the minimum of the LAI_{sha} fraction ($fLAI_{sha}$) for all solar zenith angles (Bendix et al., 2010) and the LAI_{sha} is given in Table 3-2.

Table 3-2. Physiological and morphological plant parameters.

Parameter	Symbol	Bracken	*Setaria*	Measuring unit	Method/ Source
Leaf area index	LAI	2.51	3.7	m^2 one-side leaf area m^{-2} ground	Bendix et al. (2010)
Leaf tilt angle	X	0.48	−0.37	from −1 (vertical) to 1 (horizontal) leaves	Bendix et al. (2010)
Leaf absorption	α	88.9	86.8	%	Bendix et al. (2010)
Leaf reflectance	ρ	7.4	11.7	%	Bendix et al. (2010)
Leaf transmittance	τ	3.7	1.5	%	Bendix et al. (2010)

Quantum yield	Φ	0.048	0.05	µmol CO_2 $µmol^{-1}$ quanta	Gas-exchange measurements
Carboxylation rate of sun-leaf	Vm_{sun}	68.8	32.1	µmol CO_2 m^{-2} s^{-1} ppm^{-1} CO_2	Gas-exchange measurements:
Carboxylation rate of shade-leaf	Vm_{sha}	54.4	29.6	µmol CO_2 m^{-2} s^{-1} ppm^{-1} CO_2	Gas-exchange measurements:
Q10 for kinetic parameters	Q_{10}	2.4	2.5	–	Gas-exchange measurements
Entropy factor	ΔS	649	652	J mol^{-1} K^{-1}	Gas-exchange measurements
Deactivation energy	H_d	200	200	kJ mol^{-1}	Gas-exchange measurements
Dark respiration at 25 °C of sun-leaf	Rd_{0sun}	1.55	1.92	µmol CO_2 m^{-2} s^{-1}	Gas-exchange measurements
Dark respiration at 25 °C of shade-leaf	Rd_{0sha}	1.23	1.77	µmol CO_2 m^{-2} s^{-1}	Gas-exchange measurements
Fraction of shade leaves	$fLAI_{sha}$	0.61	0.33	–	Bendix et al. (2010)
Activation energy for respiration	E_{ar}	440	484	Kelvin	Gas-exchange measurements
Root distribution	a	2	2	–	Zeng (2001)/ Pürckhauer sampling
Root distribution	b	7	20	–	Zeng (2001)/ Pürckhauer sampling
Roots/rhizomes biomass	B_{root}	3.7	4.8	kg	Pürckhauer sampling
Root/rhizome C:N	CN_{root}	111.5	50.1	g C/g N	Potthast et al. (2010)

CO_2 to biomass conversion factor	BCO_2	29	27	g biomass/mol CO_2	Potthast et al. (2010)

[a] For *Setaria* the carboxylation rate at saturating light is used, respectively for sun and shade leaves: 16 × 10^3 and 13 × 10^3 CO_2 in µmol CO_2 m^{-2} s^{-1}. The parameter m, in parenthesis, is non-dimensional and represents the efficiency of the CO_2 concentrating mechanism in the C4 plant *Setaria*.

The leaf dark respiration shows an exponential increase with temperature, which can be described by the equation of Lloyd and Taylor (1994):

$$g_r(T_l) = \exp\left(E_{ar} \cdot \left(\frac{T_l - 298.15}{71.02 \cdot (T_l - 227.13)}\right)\right) \quad (9)$$

where $g_r(T_l)$ is the temperature function, similar to Eq. (5), T_l is the leaf temperature in Kelvin and Ear is the activation energy (Table 3-2).Root maintenance respiration (Rm_{root}) is direct related to tissue nitrogen, according to the straightforward scheme of Ryan (1991):

$$Rm_{root} = r \cdot 0.643 \cdot \frac{B_{root} \cdot 10^{-6}}{CN_{root} \cdot BCO_2} \quad (10)$$

where Rm_{root} is given in µmol CO_2 s^{-1}, r is a non-dimensional respiration coefficient (Oleson et al., 2004), which in this work was set to 1. The value 0.634 is the respiration rate in s^{-1} (Ryan, 1991) multiplied by 10^6 to agree with the root dry biomass (B_{root}) in grams (Table 3-2). CN_{root} is the carbon to nitrogen relationship and BCO_2 is the conversion factor of CO_2 to dry biomass (µg biomass × µmol CO_2^{-1}).

3.2.2.4 Module for conversion of net assimilated CO_2 into dry biomass

For an estimation of biomass production, simulated net assimilation accumulated over time is converted to grams dry biomass by multiplying accumulated assimilation with a species-specific conversion factor:

$$BP = \left(\sum_{t=0}^{n} A_{net}\right) \cdot BCO_2 \cdot 10^{-6} \quad (11)$$

where *BP* is the potential dry biomass in grams, *Anet* is the net assimilation in μmol CO_2, t is the time-step and n is the time span of calculation.

3.2.3 Species- and site-specific model parameterization

The species-specific model parameters (Figure 3-2, right column) required in the model equations (Section 3.2.2) were derived from measurements at leaf and root level or from data of the study site available in the literature. A summary of used values, sources and methods is given in Table 3-2. The detailed determination of specific model parameters by using field and laboratory observations is described in the following sections for the four modules of the model. It should be emphasized that these species- and site specific plant-morphological and physiological parameters including those of the canopy radiation scheme (Bendix et al., 2010) were held constant for the model run (Section 3.3.2), representing an average individual of bracken and *Setaria* of the study site. To consider shade acclimation as required by the two-big leaf approach, typical individuals of bracken and *Setaria* were represented by data measured on productive sunlit and shade adapted leaves.

3.2.3.1 Parameterization of the radiation module

The canopy radiation scheme was based on three species-specific optical and morphological plant traits: leaf tilt angle (χ), leaf reflectance (ρ) and transmittance (τ) (Table 3-2), which were observed in the field and averaged to parameterize two typical individuals of bracken and *Setaria* (Bendix et al., 2010 and Göttlicher et al., 2011). A site-specific determination of the diffuse radiation fraction *k* from global radiation, which was measured in the field for the most years of observation (since 1998), is needed for solving Eq. (2). After Liu and Jordan (1960) *k* can be derived by using short term data on diffuse radiation taken under all local weather conditions (from sunny to completely overcast sky). The determination of *k* in this study was based on one year measurements with the BF3 sunshine sensor (Delta-T, Inc.) applied to the equation of Boland et al. (2008):

$$k = \frac{1}{1 + \exp(-4.7 + 6.5 \cdot kt)} \tag{12}$$

where the clearness index kt is the ratio of global radiation observed at ground and calculated top-of-atmosphere radiation (Bendix et al., 2010). The partitioning coefficients −4.7 and 6.5 resulted from nonlinear least squares fitting of the observed diffuse radiation fraction k to the clearness index kt.

3.2.3.2 Parameterization of the canopy photosynthesis module

Data on the photosynthetic response to radiation and CO_2 (Figure 3-3) were used for the parameterization of the photosynthesis module. To simulate shade acclimation, plant individuals were grown in a greenhouse for four months under typically incident radiation and in artificial shadow. Light intensities were controlled between 50 and 500 μmol quanta m^{-2} s^{-1} in shadow while sunlight ranged from 500 to 3000 μmol quanta m^{-2} s^{-1}. Samples from these plants were taken to represent sunlit and shade leaves after gas-exchange measurements were conducted in the greenhouse and in the field to confirm the data on sunlit leaves. Gas-exchange of sunlit and shade-adapted leaves was measured with a portable photosynthetic measurement system (LI-6400XT; LiCor, Inc., Lincoln, USA). Light response curves under ambient CO_2 and CO_2 response curves at light saturation (1200 μmol quanta m^{-2} s^{-1}) were measured following the protocol presented in Long and Bernacchi (2003). In addition, measurements were made between 11:00 and 17:00 and leaf temperature was set to 25 °C. Valid measurements were carried out under vapour pressure deficit of the air less than 2 kPa, which warranted sufficient conductance for maximum assimilation. Considering that, at least three valid measurements were selected for each sample. The arithmetic mean for each CO_2 or light level (x-axis in Figure 3-3) was then used in the parameter derivation.

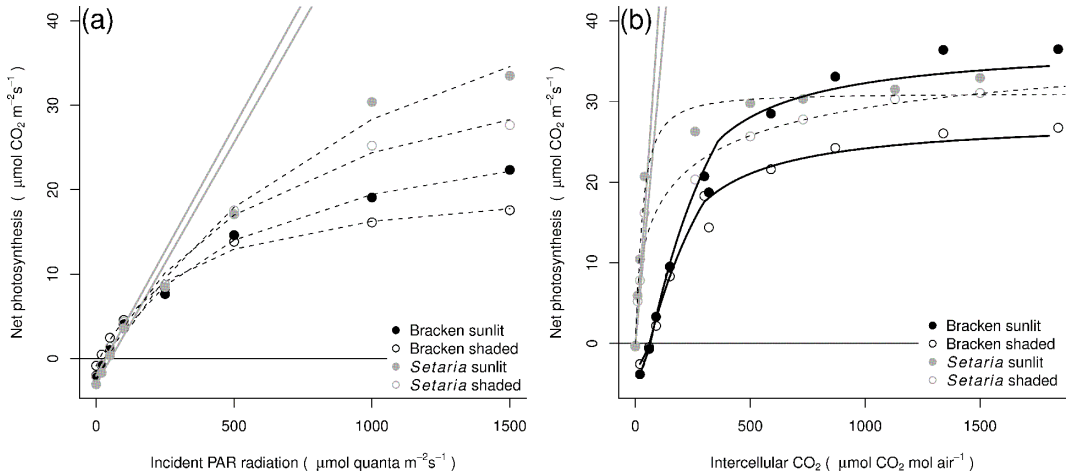

Figure 3-3. Photosynthetic light (a, left) and CO_2 response (b, right), showing the average of measurements (closed circles for sunlit and open circles for shade) at each given incident PAR radiation or intercellular CO_2. Solid lines show model results after fitting to data. Dashed curves show a quadratic fitting to the measured data. In the light response curve (a) the initial increase for *Setaria* sunlit (left line) and shade (right line) are plotted as solid lines. In the CO_2 response curve (b), the model framework distinguishes between C3 and C4 pathways. Thus, a piecewise fitting is applied to bracken (refer to text; solid black lines), while a linear fitting is used for *Setaria* (solid grey lines). The zero line at y-axis is shown in all figures as a reference for respiration (=negative net photosynthesis).

The determination of the required model parameters (i) maximum carboxylation rate and (ii) quantum yield is based on the gas-exchange measurements of Figure 3-3. The determination of the model parameters by applying linear and nonlinear regression (grey and black lines in Figure 3-3) differs between C3 and C4 plants. For the C4-plant *Setaria*, the determination relies on the work of Collatz et al. (1992). For C3-plant bracken, the work of Long and Bernacchi (2003) is considered.

The (i) maximum carboxylation rate is derived as the initial increase of the nonlinear regression on assimilation values at an internal CO_2 concentration < 250 ppm for bracken (black lines in Figure 3-3b). Eq. (4.3) was used in the regression for bracken. For *Setaria*, the region of internal CO_2 concentrations < 50 ppm was considered to estimate the efficiency of the CO_2 concentrating mechanism (m parameter in Eq. (4.4)), which equals the coefficient of the linear regression (grey lines in Figure 3-3b) divided by the maximum carboxylation. The latter is given by the asymptote of the CO_2 response curve of *Setaria* (traced lines in Figure 3-3b). The derived maximum carboxylation rates for sunlit and shade leaves (Vm_{sun} and Vm_{sha}) and the

efficiency of the CO_2 concentrating mechanism (*m* parameter) for *Setaria* are presented in Table 3-2. In general, sunlit leaves showed a higher maximum assimilation than shade leaves which shows different photosynthetic performances at saturating light.

Regarding the (ii) quantum yield (φ), estimated values for *Setaria* corresponds to the initial increase in the light response curve at an incident radiation < 150 μmol quanta m^{-2} s^{-1} (grey lines Figure 3-3a and Eq. (4.2)). For bracken, the assimilation data at the CO_2 saturating levels (>500 μmol CO_2 mol air^{-1}) was fitted to Eq. (4.1) to estimate the quantum yield (black lines in Figure 3-3b). Light absorption by leaves (α, Table 3-2) was obtained from field spectroscopy (Bendix et al., 2010 and Göttlicher et al., 2011). No significant difference was found between the quantum yield of shade and sunlit leaves. The quantum yield for *Setaria* and bracken leaves is shown in Table 3-2.

The temperature function of maximum carboxylation rate was parameterized by using CO_2 response measurements at 15 °C (not shown) and at 25 °C (Figure 3-3b). The estimated values of maximum carboxylation rate were fitted to Eq. (5) by nonlinear regression to derive new species-specific values for activation energy (E_a) and the entropy factor (ΔS). The deactivation energy (H_d) was set to 200 kJ mol^{-1} for both species (Table 3-2). For carboxylation, derived Q_{10} value was 2.4 for bracken and 2.5 for *Setaria*, and derived entropy factor (ΔS) was 650 J mol^{-1} K^{-1} for bracken and 648 J mol^{-1} K^{-1} for *Setaria* (Table 3-2). These values are within the range of those presented in Kattge and Knorr (2007).

The combined effects of temperature on carboxylation (Eq. (5)) and on leaf respiration (Eq. (9)) are shown in Figure 3-4. Parameterization of the temperature function of leaf respiration is shown in Section 3.2.3.2. The higher amplitude of leaf photosynthesis of *Setaria* with increasing temperature is due to the C4-pathway, where energy is required for the CO_2 concentrating mechanism in addition to the Calvin cycle. This observation, as well as the variation of the leaf photosynthesis with temperature, corroborates with previous findings for species similar to the bracken (Hollinger, 1987) and *Setaria* (Baruch et al., 1985).

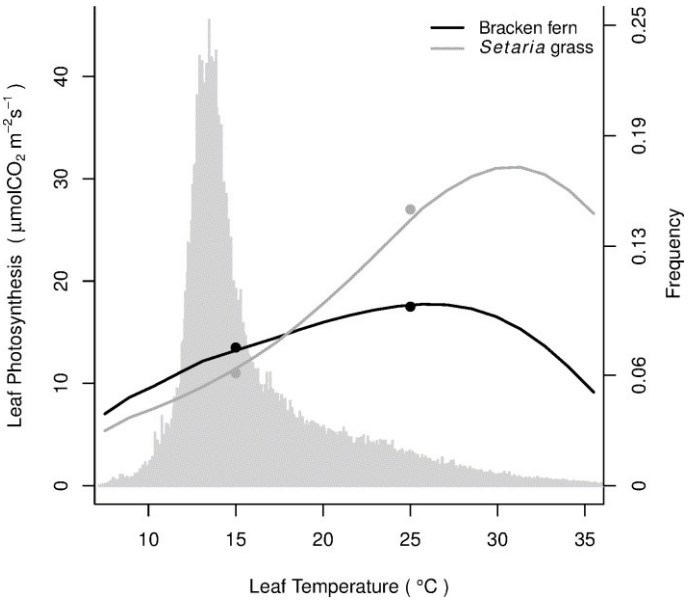

Figure 3-4. Effect of leaf temperature on net photosynthesis (assimilation minus respiration) at saturating radiation of bracken and *Setaria* adjusted to the data of maximum net photosynthesis (points). The frequency of leaf temperatures is displayed as grey bars (right y-axis).

Information on vertical profiles of soil texture and water content were needed regarding the influence of soil moisture on canopy photosynthesis. Since data on soil water content was only available for 20 cm depth (Table 3-1), its vertical extrapolation was needed. For this purpose, single measurements of soil water content were used together with a stratification function after Oleson et al. (2004). This stratification function considers eight discrete layers with increasing thicknesses down to 1 m. Single measurements of soil water profiles were carried out in the study site by using mobile soil moisture sensors in November 2008. In that relative dry season soil water content exponentially decreased with depth down to sixty centimetres from 0.53 to 0.37 (m^3 H_2O m^{-3} soil). A simple extrapolation function was used based on these data to calculate the soil water content in each layer from the continuously observed soil moisture at 20 cm depth as follows:

$$\Theta_j = \Theta_{20} \cdot (-0.46 \cdot d^2 - 0.06 \cdot d + 1.02) \qquad (13)$$

where Θj is the water content in the layer j, Θ_{20} is the water content observed at 20 cm depth, and d is the soil depth. The coefficients were obtained by least squares regression of data on soil water content with depth, using the single measurements of soil water profiles.

The required information on soil water (Eq. (6)), namely the water content at soil saturation ($\Theta_{sat,j}$), the saturated soil matric potential ($\Psi_{sat,j}$) and the parameter C_j, were obtained from empirical functions (Oleson et al., 2004):

$$\Theta_{sat,j} = 0.489 - 0.126 \cdot f_{sand,j} \quad (14)$$

$$\Psi_{sat,j} = -10 \times 10^{1.88-0.03 f_{sand,j}} \quad (15)$$

$$C_j = 2.91 + 0.159 \cdot f_{clay,j} \quad (16)$$

where $f_{sand,j}$ and $f_{clay,j}$ are the site-specific sand and clay contents, respectively, in the j_{th} layer (Figure 3-5). Clay and sand content were determined by laboratory investigations of soil samples collected at the study site and nearby (Günter et al., 2009). Figure 3-5 shows that the proportion of clay decreases with depth while that of sand slightly increases.

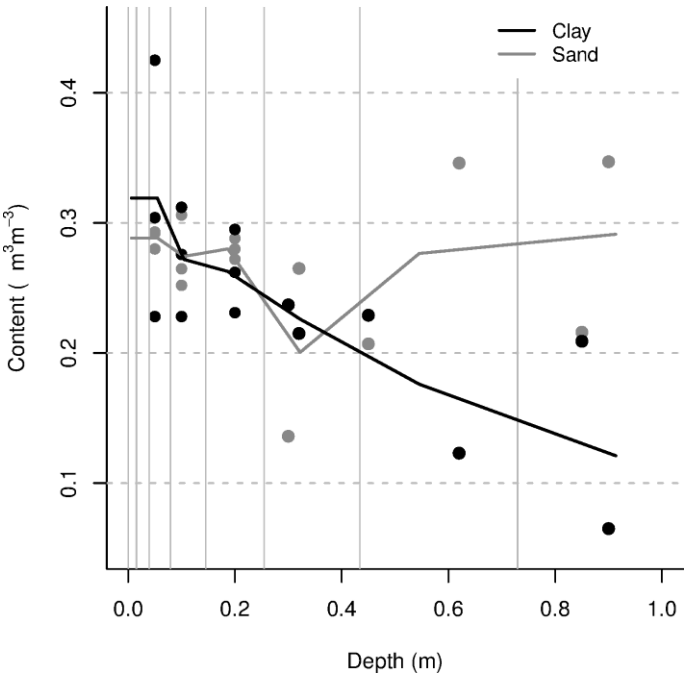

Figure 3-5. Clay and sand profiles in soils of bracken infested pastures with measurements (dots) and average profile (lines) for the eight soil layers (between the vertical lines) used in the model.

3.2.3.3 Parameterization of the respiration module

For the respiration module, species-specific dark respiration for leaves was derived from two datasets. First, dark respiration was estimated from the photosynthetic light response at 25 °C by taking the y-axis intercept from the

equation used to derive the initial slope (refer to Figure 3-3a, Section 3.2.3.2). Second, dark respiration was extracted from field measurements of CO_2 net assimilation during night when leaf temperature ranged from 14 to 16 °C (Figure 3-7, Section 3.3.1). From these observations average values of species-specific respiration oscillated around 0.63 and 0.55 μmol CO_2 m^{-2} s^{-1} for bracken (16 °C) and *Setaria* (14 °C). Average species-specific dark respiration derived from the light response curve at 25 °C ranged from 1.36 to 2.28 for bracken fronds and from 0.76 to 2.78 μmol CO_2 m^{-2} s^{-1} for *Setaria* leaves. Average values were taken to represent leaf dark respiration at 25 °C (Rd_{0sun} and Rd_{0sha}, Table 3-2). The activation energy (E_{ar}) was estimated as dependent variable in Eq. (9) with the values of dark respiration at 25 °C and at 16 or 14 °C. Root respiration was adjusted by the same temperature function applied to leaves. The relationship of tissue respiration to the carbon to nitrogen ratio (C:N) was presumed to be valid for different plant tissues of one species (Ryan, 1991). Species-specific C:N ratios for belowground biomass was available from the work of Potthast et al. (2010) (Table 3-2). Root and rhizome biomass were measured at different depths by collecting soil probes with a Pürckhauer, manually separating roots and rhizomes from mineral soil and by complete drying at 60 °C. Three Pürckhauer samples were collected in a perimeter covered solely by bracken or *Setaria*. This procedure was repeated nine times and the arithmetic average of biomass at each depth was used for deriving a species-specific root distribution function according to Zeng (2001). The total root biomass per unity area is given by B_{root} (Table 3-2). The required species-specific vertical root distribution is derived by:

$$fB_{root,j} = \frac{1}{2}\left(\left(e^{-a \cdot d_{j-1}} + e^{-b \cdot d_{j-1}}\right) - \left(e^{-a \cdot d_j} + e^{-b \cdot d_j}\right)\right) \qquad (17)$$

where $fB_{root,j}$ is the fraction of roots on the total biomass (B_{root}) of the belowground layer j, d is the depth and a and b are coefficients derived by regression between data on root biomass and depth, using the Eq. (17). Figure 3-6 shows the species-specific root and rhizome distributions. The highest fraction of bracken rhizomes and roots are observed between 20 and 30 cm. In contrast, roots of *Setaria* exponentially decrease with depth.

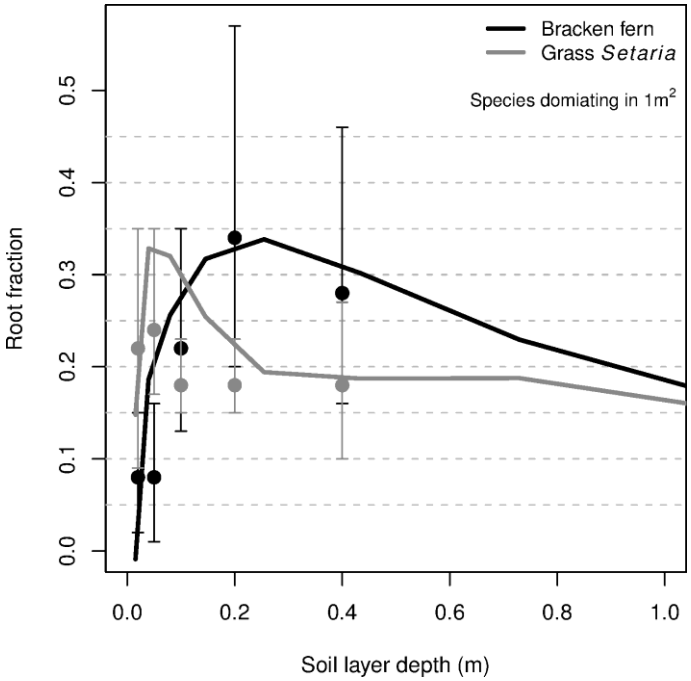

Figure 3-6. Distribution functions (solid lines) based on averages of belowground biomass data (dots). Maximum and minimum values for each biomass sample are depicted as deviation bars from the averages (n = 9 for each species).

3.2.3.4 Parameterization of the module for conversion of net assimilated CO_2 into dry biomass

A species-specific factor (BCO_2) was used to convert net assimilation into dry biomass (Table 3-2). Estimates of BCO_2 were available for bracken fern and *Setaria* grass from the work of Potthast et al. (2010). In the current version of the model, it is assumed that the total assimilated CO_2 was converted with no loss into dry biomass (in grams per square metre), which in the end of a year is composed of above and belowground living and dead biomass.

3.2.4 Model setup

The model setup is based on realistic forcing variables above- and below-ground (Figure 3-2, left column) which are continuously observed at the experimental site (Figure 3-1). After the proper parameterization (Section 3.2.3) a one-year model run was conducted with realistic external forcing (meteorological data) from January 1, 2008 to January 1, 2009 in 10-min time steps. Realistic atmospheric forcing was warranted by using data of global radiation, air temperature, relative humidity, atmospheric pressure, leaf temperature, wind speed, precipitation, soil water content and soil temperature. Radiation absorption for every time step was calculated by at-

site global radiation measurements and the novel site-specific radiation decomposition function (refer to Section 3.2.3.1). Particularly air temperature at half metre and at 2 m height as well as wind velocity at 2 m were used to calculate saturated vapour pressure and estimate the vertical profile of heat and water vapour fluxes which affect the leaf boundary layer. Infrared leaf temperatures were taken in order to calculate the saturated vapour pressure in the leaves and temperature effect on photosynthesis.

Vertical profiles of soil temperature for every time step were linearly interpolated from observations made at 10 and 20 and at 50 cm. The thermal regulation of root respiration was then calculated by considering the root biomass profile as given by the root fraction (Eq. (17)) and the total root biomass (Table 3-2). Then, root maintenance respiration was adjusted to temperature (Eq. (10)) and summed up to calculate the net assimilation. Regarding the limitation due to soil water content, observations at 20 cm depth were extrapolated to the eight soil layers of the model for every time step and used to calculate the plant wilting factor (Eq. (6)).

3.3 Results

Model-independent field measurements and simulation results of net CO_2 assimilation are compared at the leaf scale in 10 min time intervals for selected days. At canopy level, the properly parameterized model (Table 3-1 and Table 3-2) is run under realistic environmental conditions, forced by one year of high quality meteorological data from the meteorological station. The simulation results are assumed to reveal a realistic species-specific net photosynthesis and potential carbon allocation/dry matter production of bracken and *Setaria* which are used to assess the potential growth advantages of the two competing species under realistic environmental conditions.

3.3.1 Assimilation parameter validation

For validation of model parameters related to the calculation of photosynthesis, independent diurnal gas-exchange measurements in the field were compared with simulation results for bracken and *Setaria* for the same days. The root mean square error (RMSE) and the difference of sums (Δ_{sum}) are used for accuracy assessment. Figure 3-7 shows the observed and simulated assimilation for both bracken and *Setaria*. For bracken, the sum of observed values was 300 mmol CO_2 m^{-2} day^{-1}, while simulated values accumulate to 303 mmol CO_2 m^{-2} day−1 (difference of 1%). The RMSE between measurements and simulated values was 1.54 µmol CO_2 m^{-2} s^{-1}. The

Pearson's product moment correlation coefficient was 0.95 (r^2 = 0.91) which shows high association between the paired samples in time. Residuals were considered to be normally distributed after scoring a p-value less than 0.1 in the Shapiro–Wilk test. For *Setaria*, the sum of observed values was 350 mmol CO_2 m^{-2} day^{-1} while simulated values aggregated at 362 mmol CO_2 m^{-2} day^{-1}, pointing to a slight overestimation of model results of 3%. The RMSE was 2.67 µmol CO_2 m^{-2} s^{-1} and the coefficient of determination was 0.82.

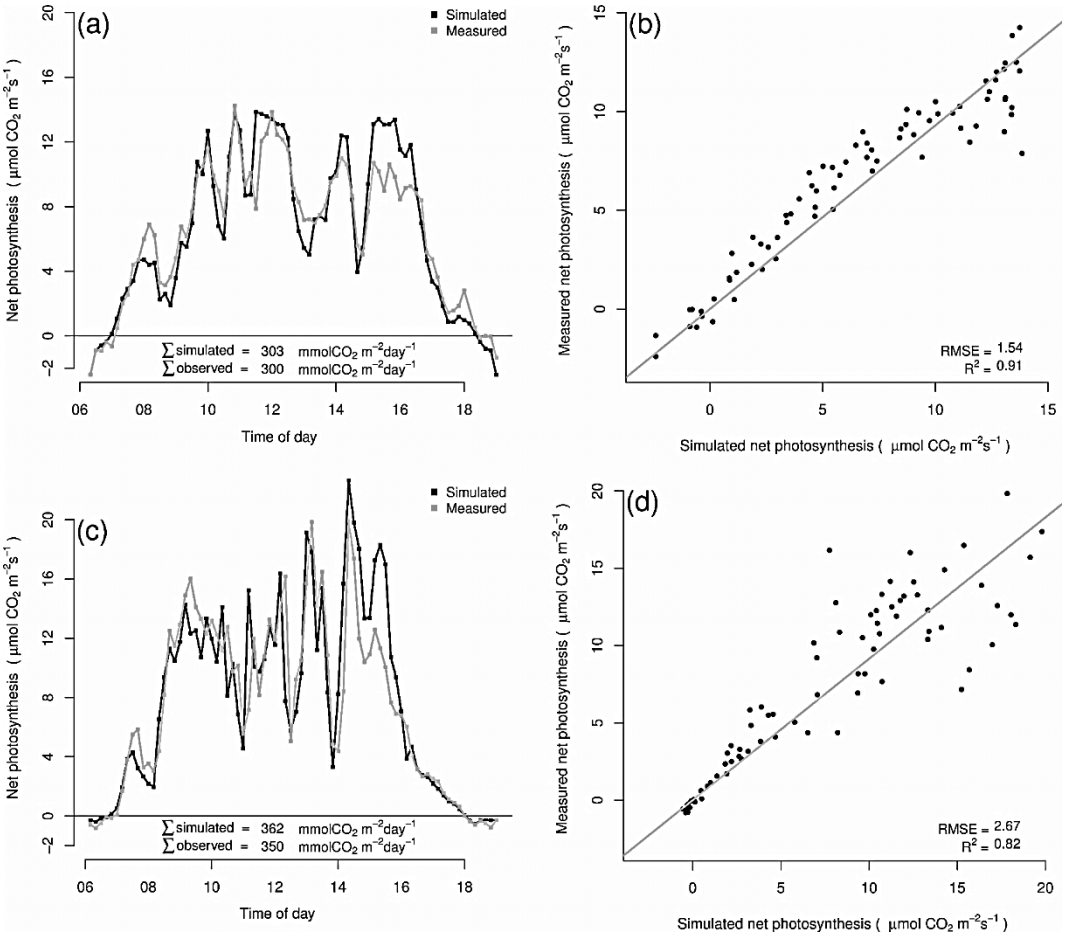

Figure 3-7. Daily measurements of net photosynthesis (in grey) and simulation results (in black) for bracken (a) and *Setaria* (c), including the difference of sums for each diurnal run. Measurements vs. simulations are shown on the right for bracken (b) and for *Setaria* (d) including the coefficient of determination.

3.3.2 Model run with realistic meteorological forcing

The canopy assimilation and the total respiration (including root respiration) resulting from the one-year model run are shown in Figure 3-8.

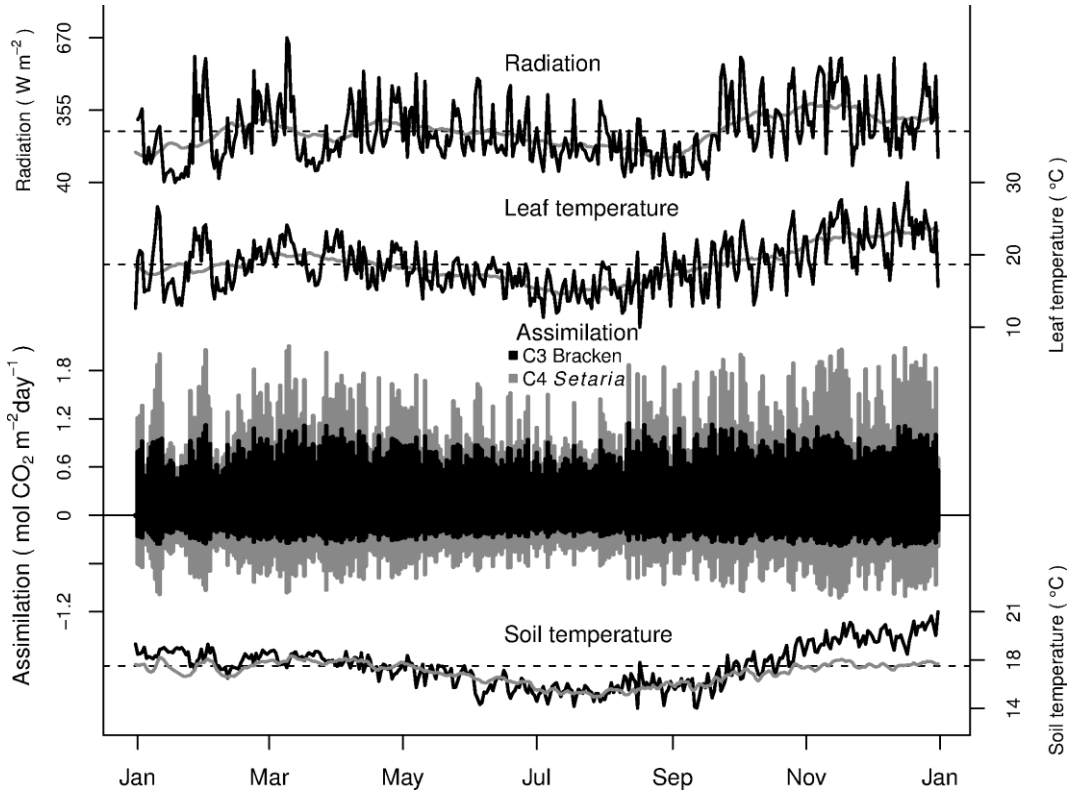

Figure 3-8. Daily means of canopy gross assimilation (positive bars) and total respiration (negative bars) for bracken (black bars) and *Setaria* (grey bars) throughout the year 2008. Main climatic variables are displayed in lines: (top) daily mean of incoming shortwave radiation, (middle) leaf temperature and (bottom) soil temperatures (black: −15 cm; grey: −50 cm) and soil water content at −20 cm. With exception of soil temperature lines are superimposed by a moving average (time lag of one month) shown in grey.

The model results show that *Setaria* is characterized by higher assimilation and respiration rates over the whole year in comparison to bracken under realistic meteorological forcing. Annual sums for *Setaria*/bracken are 430/283 mol CO_2 m^{-2} a^{-1} of gross assimilation and 158/91 mol CO_2 m^{-2} a^{-1} of respiration losses. However, annual net assimilation reveals a slight advantage for *Setaria* over the year, with 217 mol CO_2 m^{-2} a^{-1} in comparison to bracken with 191 mol CO_2 m^{-2} a^{-1}. Daily averages of net

assimilation are 522 mmol CO2 m−2 day−1 for bracken and 593 mmol CO2 m−2 day−1 for Setaria.

With regard to temperature, it can be observed that the grass Setaria is more affected by the colder conditions in the middle of the year than the bracken fern. This reflects the higher sensitivity of Setaria photosynthesis to lower temperature which is well known for C4-species. The statistical mode of air temperature at canopy level recorded at the study site during the period of the daily maximum (10:00–14:00 local time) varies from 19.5 °C in the warmest period of the year (ON) to 16 °C during the coldest period (JJA). Corresponding values of average leaf temperature were 23 °C and 18 °C for the coldest and warmest period, respectively. It is also clear from the temperature function that the higher activation energy of Setaria relative to bracken (Table 3-2) results from the more pronounced temperature dependence of the carboxylation rate. It directly affects canopy assimilation of both species, leading to lower photosynthesis in the colder rainy periods (particularly in JJAS). At the same time, root respiration is reduced as a response to lower soil temperatures in the cold season particularly for Setaria, with positive effects on net assimilation. The decrease of photosynthesis and respiration was more evident for Setaria than for bracken and thus, bracken has a more constant balance throughout the year. Consequently, *Setaria*'s net assimilation is more sensitive to intra-annual temperature variation than that of bracken.

With regard to solar radiation, *Setaria* profits from its C4-pathway particularly on sunny days, while assimilation on cloudy days is often not exceeding the capacity of bracken. The relatively long cloudy period from June to September reveals a higher decrease of gross assimilation in comparison with the reduction of respiration for both species. The same can be observed in Figure 3-9 which shows the integral assimilation for each day against total incoming solar radiation for the same day. The higher light-use efficiency of the *Setaria* grass is evident. Higher respiration levels balance this advantage, favouring bracken under totals of daily solar radiation below 12 MJ m^{-2} day^{-1}. A similar comparison may be made regarding variations in temperature. A stronger dependency of *Setaria* photosynthesis was observed on daily averages of solar radiation in comparison with temperature (Figure 3-10). Situations favouring bracken occur only at temperatures less than 17 °C.

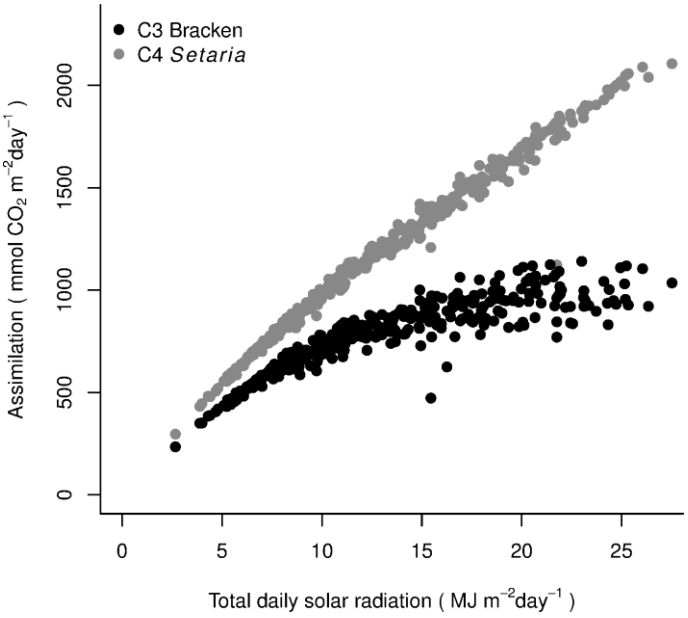

Figure 3-9. Relationship of daily gross assimilation to total global solar radiation observed over the year for bracken (in black) and *Setaria* (in grey).

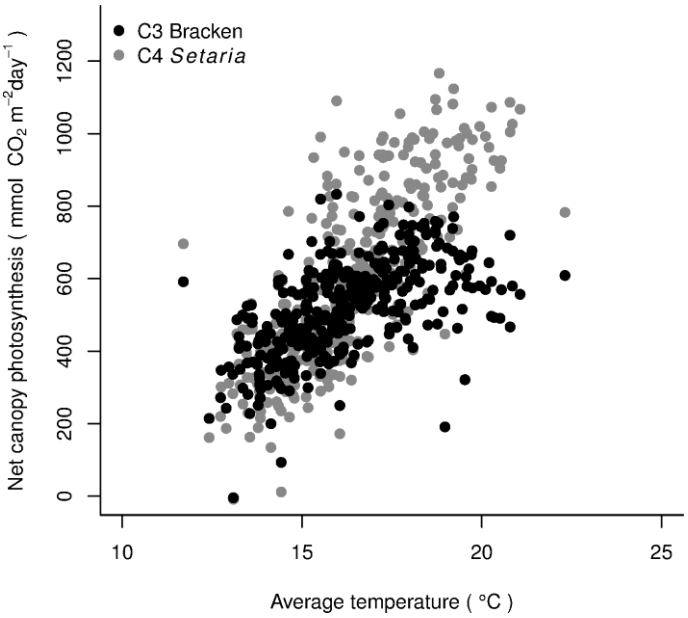

Figure 3-10. Relationship between daily canopy net photosynthesis and average temperature observed over the year for bracken (in black) and *Setaria* (in grey).

The simulated annual course of dry matter production is shown in Figure 3-11. Using the corresponding conversion factors from Table 3-2, the annual dry matter production of bracken is 5554 g m^{-2}, while *Setaria* produces 5879 g m^{-2}. The production generally follows the shape of the annual course of

assimilation and respiration and shows a slight difference between bracken and *Setaria*. An analysis of the details shows that the growth of *Setaria* particularly decreases during the colder and rainy season (May to August and between January and March) while *Setaria* can produce more dry-biomass than bracken only on warmer and sunny days in the relative dry season. It is also obvious that on colder or very cloudy days, dry matter is even produced by *Setaria*, but bracken is more productive at a quite constant level during such weather conditions.

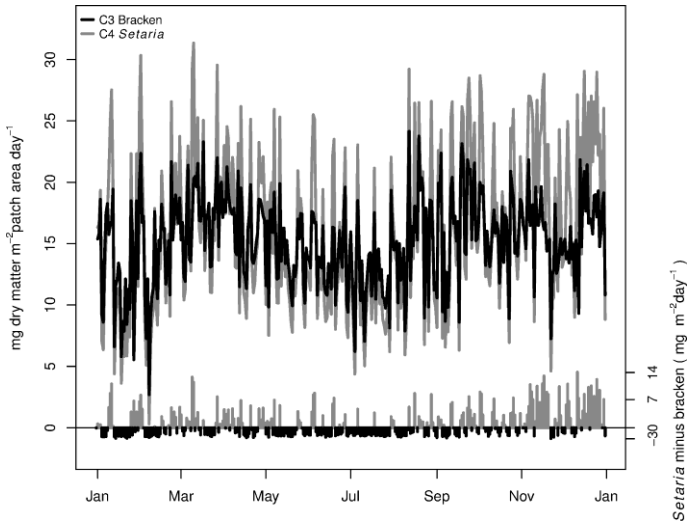

Figure 3-11. Dry matter production of bracken (in black) and *Setaria* grass (in grey) calculated over the year 2008. The bars (bottom) show the difference between the biomass increments of *Setaria* and bracken (*Setaria* minus bracken).

3.4 Discussion

The main aim of the current study was to improve and to properly parameterize a numerical model to calculate net assimilation of two species (bracken and *Setaria*) under realistic meteorological conditions.

Regarding the day runs, validation shows that the results are better than in several similar studies (refer e.g. to White et al., 2000) and in the range of expected accuracies of well-parameterized models as e.g. presented in Müller et al. (2009), Chen et al. (1994), and Vuichard et al. (2010). However, by comparing the observed and simulated assimilation curves in detail, it can be noted that the model results at distinct timesteps significantly deviate from the observed values. A possible source of uncertainty in validation data may be due to heterogeneity of stomata aperture over the leaf surface which could

change along the day (Long and Bernacchi, 2003). Despite these uncertainties, validation results correspond very well with the observed and simulated photosynthesis of both species (r^2 = 0.87–0.91). To illustrate good agreement, one may compare the slightly higher correlation of coefficient (r^2 = 0.88–0.92) found by Chen et al. (1994) under controlled environment (gas exchange measurements made in laboratory) with that of Leuning et al. (1998) (r^2 = 0.67–0.71), the latter resulted from simulations at the canopy level which is comparable to the design of the current study.

Regarding the annual run, a comparison was made with data on biomass from literature which also includes data from the study site and nearby (Roos et al., 2010). For bracken, aboveground biomass production of about 3 kg m^{-2} a^{-1} was reported in New Zealand (Bray, 1991) and southeast Brazil (Portela et al., 2009). These values are somewhat lower than the simulated value of 5554 g m^{-2} a^{-1} for the study area in Ecuador. Alonso-Amelot and Rodulfo-Baechler (1996) reported a much higher value of about 8.5 kg m^{-2} a^{-1} for the western Andes of Venezuela. Unfortunately, productivity was not measured for the same year of simulation, because of the difficulty of setting two identical plots for consecutive and destructive measurements. However, field observations of standing biomass revealed an average value of 4.4 ± 1.3 kg m^{-2} for bracken. This value can be compared with the present results, since Roos et al. (2010) found well balanced average rates of dying back and regrowth of bracken fronds.

For *Setaria*, the simulated biomass production (5879 kg m^{-2} a^{-1}) also agrees with data from literature and from the study site. In his comprehensive review on the growth of C3 and C4 grasses, Ludlow (1985) reported biomass production by *Setaria* and similar grass species of up to 8.5 kg m^{-2} a^{-1} in the lowland tropics and around 5.5 kg m^{-2} a^{-1} in the temperate region where the environmental conditions are more similar to the highland tropics as the Rio San Francisco Valley at 2100 m asl Hacker and Jones (1969) found an annual production of 3.9 kg m^{-2} a^{-1} for a grass similar to *Setaria*, considering an average of 4 years. Such values may vary significantly. Wong (1990) and Ghosh et al. (2009) presented values for above-ground *Setaria* dry weight production of around 1.2 and 3.2 kg m^{-2} a^{-1}, respectively. For the study area, an average of 5.3 ± 1.6 kg m^{-2} of standing *Setaria* biomass was observed for the study site and year of simulation. As for bracken, biomass growth may be considered close to this value, since the average leaf lifespan is about eleven months. Thus, a close agreement of simulation to observed biomass production can be concluded.

With regard to the climatic response of net photosynthesis in the study area, the model results point out that the pasture grass shows not only higher gross assimilation but also higher respiration rates in comparison to bracken.

As a consequence, canopy net CO_2 uptake of the C3-plant bracken and the C4-plant *Setaria* were close together in 2008. For bracken, total respiration per unit ground area was relatively constant throughout the year, mainly due to only small fluctuations in soil temperature. Significant oscillations were found in gross assimilation and net photosynthesis for *Setaria* from sunny to cloudy and from warmer to cooler periods.

With regard to radiation, *Setaria* is favoured during sunny days which seems at the first glance to contradict bracken's advantage in PAR absorption during sunny days due to the illumination geometry as reported in Bendix et al. (2010). However, the relation of PAR absorption and net photosynthesis is dependent on the radiation use efficiency (RUE). Pakeman et al. (1994) used a RUE value of 1.03 g MJ^{-1} in his model of the bracken in UK (*Pteridium aquilinum*). Pitman (2000) found average values of 2.77 g MJ^{-1}. At the same time, tropical C4 grasses generally show higher values of RUE, up to 4.7 g MJ^{-1} (switchgrass) under adequate soil moisture conditions (Kiniry et al., 1999). With regard to the thermal environment, the reduction of photosynthesis with decreasing temperature for bracken is lower than for *Setaria* and thus favours bracken growth, particularly under cloudy weather.

Overall, the damped response of bracken to the external climatic forcing results in less oscillation in net CO_2 assimilation throughout the year. A stronger and more sensible dependence of *Setaria* on radiation and temperature reflects the higher efficiency of the C4-photosynthetic pathway under favourable weather conditions. Taking the local environmental conditions of 2008 into account, *Setaria* has a slightly higher growth potential.

The simulation results presented in this paper cover the year 2008. However, considering a longer time period, the weather of the year 2008 might not be typical and local or regional climate changes may alter the site-specific growth potential of one or both species in future. The comparison of the weather in 2008 with longer-term averages (Bendix et al., 2008a) shows more days with lower relative humidity during the afternoon, lower temperatures and longer periods of high radiation. Drier conditions than those in 2008 favour *Setaria* because of its higher radiation use efficiency in comparison to bracken.

3.5 Conclusions

This paper has shown that the simulation of photosynthesis for bracken fern and the pasture grass *Setaria* needs a model framework that encompasses specific functions for the C3 and C4 photosynthetic pathways. This is mainly due to the more damped reaction of the C3 bracken plants to changes in

incoming radiation and temperature in comparison to the C4 pasture grass. Additionally, it is necessary to include the photosynthetic responses of both, sunlit and shade acclimated leaves/fronds by applying the same functions. Measurements of photosynthesis under varying thermal conditions are necessary to adjust the temperature dependence function for each species. With the properly parameterized model, good agreement between simulation and observations of net canopy photosynthesis was achieved. The atmospheric forcing of the model by means of a micro-meteorological station allowed the simulation of canopy photosynthesis under realistic ambient conditions. This is one reason for the good correlation between simulated and observed growth yields. However, the competition situation as observed in the field partly points to a slight growth advantage of bracken, which contradicts the higher growth potential of *Setaria*. This might be result of the common land use practise. The grass is grazed by cattle while the fern is mostly left undisturbed, apart from negligible damages by trampling. Thus, removing a major part of the growing biomass of *Setaria* might reduce the competitive strength of the pasture grass. Furthermore, recurrent burning for rejuvenation of the grass and bracken control is also hypothesized to particularly favour the regrowth of bracken after fire. However, the presented photosynthesis model does not yet allow the direct simulation of competition, e.g. as a result of disturbance. Thus, future improvements of the model will consider biomass partitioning and turnover and the influence of relevant growth disturbances (fire, cattle browsing and trampling) as well as the direct above-ground radiation competition of both species.

Acknowledgements

The current study was conducted within the framework of the DFG Research Group FOR 816 "Biodiversity and sustainable management of a megadiverse mountain rain forest in south Ecuador" and was generously funded by the German Research Foundation DFG (BE 1780/16-2; BE 473/38-1 and 2; SCHE 217/14-2). B. Silva would like to thank the Brazilian Council of Technological and Scientific Development (CNPq) for research grants (GDE 290033/2007-1). Further thanks are given to NCI (Loja) for logistic support and the Ministry of the Environment of Ecuador (MAE) for the research permission (No.: 024-IC-AGUA-DPL-MA). We are grateful to Dr. Ute Hamer who kindly provided data on soil texture, to Prof. Dr. Manfred Küppers for providing valuable data on leaf photosynthesis and to Dr. Viviana Horna for helping with the gas exchange measurements. At last we appreciate constructive contributions from anonymous reviewers.

Bibliography

Alonso-Amelot, M.E., Rodulfo-Baechler, S., 1996. Comparative spatial distribution, size, biomass and growth rate of two varieties of bracken fern (*Pteridium aquilinum* L. Kuhn) in a neotropical montane habitat. Vegetatio 125, 137-147.

Baruch, Z., Ludlow, M.M., Davis, R., 1985. Photosynthetic responses of native and introduced C4 grasses from Venezuelan savannas. Oecologia 67, 388–393.

Bendix, J., Rollenbeck, R., Göttlicher, D., Cermak, J., 2006. Cloud occurrence and cloud properties in Ecuador. Climate Res. 30,133–147.

Beck, E., Hartig, K., Roos, K., 2008. Forest clearing by slash and burn. In: Beck, E., Bendix, J., Kottke, I., Makeschin, F., Mosandl, R. (eds). Gradients in a tropical mountain ecosystem of Ecuador. Springer, Berlin, 371–374.

Bendix, J., Rollenbeck, R., Fabian, P., Emck, P., Richter, M., Beck, E., 2008a. Temporal heterogeneities – climate variability. In: Beck, E., Bendix, J., Kottke, I., Makeschin, F., Mosandl, R. (eds). Gradients in a tropical mountain ecosystem of Ecuador. Springer, Berlin, 281–290.

Bendix, J., Rollenbeck, R., Göttlicher, D., Nauß, T., Fabian, P., 2008b. Seasonality and diurnal pattern of very low clouds in a deeply incised valley of the eastern tropical Andes (South Ecuador) as observed by a cost-effective WebCam system. Meteorol. Appl. 15, 281–291.

Bendix, J., Rollenbeck, R., Richter, M., Fabian, P., Emck, P., 2008c. Gradual changes along the altitudinal gradients – the climate. In: Beck, E., Bendix, J., Kottke, I., Makeschin, F., Mosandl, R. (eds). Gradients in a tropical mountain ecosystem of Ecuador. Springer, Berlin, 63–73.

Bendix, J., Beck, E., 2009. Spatial aspects of ecosystem research in a biodiversity hot spot of southern Ecuador – an introduction. Erdkunde 63, 305–308.

Bendix, J., Silva, B., Roos, K., Göttlicher, D., Rollenbeck, R., Nauß, T., Beck, E., 2010. Model parameterization to simulate and compare the PAR absorption potential of two competing plant species. Int. J. Biometeorol. 54, 283–295.

Boland, J.W., Ridley, B., Brown, B., 2008. Models of diffuse solar radiation. Renew. Energ. 33, 575–584.

Bonan, G.B., Levis, S., 2006. Evaluating aspects of the community land and atmosphere models (CLM3 and CAM3) using a dynamic global vegetation model. J. Climate 19, 2290–2301.

Bray, J.R., 1991. Growth, biomass, and productivity of a bracken (*Pteridium esculentum*) infested pasture in Marlborough Sounds, New Zealand. New Zeal. J. Bot. 29, 169–176.

Chen, D-X., Coughenour, M.B., Knapp, A.K., Owensby, C.E., 1994. Mathematical simulation of C4 grass photosynthesis in ambient and elevated CO_2. Ecol Model. 73, 63-80.

Collatz, G.J., Ball, J.T., Grivet, C., Berry, J.A., 1991. Physiological and environmental regulation of stomatal conductance, photosynthesis and transpiration: A model that includes a laminar boundary layer. Agric. Forest Meteorol. 54, 107-136.

Collatz, G.J., Ribas-Carbo, M., Berry J.A., 1992. A coupled photosynthesis-stomatal conductance model for leaves of C4 plants. Aus. J. Plant Physiol. 19, 519–538

Cruz, D.R., Reyes, E.S., Sánchez, J.S., 2009. Effects of meteorological factors on airborne bracken (*Pteridium aquilinum* (L.) Kuhn.) spores in Salamanca (middle-west Spain). Int. J. Biometeorol. 53, 231–237.

da Silva, J.M., Arrabaça, M.C., 2004. Photosynthesis in the water-stressed C4 grass *Setaria sphacelata* is mainly limited by stomata with rapidly and slowly imposed water deficits. Physiol. Plant. 212, 409–420.

Dai, Y., Dickinson, R.E., Wang, Y.-P., 2004. A two-big-leaf model for canopy temperature, photosynthesis, and stomatal conductance. J. Climate 17, 2281–2299.

Dang, Q.-L., Margolis, H.A., Collatz, G.J., 1998. Parameterization and testing of a coupled photosynthesis–stomatal conductance model for boreal trees. Tree Physiol. 18, 141–153.

Ehleringer, J.R., Monson R.K., 1993. Evolutionary and ecological aspects of photosynthetic pathway variation. Annu. Rev. Ecol. Syst. 24, 411-439

Farquhar, G.D., von Caemmerer S., Berry J.A., 1980. A biochemical model of photosynthetic CO_2 assimilation in leaves of C3 species. Planta 149, 78–90.

Farquhar, G.D., von Caemmerer, S., Berry, J.A., 2001. Models of photosynthesis. Plant Physiol. 125, 42–45.

Feddes, R.A., Raats, P.A.C., 2004. Parameterizing the soil – water – plant root system. In: Feddes, R.A., de Rooij, G.H. and van Dam, J.C. (eds.): Unsaturated-zone modelling: Progress, Challenges and Applications, pp. 95-141. Kluwer, the Netherlands.

Fourcaud, T., Zhang, X., Stokes, A., Lambers, H., Körner, C., 2008. Plant growth modelling and applications: The increasing importance of plant architecture in growth models. Ann. Bot. 101, 1053–1063.

Franks, S.W., Beven, K.J., Quinn, P.F., Wright, I.R., 1997. On the sensitivity of soil-vegetation-atmosphere transfer (SVAT) schemes: equifinality and the problem of robust calibration. Agricultural and Forest Meteorology 86, 63-75.

Ghosh, P.K., Saha, R., Gupta, J.J., Ramesh T., Das, A., Lama T.D., Munda, G.C., Bordoloi, J.S., Verma M.R., Ngachan, S.V., 2009. Long-term effect of pastures on soil quality in acid soil of North-East India. Aust. J. Soil Res. 47(4), 372–379.

Göttlicher, D., Obregón, A., Homeier, J., Rollenbeck, R., Nauß, T., Bendix, J., 2009. Land cover classification in the Andes of southern Ecuador using Landsat ETM+ data as a basis for SVAT modelling. Int. J. Remote Sensing 30, 1867–1886.

Göttlicher, D., Albert, J., Nauß, T., Bendix, J., 2011. Optical properties of selected plants from a tropical mountain ecosystem – Traits for plant functional types to parametrize a land surface model. Ecol. Model. 222, 493-502.

Groenendijk, M., Dolman, A.J., van der Molen, M.K., Leuning, R., Arneth, A., Delpierre, N., Gash, J.H.C., Lindroth, A., Richardson, A.D., Verbeeck, H., Wohlfahrt, G., in press. Assessing parameter variability in a photosynthesis model within and between plant functional types using global Fluxnet eddy covariance data. Agric. For. Meteorol. doi:10.1016/j.agrformet.2010.08.013.

Günter, S., Gonzalez, P. , Alvares, G., Aguirre, N., Palomeque, X., 2009. Determinants for successful reforestation of abandoned pastures in the Andes: Soil conditions and vegetation cover. For. Ecol. Manag. 258, 81–91.

Hacker, J.B., Jones, R.J., 1969. The *Setaria sphacelata* complex - A review. Trop. Grasslands 3(1), 13-34.

Harnos, N., Nagy, Z., Balogh, J., Tuba, Z., 2006. Modelling net photosynthetic rate of grassland species and wheat at elevated CO_2 concentration. Appl. Ecol. Environ. Res. 4, 47–53.

Hartig K., Beck, E., 2003. The bracken fern (*Pteridium aquilinum*) dilemma in the Andes of South Ecuador. Ecotropica 9, 3–13.

Hollinger, D.H., 1987. Photosynthesis and Stomatal Conductance Patterns of Two Fern Species From Different Forest Understoreys. J. Ecol. 75(4), 925–935.

Kattge, J., Knorr, W., 2007. Temperature acclimation in a biochemical model of photosynthesis: a reanalysis of data from 36 species. Plant, Cell Environ. 30, 1176–1190

Kiniry, J.R., Tischler, C.R., Van Esbroeck, G.A., 1999. Radiation use efficiency and leaf CO_2 exchange for diverse C4 grasses. Biomass Bioenergy 17, 95–112.

Knorr, W., Heimann, M., 2001. Uncertainties in global terrestrial biosphere modeling, Part I: A comprehensive sensitivity analysis with a new photosynthesis and energy balance scheme. Glob. Biogeochem. Cycles 15, 207–225.

Lenz, K.E., Host, G.E., Roskoski, K., Noormets, A., Sôber, A., Karnosky, D.F., 2010. Analysis of a Farquhar-von Caemmerer-Berry leaf-level photosynthetic rate model for Populus tremuloides in the context of modeling and measurement limitations. Environ. Pollut. 158, 1015–1022.

Leuning, R., 1997. Scaling to a common temperature improves the correlation between the photosynthesis parameters Jmax and Vcmax. J. Exp. Bot. 48, 345–347.

Leuning, R., 2002. Temperature dependence of two parameters in a photosynthesis model Plant, Cell Environ. 25, 1205–1210.

Leuning, R., Dunin, F.X., Wang, Y.-P., 1998. A two-leaf model for canopy conductance, photosynthesis and partitioning of available energy. II. Comparison with measurements. Agr. For. Meteorol. 91, 113-125

Liu, B.Y.H., Jordan, R.C., 1960. The interrelationship and characteristic distribution of direct, diffuse and total solar radiation. Sol. Energy 4, 1–19.

Lloyd, J., Taylor, J.A., 1994. On the temperature dependence of soil respiration. Funct. Ecol. 8, 315–323.

Long, S. P., Bernacchi, C. J., 2003. Gas exchange measurements, what can they tell us about the underlying limitations to photosynthesis? Procedures and sources of error. J Exp. Bot. 54, 2393–2401.

Ludlow, M.M., 1985. Photosynthesis and dry matter production in C3 and C4 pasture plants, with special emphasis on tropical C3 legumes and C4 grasses. Australian Journal of Plant Physiology 12(6), 557-572.

Luo, Y., Medlyn, B., Hui, D., Ellsworth, D., Reynolds, J., Katul, G., 2001. Gross primary productivity in duke forest: Modeling synthesis of CO_2 experiment and eddy-flux data. Ecol. Appl. 11, 239–252.

Lynch, A.H., McIlwaine, S., Beringer, J., Bonan, G.B., 2001. An investigation of the sensitivity of a land surface model to climate change using a reduced form model. Climate Dynamics 17, 643-652.

Marrs, R.H., Johnson, S.W., Le Duc, M.G., 2000b. Control of bracken and restoration of heathland. VI. The response of bracken fronds to 18 years

of continued bracken control or 6 years of control followed by recovery. J. Appl. Ecol. 35, 479–490.

Marrs, R.H., Le Duc, M.G., Mitchell, R.J., Goddard, D., Paterson, S., Pakeman, R.J., 2000a, The ecology of bracken: Its role in succession and implications for control. Ann. Bot. (Suppl B) 85, 3–15.

Medlyn, B.E., Dreyer, E., Ellsworth, D., Forstreuter, M., Harley, P.C., Kirschbaum, M.U.F., Le Roux,X., Montpied, P., Strassemeyer, J., Walcroft, A., Wang, K., Loustau, D., 2002. Temperature response of parameters of a biochemically based model of photosynthesis. II. A review of experimental data. Plant, Cell Environ. 25, 1167–1179.

Mercado, L., Lloyd, J., Carswell, F., Malhi, Y., Meir, P., Nobre, A.D., 2006. Modelling Amazonian forest eddy covariance data: A comparison of big leaf versus sun/shade models for the C-14 tower at MANAUS I. canopy photosynthesis. Acta Amazon. 36, 69–82.

Montaldo, N., Toninelli, V., Albertson, J.D., Mancini, M., Troch, P.A., 2003. The effect of background hydrometeorological conditions on the sensitivity of evapotranspiration to model parameters: analysis with measurements from an Italian alpine catchment. Hydrology and Earth System Sciences 7, 848-861.

Müller, J., Braune, H., Diepenbrock, W., 2009. Complete parameterization of photosynthesis models. In: White, J.W., Wang, E., (eds). An example for barley crop modeling and decision support. Springer, Berlin, 12–23.

Oleson, K.W., Dai, Y., Bonan, G., Bosilovich, M., Dickinson, R., Dirmeyer, P., Hoffman, F., Houser, P., Levis, S., Niu, G.-Y., Thornton, P., Vertenstein, M., Yang, Z.-L., Zeng, X., 2004. Technical description of the community land model (CLM). NCAR Technical Note NCR/TN-461+STR.

Olioso, A., Inoue, Y., Ortega-Farias, S., Demarty, J., Wigneron, J.-P., Braud, I., Jacob, F., Lecharpentier, P., Ottl, C., Calvet, J.-C., Brisson, N., 2005. Future directions for advanced evapotranspiration modeling: Assimilation of remote sensing data into crop simulation models and SVAT models. Irrigation and Drainage Systems 19, 377-412.

Oltchev, A., Cermak, J., Nadezhdina, N., Tatarinov, F., Tishenko, A., Ibrom, A., Gravenhorst, G., 2002. Transpiration of a mixed forest stand: field measurements and simulation using SVAT models. Boreal Environment Research 7, 389-397.

Pachepsky, L.B., Acock, B., 1996. An adequate model of photosynthesis — II. Dependence of parameters on environmental factors. Agric. Sys. 50, 227–238.

Page, C.N., 1986. The strategies of bracken as a permanent ecological opportunist. In: Smith, R.T., Taylor, J.A., (eds). Bracken: ecology, land use and control technology. Parthenon, Carnforth 173–181.

Pakeman R.J., Marrs R.H., Jacob P.J., 1994. A model of bracken (*Pteridium aquilinum*) growth and the effect of control strategies and changing climate. J. Appl. Ecol. 31, 145–154.

Pitman, J.I., 2000. Absorption of photosynthetically active radiation, radiation use efficiency and spectral reflectance of bracken [*Pteridium aquilinum* (L.) Kuhn] canopies. Ann. Bot. 85,101–111.

Portela, R.C.Q., Matos, D.M.S., Siqueira, L.P., Braz, M.I.G., Silva-Lima, L., Marrs, R.H., 2009. Variation in aboveground biomass and necromass of two invasive species in the Atlantic rainforest, Southeast Brazil. Acta Bot. Bras. 23(2), 571-577.

Potthast, K., Hamer, U., Makeschin, F., 2010. Impact of litter quality on mineralization processes in managed and abandoned pasture soils in Southern Ecuador. Soil Biol. Biochem. 42, 56–64.

Richter, M., 2003. Using plant functional types and soil temperatures for eco-climatic interpretation in southern Ecuador. Erdkunde 57,161–181.

Roos, K., Rollenbeck, R., Peters, T., Bendix, J, Beck, E., 2010. Growth of tropical bracken (*Pteridium arachnoideum*): Response to weather variations and burning. Invasive Plant Sci. Manag. doi: 10.1614/IPSM-D-09-00031.1.

Ryan, M.G., 1991. Effects of climate change on plant respiration. Ecol. Appl. 1,157–167.

Schneider, L.C., 2004. Bracken fern invasion in southern Yucatán: a case for land-change science. Geogr. Rev. 94, 229–241.

Shena, W., Wua, J., Kemp, P.R., Reynolds, J.F., Grimm, N.B., 2005. Simulating the dynamics of primary productivity of a Sonoran ecosystem: Model parameterization and validation. Ecol. Model. 189, 1–24.

Thum, T., Aalto, T., Laurila, T., Aurela, M., Kolari, P., Hari, P., 2007. Parametrization of two photosynthesis models at the canopy scale in a northern boreal Scots pine forest. Tellus B 59, 874–890.

Vuichard, N., Ciais, P., Belelli-Marchesini, L., Valentini, R., 2010. New parameterization of a global vegetation model for steppe ecosystem from southern Siberian in situ measurements. Rangel. Ecol. Manag. 63, 51–61.

Wang, Y.-P., Leuning, R., 1998. A two-leaf model for canopy conductance, photosynthesis and partitioning of available energy I: model

description and comparison with a multi-layered model. Agr. For. Meteorol. 91, 89–111.

White, M.A., Thornton, P.E., Running, S.W., Nemani, R.R., 2000. Parameterization and sensitivity analysis of the BIOME-BGC terrestrial ecosystem model: Net primary production controls. Earth Interact. 4, 1–85.

Wong, C.C., 1990. Shade Tolerance of Tropical Forages: A Review. In: Shelton, H.M, Stür, W.W, (eds). Forages for plantation crops (Proceedings 32). ACIAR.

Zeng, X., 2001. Global vegetation root distribution for land modeling. J. Hydrometeor. 2, 525–530.

Zhang, L., Moran, M.D., Brook, J.R., 2001. A comparison of models to estimate in-canopy photosynthetically active radiation and their influence on canopy stomatal resistance. Atmos. Environ. 35, 4463–4470.

Chapter 4

4. Climate Change and its Impact on Current and Future Vegetation Dynamics and Carbon Cycling

Brenner Silva[1], C. Dislich[2], I. Voss[3], K. Roos[4], R. Scheibe[3], P. Vorpahl[5,6], B. Schröder[5,6], A. Huth[2], E. Beck[4], J. Bendix[1]

[1] Faculty of Geography, University of Marburg, Germany

[2] Helmholtz Centre for Env. Research UFZ Leipzig, Dept. Ecol. Modelling

[3] University of Osnabrück, Dept. of Plant Physiology, Germany

[4] University of Bayreuth, Dept. of Plant Physiology and Bayreuth Centre of Ecology and Environmental Research, Germany

[5] Landscape Ecology, Technische Universität München, Germany;

[6] University of Potsdam, Potsdam, Germany

In review: Ecological Studies Book (Chapter 24). Springer, Heidelberg

Abstract

In this chapter, pasture and forest productivity and dynamics are investigated under global climate change impacts. Due to unsustainable management, pasture areas, mostly covered by *Setaria sphacelata*, are invaded by the aggressive Southern Bracken (*Pteridium arachnoideum*). The Southern Bracken Competition Model (SoBraCoMo) was applied to predict the development of the pasture-weed competition under IPCC-SRES A1B conditions. The model and respective physiological observations reveal a higher performance of *Setaria* under global warming. In the forest, a potential increase in precipitation could boost landslide activity and thus affect growth dynamics. The forest-gap FORMIND model predicts a higher fraction of early successional species in tree species composition, which would reduce the aboveground carbon stocks. In summary, climate warming might improve regulating and supporting services on the pasture side (increased carbon

sequestration, higher pasture yield), but also lead to a reduction of above ground carbon stocks in the natural forest.

4.1 Introduction

The future development of vegetation dynamics and components of the carbon cycle sensitive to environmental change should be considered separately for both parts of the ecosystems in the San Francisco Valley, i.e. the natural forest and the pastures as a widespread anthropogenic replacement system. Useful tools to predict an impact of environmental change on vegetation are numerical growth models (Bonan et al. 2003). Process-oriented photosynthesis models allow for an estimation of changes in photosynthesis, biomass and thus, carbon allocation, which is applied to the pasture system. To analyze the dynamics of forest stands under environmental change impacts, process-based forest-gap models can be used. In addition, soil mechanical and hydrological properties as well as tree morphology should be considered, because of the intensity of landslides in the mountain forest. Both model types need extensive parameterization to adapt the models to the local situation. The parameter values were derived from field surveys for single species or representative plant functional types.

Climate change might affect the forest and the pasture in the San Francisco Bio-sphere Reserve (RBSF) in different ways:

- On pastures, an increase of the temperature might stimulate the growth of the C4-type pasture grass *Setaria sphacelata* over that of the C3-type bracken (*Pteridium arachnoideum*) and thus might shift the competitive interaction of both species in favour of the grass. This was investigated by means of temperature-driven runs of the Southern Bracken Competition Model (SoBraCoMo).

- In the natural forest, increase of precipitation may lead to a higher land-slide activity, and thus to an enhanced forest turnover with impacts on carbon sequestration. The effect of the natural disturbance factor 'land-slides' on the dynamics of the natural forest was investigated with the forest-gap model FORMIND.

4.2 Methods

4.2.1 The SoBraCoMo Model

The SoBraCoMo is a canopy-photosynthesis model based on the two-big-leaf approach (Dai et al. 2004). As described by Silva et al (2012), the general compo-nents of the SoBraCoMo are (i) a radiation module, including canopy radiation and radiation partitioning, (ii) a canopy-photosynthesis module, (iii) a respiration module for leaves and subterraneous plant parts, and (iv) a module for conversion of net assimilated CO_2 into biomass (dry matter). All modules are parameterized for two species, the main pasture grass *Setaria* and the Southern Bracken. For the radiation scheme, species-specific optical and morphological plant traits were derived from field measurements (Bendix et al. 2010). The parameterization of the photosynthesis model was done by determining species-specific values of quantum yield and carboxylation rate. To assess the thermal influence on biomass production and the competitive strength at leaf and canopy level, leaf measurements were made under controlled conditions and used to parameterize the SoBraCoMo, which is run at canopy level using meteorological forcing data of the year 2008. Further parameterization concerned respiratory carbon losses and the conversion of net assimilation to dry matter. Environmental forcing of the model is conducted with data of global radiation, air temperature, relative humidity, atmospheric pressure, leaf temperature, wind speed, precipitation, soil water content and soil temperature which were continuously recorded in the field. In the following, the model is applied to calculate scenarios at different ambient temperatures. To force the model the downscaled meteorological data sets of air temperature (for more information on climate scenarios refer to Chap. 19) are used on a daily basis. All variables which are directly dependent on air temperature (soil and leaf temperatures) are projected to the IPCC-SRES A1B scenario periods (Nakicenovic and Swart 2000) by regression analysis. In the regression analysis, the residuals were tested for normal distribution (Shapiro-Wilk test > 0.99) and a linear model was fitted by least-squares between the temperatures of the soil, or the leaf and the average air temperature (reference period).

4.2.2 The FORMIND Model

FORMIND belongs to the class of process-based forest-gap models. It is designed to analyze the dynamics of uneven-aged, species-rich forest stands with a focus on the impact of natural or anthropogenic disturbances on forest structure and composition (Köhler and Huth 2004, Huth and Ditzer 2001). It

has been suc-cessfully applied to various forests throughout the tropics (e.g. Rüger et al. 2008, Köhler and Huth 2010, Pütz et al. 2011). The main processes of the model are the competition for light and space which influences tree growth, tree mortality, and the establishment of young trees. To handle the high number of tree species in the San Francisco valley (many of them are extremely rare), tree species within the model are grouped into seven plant functional types (PFTs) according to selected attributes like maximum attainable diameter or maximum height of tree species. In this chapter we analyzed one forest type, the ridge forest (1900-2100 m asl) harbouring ~70 tree species. A parameterization of the FORMIND model for the ridge forest within the RBSF tropical mountain forest was developed and the pre-dicted forest succession dynamics were examined (Dislich et al. 2009). Data from repeated field inventories (2004, 2005, and 2007) of 4.88 hectares, in which the diameter at breast height (1.3 m) of all trees with diameters > 20 cm was meas-ured, and from 0.12 hectares, in which all trees above 5 cm were measured, were used for model calibration (Homeier 2004).

Landslides are an important natural disturbance factor in the RBSF forest and a strong driver of spatio-temporal vegetation turnover (Restrepo et al. 2003, Wilcke et al. 2003, Bussmann et al. 2008). Apart from different soil mechanical, hydrological and vegetation related factors, precipitation is an important external trigger of landslides (Sidle 1992, Stoyan 2000, Muenchow et al. 2012). The current rainfall in our study area lies around 1800 mm a^{-1} (Rollenbeck et al. 2007). Since the downscaled climate scenarios suggest an increase in rainfall by ~+515 mm a^{-1} (IPCC-SRES scenario A1B), future changes in frequency and/or magnitude of extreme rain events will also affect landslide dynamics. Consequently, we assume shifting landslide regimes under climate change.

In the FORMIND model, landslides are implemented as a spatially explicit form of disturbance (Fig. 4-3a). The local forest succession after landslide disturbance might follow different trajectories (Velázquez and Gómez-Sal 2008, Dislich and Huth, 2012). In the current chapter it is assumed that reduced tree growth on landslide sites occurs due to nutrient limitation (Wilcke et al. 2003). Since it is not clear, to which extent increasing rainfall will affect landslide frequencies, we applied the current landslide frequency as well as doubled and a fourfold landslide frequencies to analyse the effect of changing landslide activity on above ground biomass and tree species composition.

4.3 Results and Discussion

4.3.1 Biomass Production and Competition on the Pastures upon Local Warming

For the comparison of photosynthetic productivity of the two species in the pasture system, temperature is an essential environmental parameter. Photosynthetic performance strongly depends on temperature, especially when comparing a high-temperature C4-type grass (*Setaria*) with a moderate-temperature C3-type species (bracken). Due to a higher photosynthetic efficiency C4-plants often prevail in habitats with warm and humid or dry conditions and high or moderate irradiation, whereas under cooler conditions C3-plants have the edge on photosynthetic biomass production and growth (Sage et al. 1999), particularly because C3-photorespiration decreases with lower temperatures. In our days, the daily average air temperature is 14.8 °C on the pastures (Silva et al. 2012) which is suboptimal for *Setaria*, and thus, should favour the competitive strength of bracken.

The results of the laboratory measurements at leaf level (Fig. 4-1a-c) show that the photosynthetic performance of bracken is better than that of *Setaria* at temperatures below 20 °C when both plants were cultivated at 20 °C (Fig. 4-1a). For measurements with leaf temperatures above 20 °C, the photosynthetic production of *Setaria* increases and outperforms that of the bracken fern. Even more pronounced trends of photosynthetic temperature dependence were observed for plants which were grown and examined at 10, 20 and 30 °C, respectively (Fig 4-1b). In that case the amount of bracken-RubisCO appears to correlate inversely with the temperature, being higher at 10 °C growth temperature than at 20 and 30 °C (Fig. 4-1c). Such an effect of the growth temperature has also been described by Hurry et al. (1995). In contrast, no temperature-related change in the RubisCO amount is apparent in the fodder grass.

In contrast to single leaf measurements of photosynthetic activity, the model describes net photosynthetic CO_2-uptake at the canopy level (Fig. 4-1d-e) which generally confirms the contrasting thermal dependency of CO_2 assimilation for bracken and *Setaria* (Fig. 4-1a-b). For biomass production, the temperature de-pendency of mitochondrial respiration (leaf and root tissues) was calculated as 0.23 and 0.16 μmol CO_2 m^{-2} s^{-1} for bracken and *Setaria* leaves respectively, and as 0.9 and 2.0 μmol CO_2 kg^{-1} s^{-1} for rhizomes and roots of the two species at 20 °C (Silva et al. 2012). At canopy level, the turning point towards a growth ad-vantage of the C4-plant was at a daily mean of the leaf temperatures between 14 and 16 °C. Of course mean daily leaf temperatures are characteristic of the special experimental sites in the San Francisco valley.

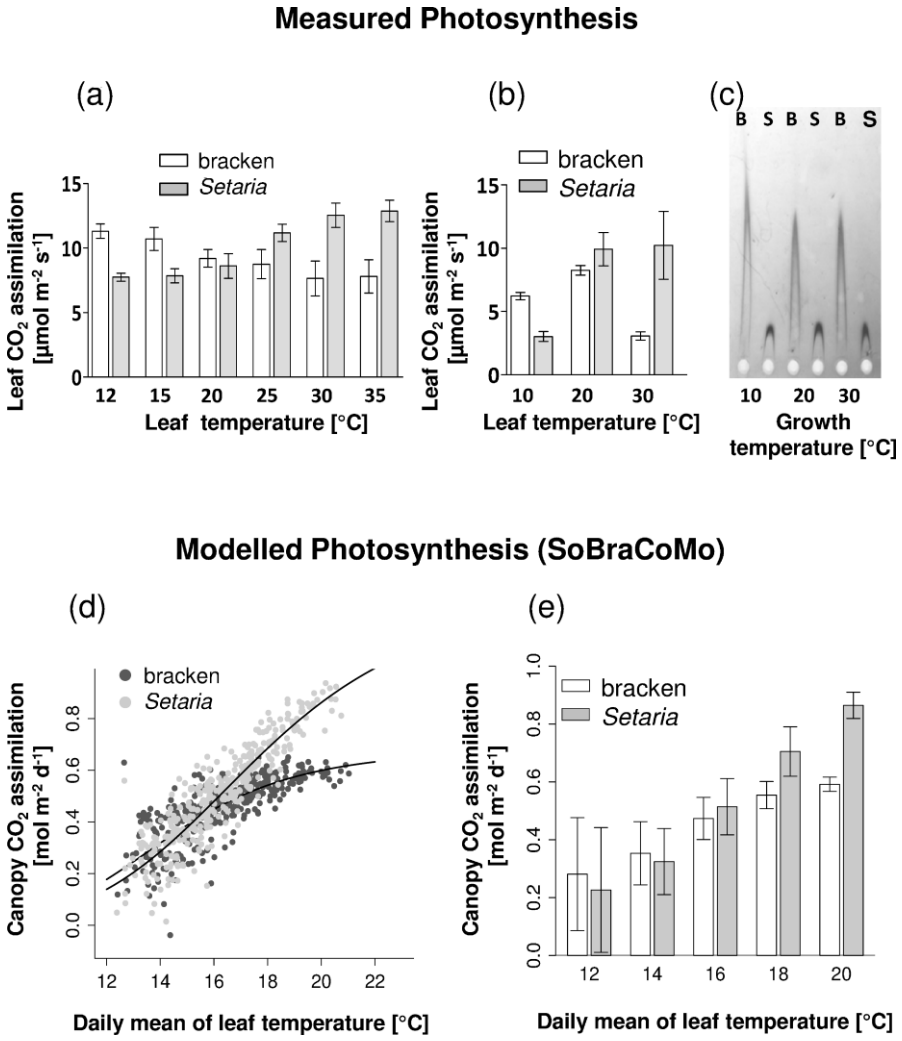

Figure 4-1. Temperature dependency of photosynthesis in Southern Bracken (*Pteridium arachnoideum*) C3-plant) and *Setaria sphacelata* (C4-plant). Measurements (a): Southern Bracken (white bars) and *Setaria* (grey bars) were cultivated at 20 °C, and net CO_2 assimilation was determined at different leaf temperatures at 1200 µmol quanta m^{-2} s^{-1}. (b): Southern Bracken (white bars) and *Setaria* (grey bars) were cultivated at 10, 20, and 30 °C, respectively, at 500 µmol quanta m^{-2} s^{-1}, and CO_2 assimilation was measured at the growth temperatures. (c): Amount of RubisCO protein in leaves of bracken and *Setaria* which were grown under 10, 20, and 30 °C, respectively. The relative amounts of the protein were determined by rocket immuno-electrophoresis of leaf extracts. Simulations (d): Scatter plot of canopy net CO_2 assimilation with daily means of leaf temperature in the year 2008. (e): Canopy net CO_2 assimilation depending on leaf temperature.

Following the most likely IPCC-SRES A1B emission scenario – which presumes a fast growing world population and a balanced use of fossil and non-fossil fuels – and the corresponding ensemble calculations, ambient air temperature at the altitudinal level of the pasture (RBSF meteorological station) will increase by 1.1 °C (σ = 0.5) by 2039, 2.1 °C (σ = 0.6) by 2069 and 2.9 °C (σ = 0.9) by 2099 (Fig. 4-2a).

As a result, global warming might alter the growth potential and competitive strength of bracken and *Setaria* in favour of the grass. Fig. 4-2 (b-d) reveals that particularly *Setaria* can respond to an increase of the temperature by 2.9 °C (year 2099) with an increase of gross CO_2 assimilation from 21 to 47 mol CO_2 uptake per m2 and year whereas increase of bracken photosynthesis will be only from 1 to 2 mol CO_2 m^{-2} a^{-1}. At the same time, respiration losses will also increase differently in both species, being higher in *Setaria* (+ 13%) than in bracken (+ 4%). Biomass production of *Setaria* will double until 2099 while that of bracken, due to a stronger increase of respiration than of gross photosynthesis will slightly de-crease. Notably, according to a steeper rate of temperature increase between 2010 and 2069 the increase in biomass production of *Setaria* will also be higher during that time period than in the course of the following decades until 2099.

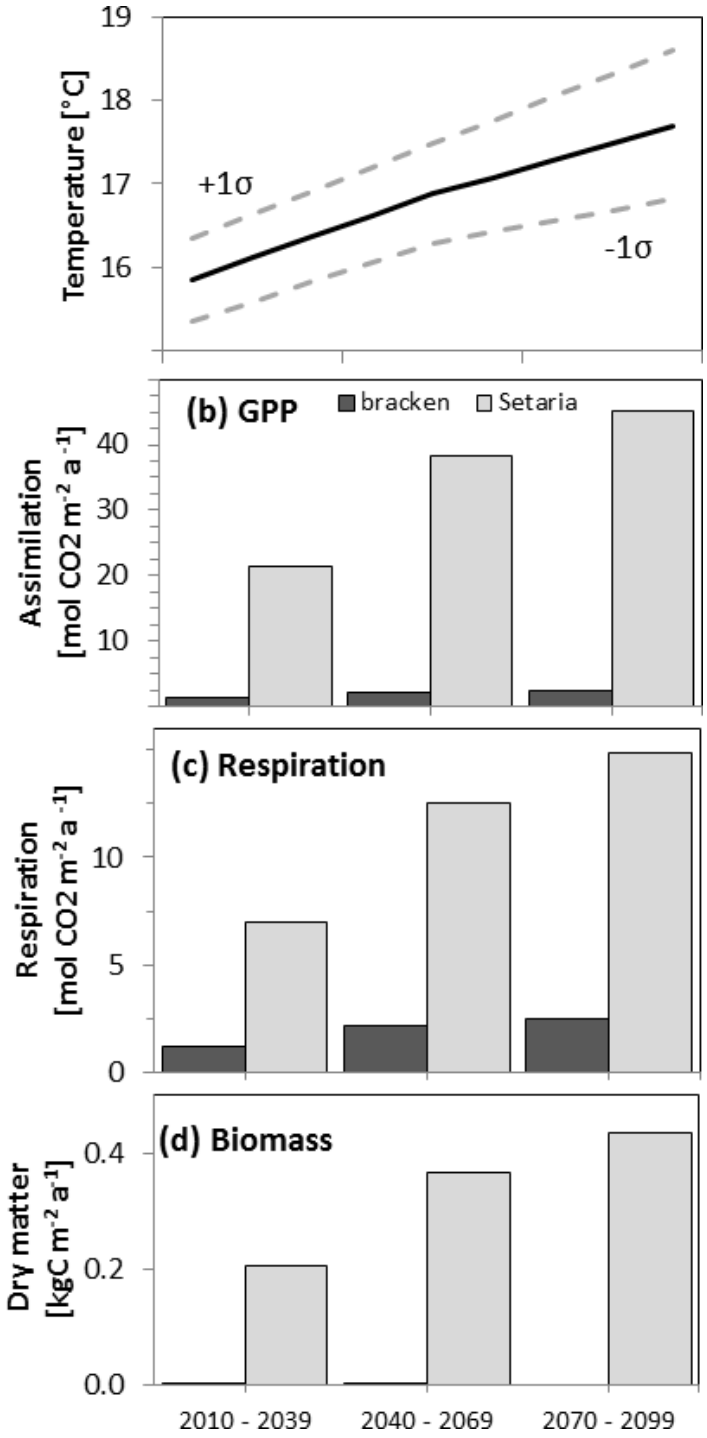

Figure 4-2. Modelled influence of increasing temperatures on *Setaria* and bracken for future years. (a) Air temperature of the research site (at 2 m height) according to the IPCC-SRES A1B scenario (average and standard deviation of 10 models) and (b) resulting changes (= difference be-tween scenario – present day values) of gross photosynthesis (GPP), (c) respiration (sum of maintenance and growth respiration), as well as (d) dry matter production for Southern Bracken and the pasture grass *Setaria*.

4.3.2 Forest Dynamics after Natural Disturbance

The simulated impact of landslides is presented in Fig. 4-3. On the entire surface of the landslide, the complete tree biomass is removed and remains lower than the original one during the first 50 years after the event (Fig. 4-3c). The subsequent accumulation of new tree biomass initially originates from the fast growing pioneer species (PFT 1 and 2) with an increasing share from mid-successional species (PFT 3 and 4) and eventually also from slow growing species (PFT 5, 6 and 7). After 75 years, the overall biomass attains a close to pre-disturbance level, but even after 150 years the composition of the different plant functional types is biased towards fast growing tree species. It takes around 350 years, until all species groups reach their mature biomass. Interestingly, even in the mature ridge forest, the fast growing species (PFT 1 and 2) account for a major share of tree biomass which might be attributed to a generally high frequency of disturbances and poor edaphic conditions that prevent a dominance of late successional species.

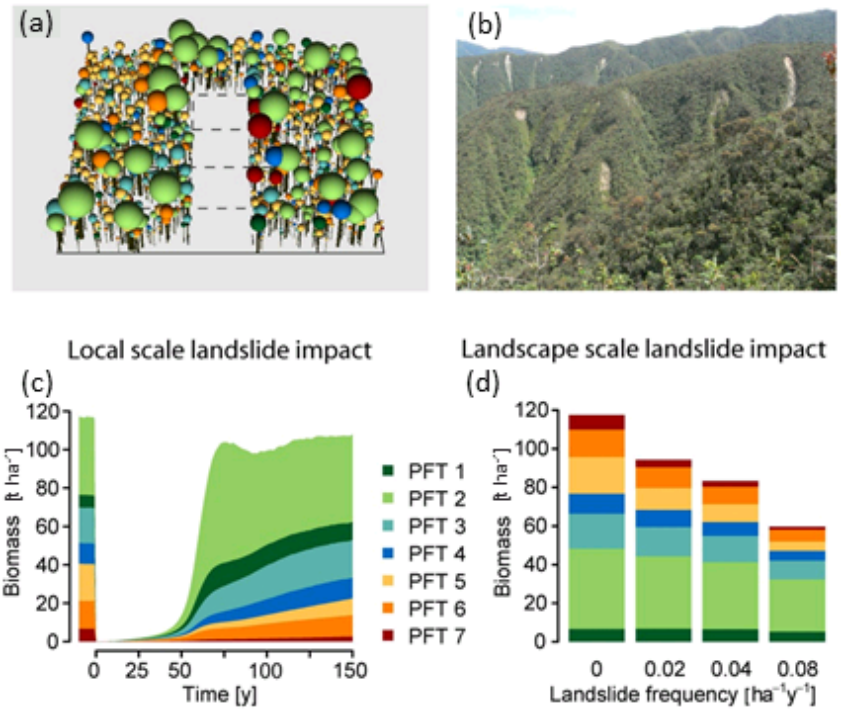

Figure 4-3. Simulated impact of landslides on the forest. (a): Visualisation of the forest model (area 1 ha) with recent landslide disturbance (cf. Dislich and Huth 2012, Fig. 1). (b): Photograph of the RBSF forest with several visible traces of landslides. (c): Simulated accumulation of above-ground tree biomass after landslide disturbance from different plant functional types (PFT). (d): Aboveground tree biomass under different landslide frequencies (current landslide frequency is 0.02 ha^{-1} $year^{-1}$). All simulation runs apply a reduced growth rate of trees on landslide-disturbed areas due to nutrient limitation. The functional types of the tree-species are classified as: fast-growing pioneer species (PFT 1 and 2, green), mid-successional species (PFT 3 and 4, blue), slow growing species (PFT 5, 6 and 7, orange and red).

On the landscape level, landslides increase the heterogeneity of biomass distribution and therefore increase landscape heterogeneity by creating a mosaic land-scape structure consisting of forest patches with different successional stages (Yamamoto et al. 1995, Geertsema and Pojar 2007). The simulation experiment demonstrates the effect of landslides on aboveground carbon stocks in the RBSF forest ecosystem. Applying a realistic current landslide frequency (0.02 landslides per hectare and year) and landslide size distribution which were derived from aerial photographs, the average aboveground tree biomass is predicted as 94 tons per hectare (Fig. 4-3d). An increase of the current landslide frequency following an increase of precipitation reduces the aboveground carbon stocks considerably – doubling

or even quadruplicating the current landslide frequency would result in 12% or 37% less tree biomass, respectively. In the opposite case of diminishing landslide frequencies, the upper limit of tree biomass was calculated as 117 tons per hectare, representing a 25% increase compared to the current biomass. De-pending on the landslide frequency the model predicts changes in the community composition. With increasing disturbance frequency, the relative abundance of fast growing pioneer tree species (PFT 1 and 2) slightly increases at the cost of slow growing species (PFT 5, 6 and 7).

The influence of landslide disturbances on forest productivity is ambiguous – while the area with undisturbed forest productivity decreases due to landslides, the disturbed area provides new space for forest succession, but under unfavourable environmental conditions, like low nutrient availability, instable substrates, and strong exposition to wind (Walker 1994, Walker and del Moral 2003). The investigation of the effect of landslides on forest productivity with the model showed moderate reductions in forest productivity due to this type of disturbance (Dislich and Huth, 2012).

4.4 Conclusion

The performance of the C4-pasture grass *Setaria* under current day thermal conditions of the research area shows that the grass is not optimally adapted for the competition with the C3-bracken fern. Currently, *Setaria* is striving close to the thermal turning point towards a better competitive strength in comparison to bracken which is doing very well. Planting a C3-grass instead of *Setaria* would possibly improve pasture yields, as long as the temperature (and other climate variables will remain the same. With the expected increase in temperature without significant decrease in humidity, however, the growth potential of the C4-grass will steadily increase. Regarding to supporting and regulating services, this means that global warming will foster the growth of the pasture grass, leading to an enhanced carbon sequestration by the pastures. Additionally, the growth advantage of *Setaria* will induce an increase of its competitive strength against the Southern Bracken which should facilitate pasture management, particularly bracken control.

Future changes in precipitation amounts and intensity might affect landslide regimes in the RBSF area. Increased landslide frequencies reduce the aboveground carbon stocks, e.g. a fourfold increase would result in a 37% reduction of aboveground tree biomass. This reduction would be accompanied by changes in the community composition towards a higher fraction of early successional species and species that can tolerate the harsh conditions on landslide sites (e.g. *Clethra revoluta*, *Tibouchina lepidota*).

Naturally, landslide occurrence does not only depend on the rainfall regime. Various other biotic and abiotic triggering factors of landslides, for example soil characteristics and wind, will also have to be taken into account to predict changes in future landslide frequencies (Chap. 12, Vorpahl et al. in press). To analyze the effect of landslides on the entire ecosystem carbon cycle, the influence of this particular disturbance type on soil carbon dynamics is an additional important aspect that needs to be considered. Landslides induce increased soil erosion and contribute to landscape evolution over long timescales (Walker and Shiels, 2008, Muenchow et al. 2012).

The investigated changes of landslide regimes are just one facet of change that might affect forest carbon cycles in the future: increasing temperatures might lead to an upward shift of species, and changes in precipitation as well as remote fertilization (cf. Chap. 23) might change species composition. Predicting such changes is much more difficult for the highly diverse forest ecosystem compared to the pasture system due to the extremely complex interactions (across and within different trophic levels). In this sense we are still at an early stage of understanding future regulations of important ecosystem services like carbon sequestration and carbon storage capacity in tropical mountain forests.

Acknowledgments

The authors are indebted to the German Research Foundation (DFG) for funding the Research Unit 816 (projects BE 1780/16-2, BE 473/38-1, Hu 741/4-2, SCHE 217/14-2 and SCHR1000/4-1). The first author B. Silva would like to thank the Brazilian Council of Technological and Scientific Development (CNPq) for research grants (GDE 290033/2007-1). We thank Rütger Rollenbeck (Univ. Marburg) and Nicolas König (Univ. of Osnabrück) for their help in the field experiments on the pastures.

Bibliography

Bendix J, Silva B, Roos K, Göttlicher D, Rollenbeck R, Nauß T, Beck E (2010) Model parame-terization to simulate and compare the PAR absorption potential of two competing plant species. Int J Biometeorol 54: 283–295

Bonan, GB, Levis S, Sitch S, Vertenstein M, and Oleson KW (2003) A dynamic global vegeta-tion model for use with climate models: concepts and description of simulated vegetation dynamics. Global Change Biol., 9: 1543-1566.

Bussmann RW, Wilcke W, Richter M (2008) In: E. Beck, J. Bendix, I. Kottke, F. Makeschin, R. Mosandl (eds): Gradients in a Tropical Mountain

Ecosystem of Ecuador. Ecol. Stud. 198: Gradients in a Tropical Mountain Ecosystem of Ecuador. Springer, Berlin, pp. 319-330

Dai Y, Dickinson RE, Wang Y-P (2004) A two-big-leaf model for canopy temperature, photo-synthesis, and stomatal conductance. J Climate 17: 2281–2299

Dislich C, Günter S, Homeier J, Schröder B, Huth A (2009) Simulating forest dynamics of a tropical montane forest in South Ecuador. Erdkunde 63: 347-364

Dislich C, Huth A (2012) Modelling the impact of shallow landslides on forest structure in tropical montane forests. Ecol Model 239: 40-53

Geertsema M, Pojar JJ (2007) Influence of landslides on biophysical diversity - A perspective from British Columbia. Geomorphology 89: 55-69

Homeier J (2004) Baumdiversität, Waldstruktur und Wachstumsdynamik zweier tropischer Bergregenwälder in Ecuador und Costa Rica. PhD-thesis, University of Bielefeld

Hurry V, Keerberg O, Pärnik T, Gardeström P, Öquist G (1995) Cold-hardening results in in-creased activity of enzymes involved in carbon metabolism in leaves of winter rye (Secale cereale L.). Planta 195: 554–562

Huth A, Ditzer T (2001) Long-term impacts of logging in a tropical rain forest – a simulation study. Forest Ecol and Manag 142: 33-51

Köhler P, Huth A (2004) Simulating growth dynamics in a South-east Asian rainforest threat-ened by recruitment shortage and tree harvesting. Climatic Change 67: 95-117

Köhler P, Huth A (2010) Towards ground-truthing of spaceborne estimates of above-ground life biomass and leaf area index in tropical rain forests. Biogeosciences 7: 2531-2543

Muenchow J, Brenning A, Richter M (2012) Geomorphic process rates of landslides along a humidity gradient in the tropical Andes. Geomorphology 139: 271-284

Nakicenovic N, Swart, R (eds, 2000) Special Report on Emissions Scenarios: A Special Report of Working Group III of the Intergovernmental Panel on Climate Change, Cambridge Uni-versity Press, Cambridge, U.K., 599 pp

Pütz S, Groeneveld J, Alves LF, Metzger JP, Huth A (2011) Fragmentation drives tropical forest fragments to early successional states: A modelling study for Brazilian Atlantic forests. Ecol Model 222: 1986-1997

Restrepo C, Vitousek P, Neville P (2003) Landslides significantly alter land cover and the distribution of biomass: an example from the Ninole ridges of Hawai'i. Plant Ecol 166: 131-143

Rollenbeck R, Bendix J, Fabian P, Boy J, Wilcke W, Dalitz H, Oesker M, Emck P, 2007: Com-parison of different techniques for the measurement of precipitation in tropical montane rain forest regions. J. Atmos. Oceanic Technol., 24, 156–168.

Rüger N, Williams-Lineara G, Kissling WD, Huth A (2008) Long-term impacts of fuelwood extraction on a tropical montane cloud forest. Ecosystems 11: 868-881

Sage RF, Wedin DA, Li M (1999) The biogeography of C4 photosynthesis: patterns and controlling factors. In: C4 Plant Biology (eds R.F. Sage & R.K. Monson), pp. 313–373, Academic Press, Toronto, Canada.

Sidle RC (1992) A theoretical model of the effects of timber harvesting on slope stability. Water Resour Res 28: 1897-1910

Silva BSG, Roos K, Voss I, König N, Rollenbeck R, Scheibe R, Beck E, Bendix J (2012) Simu-lating canopy photosynthesis for two competing species of an anthropogenic grassland community in the Andes of southern Ecuador. Ecol Mod : doi:10.1016/j.ecolmodel.2012.01.016

Stoyan R (2000) Aktivität, Ursachen und Klassifikation der Rutschungen in San Francis-co/Südecuador. Diploma thesis, University of Erlangen-Nürnberg

Velázquez E, Gómez-Sal A (2008) Landslide early succession in a neotropical dry forest. Plant Ecol 199: 295-308

Vorpahl P, Dislich C, Elsenbeer H, Märker M, Schröder B (in press) Biotic controls on shallow translational landslides Earth Surf Proc Land.

Walker LR (1994) Effects of fern thickets on woodland development on landslides in Puerto Rico. J Veg Sci 5: 525-532

Walker LR, Shiels AB (2008) Post-disturbance erosion impacts carbon fluxes and plant succession on recent tropical landslides. Plant Soil 313: 205-216

Walker LR, del Moral R (2003) Primary Succession and Ecosystem Rehabilitation. Cambridge University Press, UK

Wilcke W, Valladarez H, Stoyan R, Yasin S, Valarezo C, Zech W (2003) Soil properties on a chronosequence of landslides in montane rain forest, Ecuador. Catena 53: 79-95

Yamamoto S Nishimura N, Matsui K (1995) Natural disturbance and tree species coexistence in an old-growth beech - Dwarf bamboo forest, southwestern Japan. J Veg Sci 6: 875-886

Chapter 5

5. Low-altitude, cost-effective aerial photography of two competing grassland species

Brenner Silva[1], L. Lehnert[1], K. Roos[2], A. Fries[3], R. Rollenbeck[1], E. Beck[2], and J. Bendix[1]

[1] Department of Geography, University of Marburg, Germany

[2] Bayreuth Centre of Ecology and Environmental Research, Germany

[3] Technical University of Loja, Ecuador

Submitted to IEEE-Journal of Selected Topics in Applied Earth Observations and Remote Sensing

Abstract

A cost-effective approach using low-altitude remote sensing and leaf area measurements was developed for monitoring the post-fire canopy recovery of two competing grassland species in an experimental plot. A tethered balloon with a digital camera was deployed to record a time-series of very high-resolution photos of the two species covering the plot: the pasture grass, *Setaria sphacelata*; and the aggressive southern bracken, *Pteridium arachnoideum*. Image processing techniques were combined to solve geometric issues and construct quality mosaics for image classification. A customised automatic classification, based on geometric and textural features of image segments, showed promising results for detecting the invasive bracken fern in *Setaria* pastures. In addition, allometric functions were used to convert the projected cover into species-specific maps of the leaf area index. The developed method constitutes an important and accessible tool for both ecological investigation of competing species in pasture and validation of remote sensing information on mountain environment.

5.1 Introduction

The Andes in southern Ecuador are a global hotspot of biodiversity [1], as is the Rio San Francisco valley, which breaches the eastern Andean cordillera, connecting the provincial capitals of Loja and Zamora [2]. However, the high biodiversity harboured by the natural mountain rain forest is threatened by human activities, in particular the conversion of forest to pasture. Satellite image interpretation has revealed that this problem is especially evident on the lower slopes of unprotected forest areas close to the main Loja-Zamora connection road [3]. On the cleared slopes, the pasture grass, *Setaria sphacelata*, is planted by the local farmers. Unfortunately, an aggressive weed, the southern bracken fern (*Pteridium arachnoideum*), is invading the pastures after recurrent burning, which is the primary pasture management method of the local population. Bracken outcompetes the pasture grass, and the pastures are abandoned, which increases the pressure to clear more of the natural forest [4]. A numerical growth model for both species was developed to determine the mechanism for the competitive dominance of bracken [5],[6]. However, to understand the spatial spread of bracken over time and spatially validate the results of the growth model, an effective tool is required to map the bracken and pasture grass coverage (e.g., in terms of the foliage projective cover). This tool must be adapted to the difficult conditions of a remote, partly inaccessible and steep high-mountain area. Satellite remote sensing might be an option, but spatial and temporal resolution of the current operational sensors (e.g., Quickbird) is not sufficient to delineate the two competing species and the local cloud frequency (>80%) [7] severely complicates image acquisition from space.

In this context, Low-Altitude Remote Sensing (LARS) has the advantage to provide greater details of plant species [8], which can be acquired in near-real time below cloud cover. Depending on the system, investment and maintenance costs are rather marginal, particularly if the unmanned vehicle is equipped with light-weight, low-cost commercial digital cameras [9]. Several approaches based on LARS vehicles are reported in the literature. For instance, deploying kite aerial photography [10] to classify vegetation in mountainous areas, using both supervised and unsupervised methods. Seven different species mixes were successfully delineated by using balloon aerial photography based on a standard 28-mm non-metric camera [11]. True-colour balloon images can also be used either to single-point hyperspectral investigations [12] or to assess the accuracy of a hyperspectral image classification [13]. The latter usually requires LARS platforms with a very large payload [14],[15],[16]. The advantage of balloon-borne vegetation classification is the low-cost of platform and digital cameras, which from

flight levels of 50-80 m, warrant a spatial image resolution of better than 2 cm [17].

The segmentation of different species based on airborne digital images is mostly conducted for trees by using structural information [18],[19]. For scrubby and herbaceous vegetation, a combination of spectral and structural attributes is frequently used for this purpose. Landscape metrics based on balloon aerial photographs were applied to classify Mediterranean vegetation and assess fine-scale landscape fragmentation [20]. Vegetation pattern analysis to investigate the development of spatial heterogeneity was conducted based on a digital Canon IXUS 500 camera by using the supervised maximum likelihood method and pattern metrics, such as the mean patch size and density [21]. For instance, a database containing image examples of 19 weed species was constructed for an active shape model applicable to image classification [22]. Vegetation shape parameters, such as roundness, aspect and perimeter, have been used for species image segmentation [23]. The discrimination between broadleaf and grass plant categories was accomplished by combining a low–level, Gabor wavelets–based feature extraction technique with a neural network–based pattern recognition algorithm [24]. Colour information was also used to discriminate between vegetation and background, whilst shape analysis techniques were applied to distinguish between crop and weed plants [25]. With regard to bracken, several authors have stressed that discrimination might be facilitated by the specific reflectance properties of the fronds [26],[27]. Compared with matorral vegetation, strong relationships were found between pigment concentrations per unit of leaf mass and reflectance in the red, blue, and near-infrared region for bracken [28].

The objective of this paper is to describe a methodology to use balloon-borne, standard digital cameras to delineate two competing species, bracken and the pasture grass, *Setaria*. In the presented methodology the cameras provide non-calibrated images in the visible (RGB) and near-infrared (NIR) spectral ranges, and the species cover was observed in different phases of pasture management; i.e., before and directly after burning, the common pasture management practice in the study area, and after re-growth of the plants. A time-series of image mosaics is recorded and analysed at the different time steps to monitor changes in foliage projective cover. Finally, foliage projective cover is converted into leaf area index (LAI) by using species-specific allometric functions.

The paper is structured as follows. First, we present the study site, balloon-borne photo acquisition and ground measurements. Then, we describe the developed image processing method, which includes stitching of photo-tiles, geometric rectification, image enhancement, segmentation, and

classification of foliage projective cover. Foliage projective cover is then blended with ground measurements to produce LAI maps. Last, validation of the produced maps is presented by using independent ground observations of fractional cover and leaf area.

5.2 Study area, data, and methods

5.2.1 Study area

The current project was conducted in the framework of an interdisciplinary, ecological research project situated at the eastern slopes of the eastern Andean cordillera of southeast Ecuador in the San Francisco River valley (Fig. 5-1) [2]. To investigate the competition between pasture grass and bracken, an experimental site was established for the ecological fire experiment (Fig. 5-2), which was used to develop the low-cost LARS methodology presented in this work. The plot is 50 x 20 m and has a slope inclination of 38 degrees. It is located at S 3° 58′ 18′′ (latitude), W 79° 4′ 45′′ (longitude) at 2,107 m a.s.l.. The plot is mostly covered by the common pasture grass (*Setaria sphacelata*), planted in rows, and the invasive southern bracken (*Pteridium arachnoideum*). The area was completely burned in September 2008 and again in November 2009 to mimic the current pasture management practice of recurrent burning and to evaluate its impact on vegetation succession. We used the balloon platform to monitor vegetation succession after November 2009.

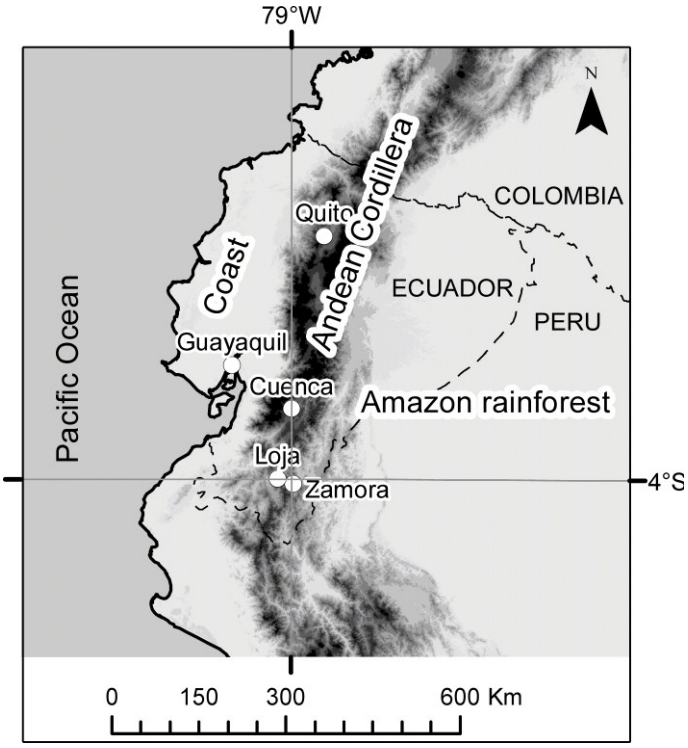

Figure 5-1. Site location.

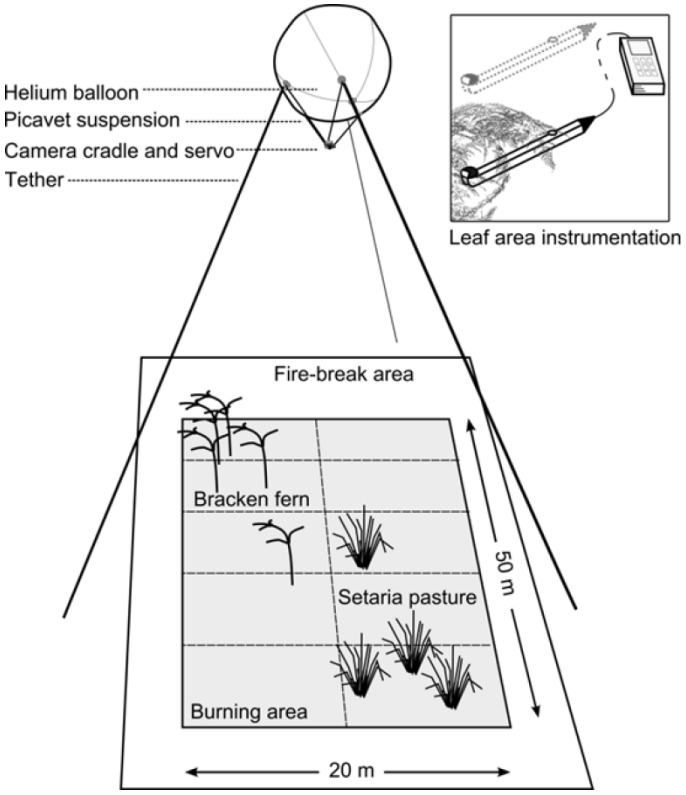

Figure 5-2. Experimental setup.

5.3 Balloon photos and ancillary data

Aerial images were captured with a standard digital camera (Ixus-90; Canon, Inc., Tokyo, Japan) mounted on a tethered, 3 m^3 helium balloon, which can lift a 1.3 kg payload. The camera was attached to the balloon with an automatic shutter using a light metal frame and a cross-wired *picavet* [29]. A second camera, modified with an IR transmitting filter RG715 (SCHOTT AG, Mainz, Germany), was deployed on a consecutive flight to obtain images in the near-infrared. The 35 mm-equivalent camera records images of 2736 x 3648 pixels, which, at a height of 35 m, corresponds to a field of view of 26 x 34 m, with 1 cm ground resolution. The total cost of the platform and camera was US$1,200 (€ 900). During each flight, the automatic shutter released one photo every ten seconds while the tethered balloon was towed over the plot. Due to frequent air turbulence, a complete imaging of the target area was only possible using oblique shots at different heights. After each flight, the set of tiles with the best image quality, while covering the entire plot, was visually selected for processing. These photos are referred to as "image-tiles" in the processing workflow (see Section 5.3.3). Table 1 summarises the images and ancillary data used.

Table 5-1. Summary of image and ancillary data. The date of the flight is shown in the leftmost column. "MAB" is the number of months post-burn. "Mode" is the camera mode (VIS: visible; NIR: near-infrared). "Shots" is the number of images captured per flight. "Tiles" refers to the selected image-tiles from shots. Leaf area index (Ground LAI) measurements (n=40 per date and species) are shown by date and "MAB". A summary of the DGPS survey is shown in the rightmost column.

Balloon flight					Ground LAI		GPS
Date	MAB	Mode	Shots	Tiles	Date	MAB	Date
31.10.2009	-1	VIS	156	9	15.03.2008	-1	03.11.2009
		NIR	256	10	18.09.2008	-1	
8.11.2009	0	VIS	166	13	25.09.2008	0	N. Points
		NIR	87	9	28.09.2008	0	36
6.12.2009	1	VIS	161	10	1.12.2008	2	
		NIR	144	8	14.01.2009	4	Horiz. Prec.
14.03.2010	4	VIS	332	3	11.3.2009	6	0.76
		NIR	149	8	24.10.2009	-1	
27.10.2010	12	VIS	535	4	7.11.2009	0	Vert. Prec.
		NIR	185	4	10.11.2009	0	1.36
					15.05.2010	6	
					23.10.2010	12	

5.3.1 Ground control points and elevation model

To facilitate geometric correction, a set of DGPS-located (Differential Global Positioning System) landmarks (10 x 10 m) was installed at canopy height (~50 cm above ground). Additional DGPS coordinates were taken and interpolated using "kriging" to construct a digital elevation model (DEM). The collected DGPS data were processed with a mean horizontal and vertical precision of 0.76 and 1.36 m, respectively. The generated DEM has a grid resolution of 2 cm and is used - as a representation of the bare ground - in the ortho-rectification of the balloon imagery.

5.3.2 Leaf area index data

LAI was measured based on near-hemispherical light transmittance with a LI-COR LAI-2000 Plant Canopy Analyser (LI-COR, Inc., Lincoln, NE, USA). A measuring protocol [30] was used with a view restrictor (45°) and under diffuse light conditions to avoid multiple scattering. Five sample areas (1 m^2) were marked on the ground within a 25 m^2 area predominantly occupied by only one species (bracken or *Setaria*). Four LAI measurements were made for each sample area for a total of 40 LAI measurements for each species per sampling date.

5.3.3 Image processing

The workflow can be divided into three consecutive processing steps, separated by dotted lines in Fig. 5-3. The first processing step (Fig. 5-3, left) is the mosaic construction. Here, the images were processed to reduce contrast between images. Then, the mosaic was obtained by ortho-rectification to the surface. The second process step (Fig. 5-3, centre) is classification. First, the image was enhanced by band differencing. Second, individual segments were delineated. Third, statistics from NIR and RGB images, as well as geometry indices, were calculated to the segments attribute table. The extracted entities were classified into bracken and pasture grass based on the attribute table. Then, the automatically extracted segments were visually classified for validation. The third process step (Fig. 5-3, right) is the conversion of the projective cover to leaf area, which consists of a single step. The LAI data-set was bisected. One set was used to derive the allometric conversion function, and the other was used for validation.

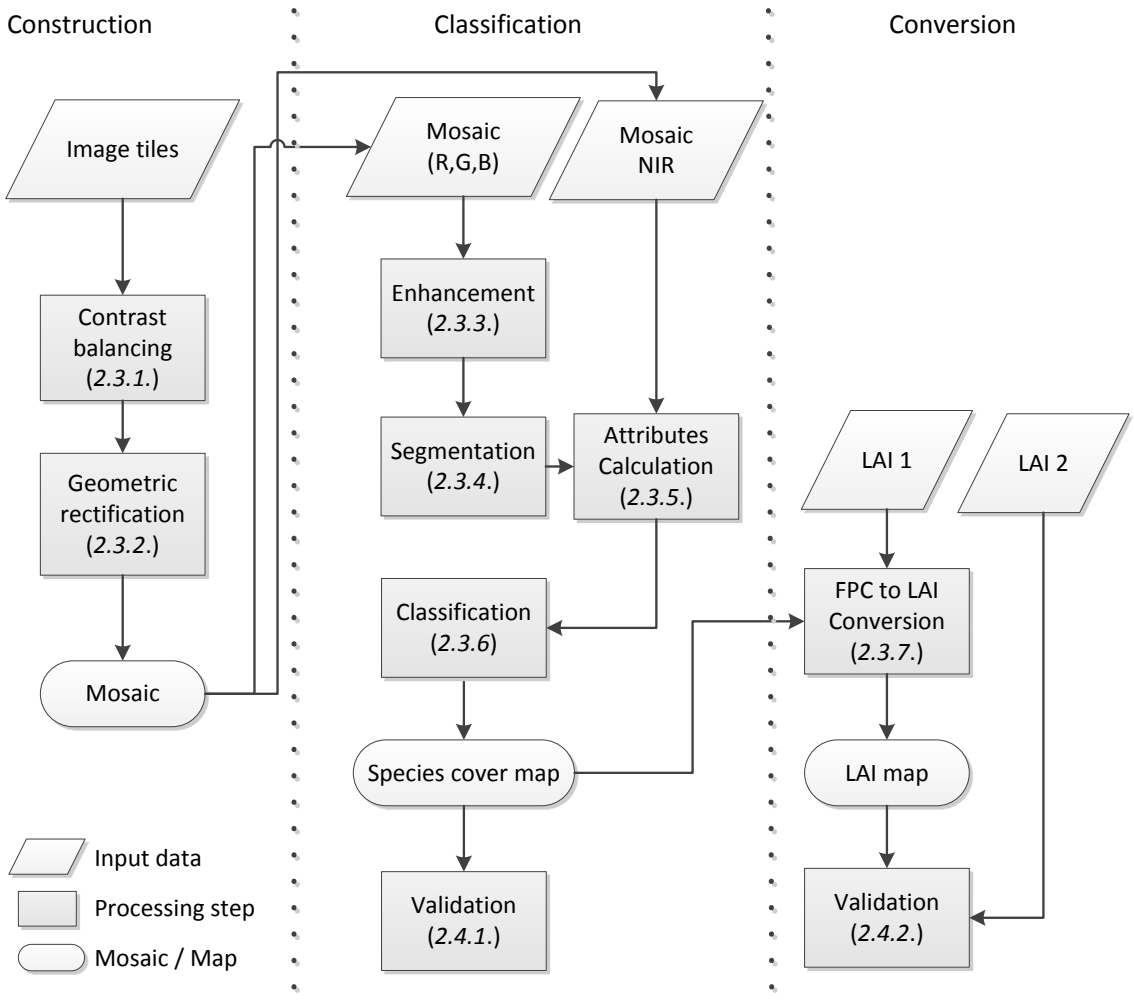

Figure 5-3. Main processing workflow. The numbers in brackets refer to the following sections.

5.3.4 Contrast balancing

To analyse the contrast balancing using the produced mosaics, spectral data and digital photos were taken on ground from fresh green leaves of bracken and *Setaria*. Nine samples of spectral reflectance for each species were collected with the Handyspec-14 field spectrometer (Tec5, AG, Oberursel, Germany) using the method of [31]. The spectral data were integrated to the corresponding spectral ranges of the image-tiles (blue 450-520 nm, green 520-600 nm, red 630-900 nm, NIR 760-900 nm). The same samples were photographed using the balloon digital camera (IXUS-95, Canon, Inc.).

The contrast balancing was done by taking a nearly horizontal image-tile, containing *Setaria* and bracken cover, as reference. The image contrast of each tile was matched to the reference image using the contrast balance method [32]. A comparison between the digital value after contrast matching

and field spectroscopy of the same surfaces (bracken, grass) was made to assure that the relative spectral differences of bracken and *Setaria*, as observed in the mosaic, are realistic. On the final mosaic, 50 digital values were randomly sampled on green leaves of bracken and *Setaria* and compared with spectroscopy and digital photos made on ground.

5.3.5 Geometric rectification

The first step was to obtain a well rectified image, which was based on the digital elevation model (DEM) and DGPS-coordinates. First, the landmark coordinates were used as ground control points (GCP) to ortho-rectify the RGB image of 27.10.2010, which was then taken as reference for assisted rectification of the time-series. Then, we used landmarks and image-to-image GCPs together with the camera constants (field of view) to calculate camera coordinates for each image-tile. Camera coordinates were used to calculate the angle of acquisition for each pixel, which are based on the camera attitude (pitch, roll, and yaw) and the DEM. Fig. 5-4 shows the acquisition geometry of each tile for a single flight in October 2010. In this example, the image mosaic is composed of four image-tiles from which the image number 2 is taken as reference for contrast matching (see Section 5.3.3). Camera coordinates were calculated for each footprint based on the ortho-rectification. A script for visualization of the acquisition geometry (Fig. 5-4) helped to improve the selection of ground control points, for instance, by avoiding areas of high obliquity during the collection of GCPs.

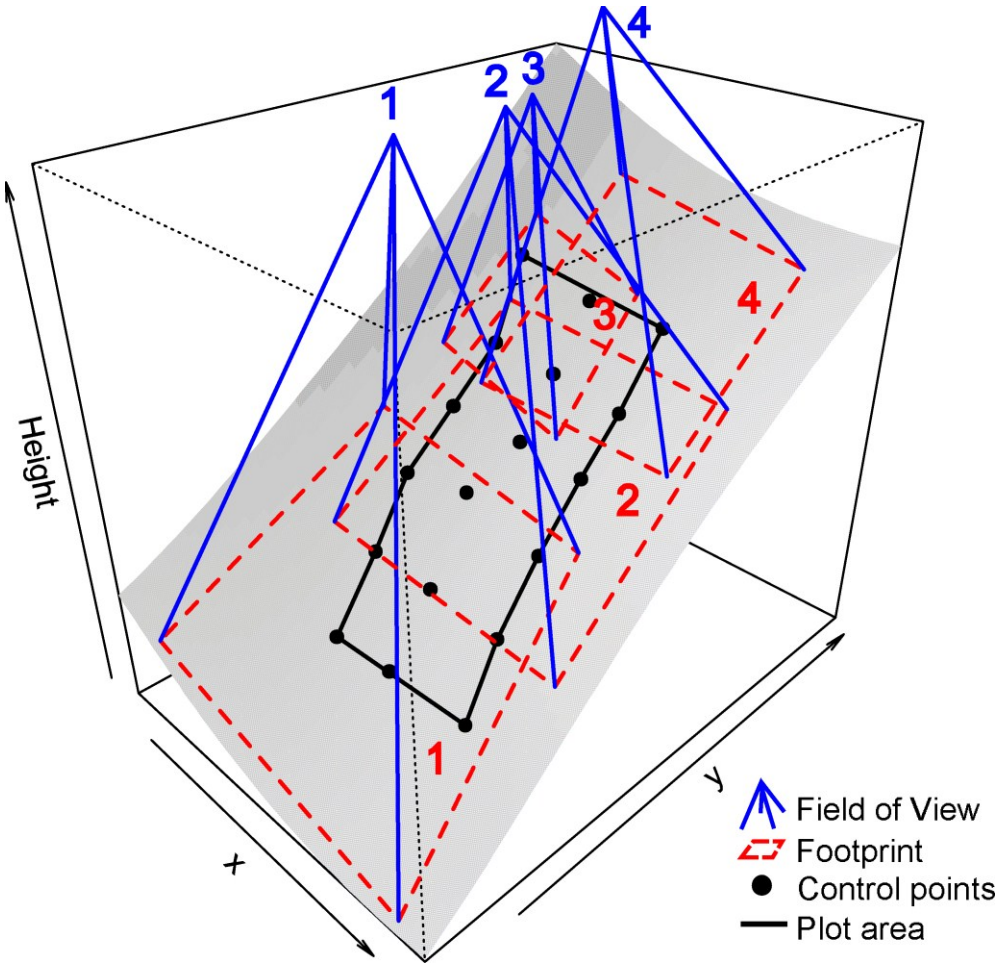

Figure 5-4. Acquisition geometry for flight 27-10-2010.

For each date, the corresponding image-tiles were ortho-rectified using GRASS software [33] and composed into a mosaic. The quality of the ortho-rectification has been recently assessed [34]. We used the root mean square error (RMSE) to estimate spatial accuracy of each mosaic, after ortho-rectification. The mean square error is the average of the squared residuals in the x and y axes for ten additional control points. To construct the time-series, coordinates from image features common to all mosaics were used in the same way to calculate the overall RMSE.

5.3.6 Enhancement

To reduce the RGB bands aiming a single-band based segmentation, band difference images were calculated to enhance green vegetation (1). Enhancement of overlaying green leaves by the chosen bands was already confirmed by spectroscopy [5],[35]. In the non-calibrated camera, the resulting image (*eRGB*) is given as follows:

$$eRGB = 2 \times g - r - b \quad (1)$$

where g, r, and b are the digital values in green, red, and blue channels, respectively. Finally, the image histogram was stretched linearly to obtain a contrast-rich canopy foreground and ground with null values. This resulting image is similar to the NIR-mosaic, but higher in contrast. Therefore the enhanced image (*eRGB*) was used for segmentation, while the NIR-mosaic fed the classification (Section 5.3.3).

5.3.7 Segmentation

Image segmentation by seeded region-growing was applied to the image in successive iterations of two basic steps: (i) the seeding by delineation of initial segments; and (ii) the spatial expansion of the segment by the region growing technique. The first step is similar to that used to detect individual tree crowns using LiDAR data, where the seeds are given by the highest points in the canopy point cloud. Here, the segmentation was based on the enhanced brightness values, which are related to the greenest parts of the canopy, which in this case are mostly central parts of each individual plant. The initial segments resulted from a high cut-off digital value (s_i) applied to the enhanced image. These small initial areas were delineated and used as seeds for region growing [36]. The region growing built the entities limited by a second cut-off value. Next, region growing was applied on the rest of image with a lower cut-off value ($s_{i+1} = s_i - 25$), which was used to include entities with different brightness from previous iteration. The successive thresholding and region growing permitted to control the change from one to the next iteration in either brightness or geometric dimensions.

5.3.8 Attributes calculation

Two sets of attributes representing texture and geometry were calculated and assigned to each image-segment. Image texture was calculated from NIR and the RGB channels based on the pixels within the area of each image-segment. The texture attributes-set were calculated either directly from NIR and RGB images (“mean”, “variance”, “number of horizontal maxima”, “number of vertical maxima”, and “maxima per area”) or derived from a grey-level co-occurrence matrix on the enhanced image. The latter include nine variables (“entropy”, “contrast”, “correlation”, “inverse difference”, “inverse difference moment”, “standardised inverse difference”, “uniformity”, “dissimilarity”, and “maximum”). The reader should refer to [37] for corresponding equations to the texture attributes. Geometry attributes used were “area”, “seed size”, “perimeter”, “height”, “width”, “height”, “compactness”, “circularity”,

“elongateness”, “circularity ratio”, “circularity”, “ellipticity index”, “shape factor”, and “grain shape index”. For the corresponding equations of the geometry attributes see [38].

5.3.9 Classification

The image mosaics were classified individually. Since the grass cover was composed of two species (>97% is “bracken” or “*Setaria*”), a supervised classification based on attributes of the segmented image was applied to detect "bracken" under the "*Setaria*" pasture.

In the classification we used a boosted regression tree (BRT) model [39] and combined the “gbm” package [40] and custom code [41] in R-language [42]. Training sites were segments within two sample areas of 100 m² size, where bracken segments were visually identified. In attribute pairs with a correlation coefficient higher than 0.7, the variable with the lower predictive performance was excluded. Then, the BRT model was fitted to the training sites and run on the entire segmented image. In this approach, the attributes are combined in regression trees by controlling the learning rate and tree complexity until the number of trees in the BRT model reaches 1000. The final result is the probability of each segment to pertain to the class bracken. A separation threshold for the definition of the two classes (bracken and *Setaria*) was chosen based on the highest hit rate on the validation area (see Section 5.4).

5.3.10 Conversion of FPC to LAI

The foliage projective cover (FPC) was calculated from the gap fraction in light transmittance measurements:

$$\mathrm{FPC} = 1 - G \tag{2}$$

where G is the diffuse non-interceptance perpendicular to the ground, or the gap fraction. The difference between G and LAI is in the instrument configuration, which allows tilted measurements of transmittance. While LAI is based on hemispherical gap fractions, G is the transmittance projected to the horizontal plane. Thus, considering measurement assumptions [29] and the foliage orientation, a direct relationship can be used to convert FPC to LAI:

$$\mathrm{LAI} = -\ln(a - \mathrm{FPC}) \times b \tag{3}$$

where a and b are coefficients to be fitted to species-specific LAI and FPC data. These parameters are used to explain the species-specific divergence in the LAI to FPC relation due to the predominant leaf angle of

each species [5]. Because of measurement uncertainties in areas with a sparse plant cover or the extremes in areas of closed vegetation cover, the dynamic range of LAI was limited to that corresponding to 0.15 < FPC < 0.95. In addition, we can assume LAI equals green-LAI for the first year after burning because the average lifespan of *Setaria* leaves and bracken fronds is approximately eleven months [4].

5.4 Validation

5.4.1 Validation of classification:

Validation maps were constructed for two sample areas (100 m² size, disjoint with training sites) by visual identification of bracken segments using the RGB photo-mosaic. To assess the classification accuracy, we calculated the area under the curve (AUC) given by the receiver operating characteristic (ROC) accuracy method [43]. The area under the ROC curve (AUC) express the general probability of a given detection to be correct in the space of all occurrences of hit rate (h) in relation with the false alarm rate (f), which are given by:

$$h = p \div (p + n) \quad (4)$$

$$f = q \div (q + m) \quad (5)$$

where p (true positive) is the fraction of the map assigned to a class (bracken or *Setaria*), which is in agreement with automatic and visual selection of bracken entities. Similarly, m (true negative) is the fraction correctly not assigned to bracken, thus to *Setaria*. The variables expressing disagreements are q (false positive) and n (false negative). The first computes the fraction of bracken incorrectly detected by the automatic classification, but not by the visual interpretation, while n computes the opposite. The AUC is calculated using the Wilcoxon statistic method [43]. Values higher than 0.7 are considered reasonable performances and very good performances are obtained with AUC higher than 0.9 [44]. The final map is given by the selection of a decision threshold, which results in the pair of highest h and lowest p coordinates.

5.4.2 Validation of LAI maps

We used the ground measurements (FPC and LAI) to validate the final FPC maps. From the FPC maps, two extents (5 x 5 m²) containing the ground sample areas were extracted and converted to LAI (see Section 5.5.7). Mean

values were compared with ground data, either directly or after linear interpolation in time. In the validation of LAI, the RMSE was calculated by averaging the square of the difference between LAI measurements and values derived from FPC maps.

5.5 Results

5.5.1 Image acquisition

A time-series of balloon-borne aerial photos from the experimental plot was acquired, processed into image mosaics, and classified to obtain the projective cover of the two species of interest. A summary of acquisition parameters is given in Table 2 and exemplifies the main issue regarding the quality of balloon-borne photos: the instability of the platform. Only in 14-03-2010 was it possible to obtain complete coverage with three photo tiles. For the other dates, the relatively high numbers of photos (from 8 to 13) are due to either obliquity or recording at low height. For instance, the mosaic of 31-10-2009 is composed of nine tiles and has maximum obliquity (roll or pitch) of 22° and a mean height of 21 m. The mosaic of 14-03-2010 has a maximum obliquity of 17° at 23.7 m mean height. Despite the obliquity ortho-rectification resulted the best geometric precision for the mosaic of 27-10-2010 (RGB to NIR) (RMSE = 7 cm).

Table 5-2. Summary of acquisition, post-hoc geometry (maximum roll , maximum pitch, and mean height) and spatial accuracy (root mean square error after geo-rectification) for the VIS and NIR aerial image-tiles.

Date	Max. roll	Max. pitch	Mean height	Geo. RMS
31.10.2009	22	16	21	0.09
8.11.2009	16	9	18	0.10
6.12.2009	19	28	20	0.09
14.03.2010	17	8	23.7	0.08
27.10.2010	-19.1	-4.7	23.9	0.07*
Overall				0.11**

*used as reference for collecting gorund control points.
**calculated based on features common to all mosaics

.

5.5.2 Geometric processing

The acquisition geometry is an indicator of spatial accuracy and mapping quality. The overall displacement of the time-series was 11.1 cm, which is high considering the nominal resolution (2 cm). Consequently, the time-series was considered adequate for analyses only in a grid resolution of 1 meter. The maximum displacement between NIR and RGB was 10 cm. Thus, in the classification step (see Section 5.3.3), the assumption of topological inclusion of NIR image features to the first-image-segments depended on size of objects and acquisition geometry at each location. These relatively high displacement values were mainly due to perspective effects (parallax) on canopy cover. Therefore, the higher the number of tiles or the maximum roll or pitch (Table 2), the lower the quality and spatial accuracy of the mosaic. This concept holds for the calculated height above ground, which is inversely correlated to the number of photo-tiles, but, in this case, increasing the ground sampling distance. Due the combination of these factors, the mapping quality for the study site generally decreased from the centre to the extreme north and south part of the plot.

5.5.3 Relationship between brightness and reflectance

Fig. 5-5 shows the reflectance integrated for the visible (RGB) and near-infrared (NIR) channels of green leaves of bracken and *Setaria*. As observed in the spectroscopy (Fig. 5-5(a)), *Setaria* has higher values in RGB but slightly lower in the NIR compared to bracken. This relationship is reproduced by the non-calibrated camera using the same measuring setup as for spectroscopy (Fig. 5-5(b)). As observed in mosaic 27-10-2010, the relative difference between *Setaria* and bracken are similar (Fig. 5-5(c)). Due to contrast matching, less represented values in the red channel are reduced in comparison to the blue and green channels (Fig. 5-5(c)). However, *Setaria* is still brighter in the visible (especially in the blue and green channels) and tends to be darker than bracken in the NIR channel. Therefore, despite the use of a non-calibrated sensor, relative differences in brightness values between bracken and *Setaria* were maintained for image classification.

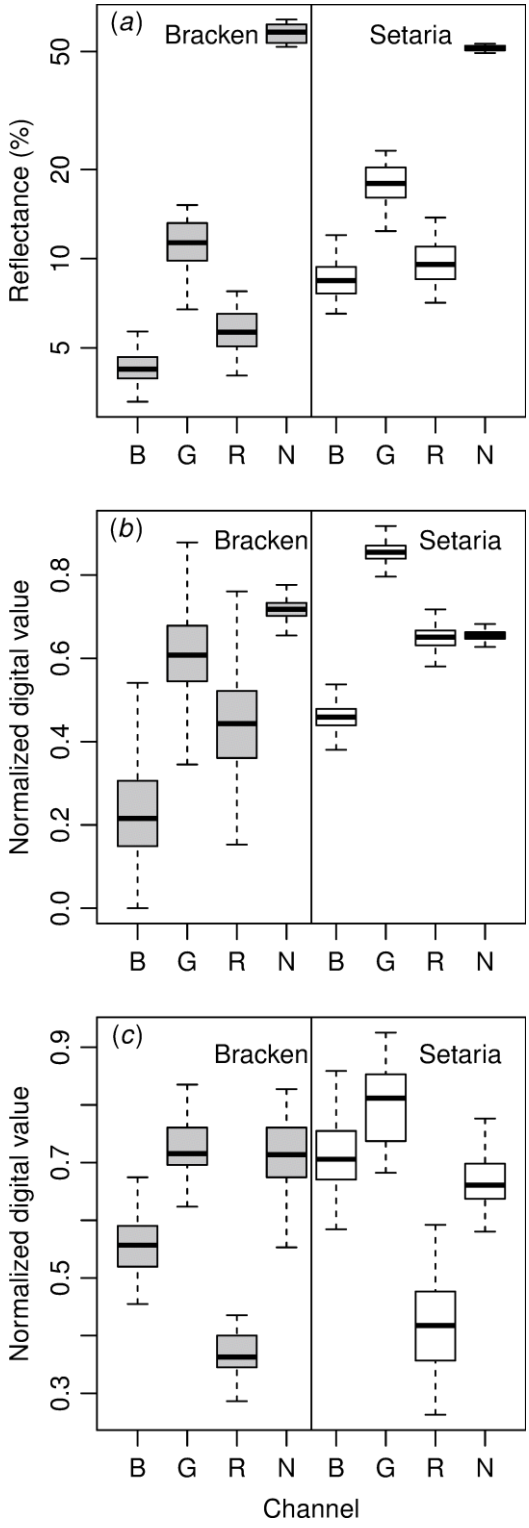

Figure 5-5. Reflectance of green leaves in red (R), green (G), blue (B) and near infrared (N) channels by (a) field spectroscopy, (b) camera digital values measured in the field spectroscopy setup, and (c) camera digital values in the image mosaic of 27-10-2010.

5.5.4 Segmentation and classification

Relative to the RGB image (Fig. 5-6a) a high contrast was observed between green canopies (bright) and the background (dark) after image transformation (Fig. 5-6b). The more leaves were clumped, side by side and/or directly overlaying, the brighter the digital values. These dense, covered areas resulted in the construction of single plant segments, mostly smaller, and segmented in the first segmentation iteration (Fig. 5-6c). Partially overlaying individuals were separated only if digital numbers of all features differed by more than the cut-off value. This pattern was observed in fern fronds, in contrast to *Setaria* leaves. The contrast within the *Setaria* canopy was higher than that of bracken, which led to more than one segment per grass bunch (Fig. 5-6d). Fig. 5-6 shows also the NIR image with the classified segments as overlay. The displacement (~ 10 cm) between NIR and RGB images can be observed. Despite that, in the case of Fig. 5-6, image of 27-10-2010, the BRT-classification pointed the NIR "maxima per area" values and *eRGB* "mean" values as the most important pairwise interaction for classification. It shows that the maximum value can be used to overcome the spatial displacement between the NIR image and *eRGB* derived segments. In general, "texture" contributed more to classification than "geometry". However geometry attributes were significantly important in the two dates of growing phase after fire, which is reflected in the validation.

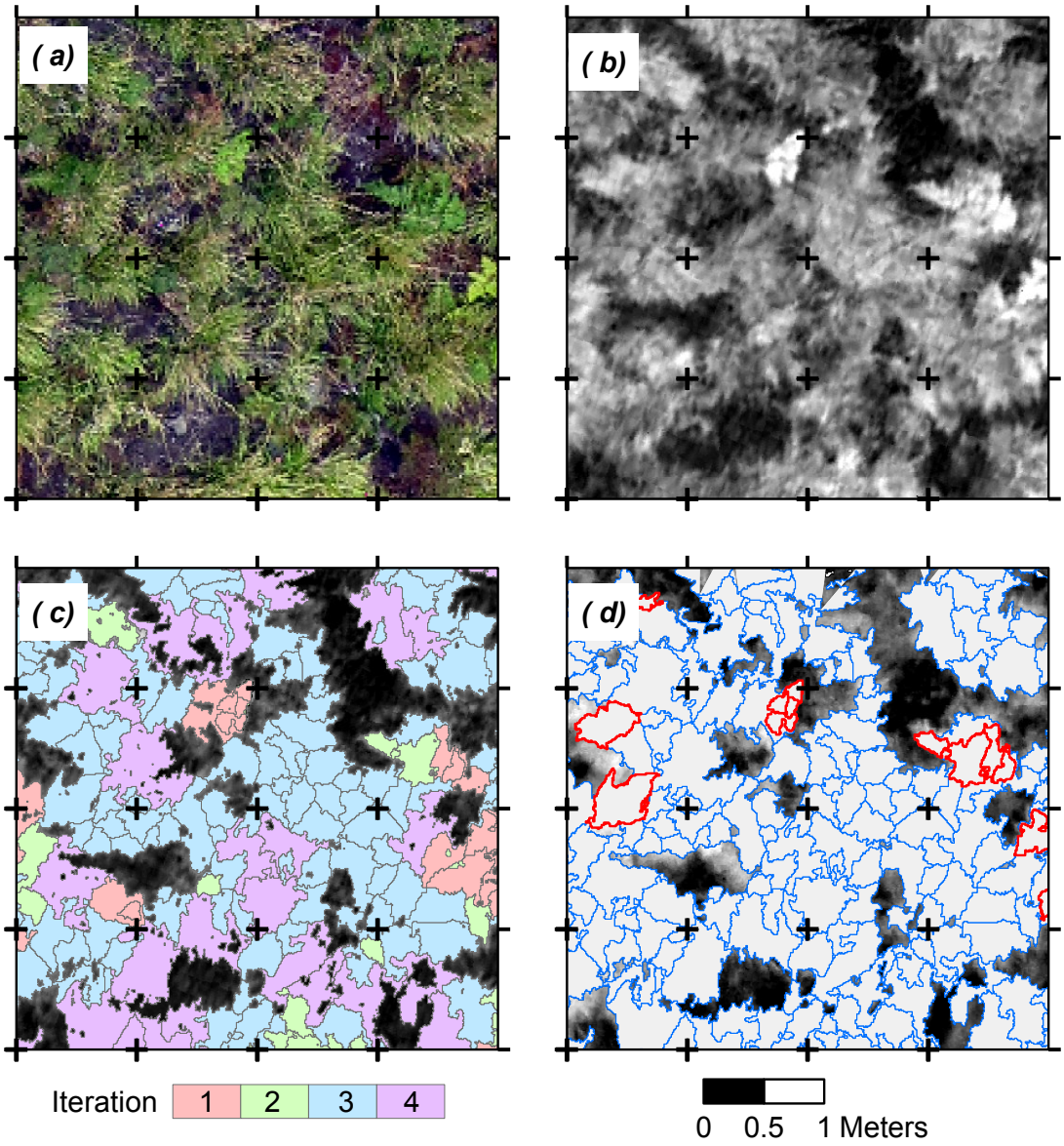

Figure 5-6. Aerial image mosaic (a) before and (b) after enhancement and (c) after segmentation. In (c), objects resulting from four consecutive segmentation steps are shown. In (d) the classified segments are plotted as overlay on the NIR image (bracken fern is in red, *Setaria* in blue).

5.5.5 Validation of classification

Table 3 shows the validation results based on the area under the ROC curve (AUC). Classification performance was between reasonable and very good for the images before (31-10-2009) and after one year (27-10-2010) of canopy recovery after burn. In both situations the densely canopy of *Setaria* resulted in small areas of reflection spots within the canopy in the enhance image. These areas caused confusion with bracken segments, because of the

similarity of patterns found in the attribute table. The time of canopy recovery can be observed in the accuracy table Table 3. Four months after burn (06-12-2009), isolated bracken segments were much easier to classify than when mixed canopies started to cover the area (14-03-2010). The general classification performance is relative high (AUC = 0.88 in average), which corresponds to the detection of bracken fronds in a *Setaria* pasture.

Table 5-3. Area under the ROC curve for the classification of each mosaic/date.

Mosaic	31/10/2009	06/12/2009	14/03/2010	27/10/2010
AUC	0.81	0.99	0.91	0.83

5.5.6 Maps of vegetation development

The time-series of images and canopy cover classification is presented in Fig. 5-7. Image mosaics are shown in line (*a*). Line (*b*) shows the species canopy maps. Lines (*c*) and (*d*) show the maps of foliage projective cover for *Setaria* and bracken, respectively. The plot was completely burned in November 2009 (column (*ii*)). After one month, the recovery of the *Setaria* canopy was faster than that of bracken (column (*iii*)). Field observations showed that the bracken area was occupied by small and sparse unfolded fronds. However, the status after four months (column (*iv*)) shows a more intensive recovery of bracken in the medium term (prior three months). After one year (column (*v*)), the canopy recovered to the pre-burn status with differently distributed bracken fronds in the *Setaria* (south) area. This pattern suggests the sprouting of fronds from the existing living rhizomes, which are present in the whole area.

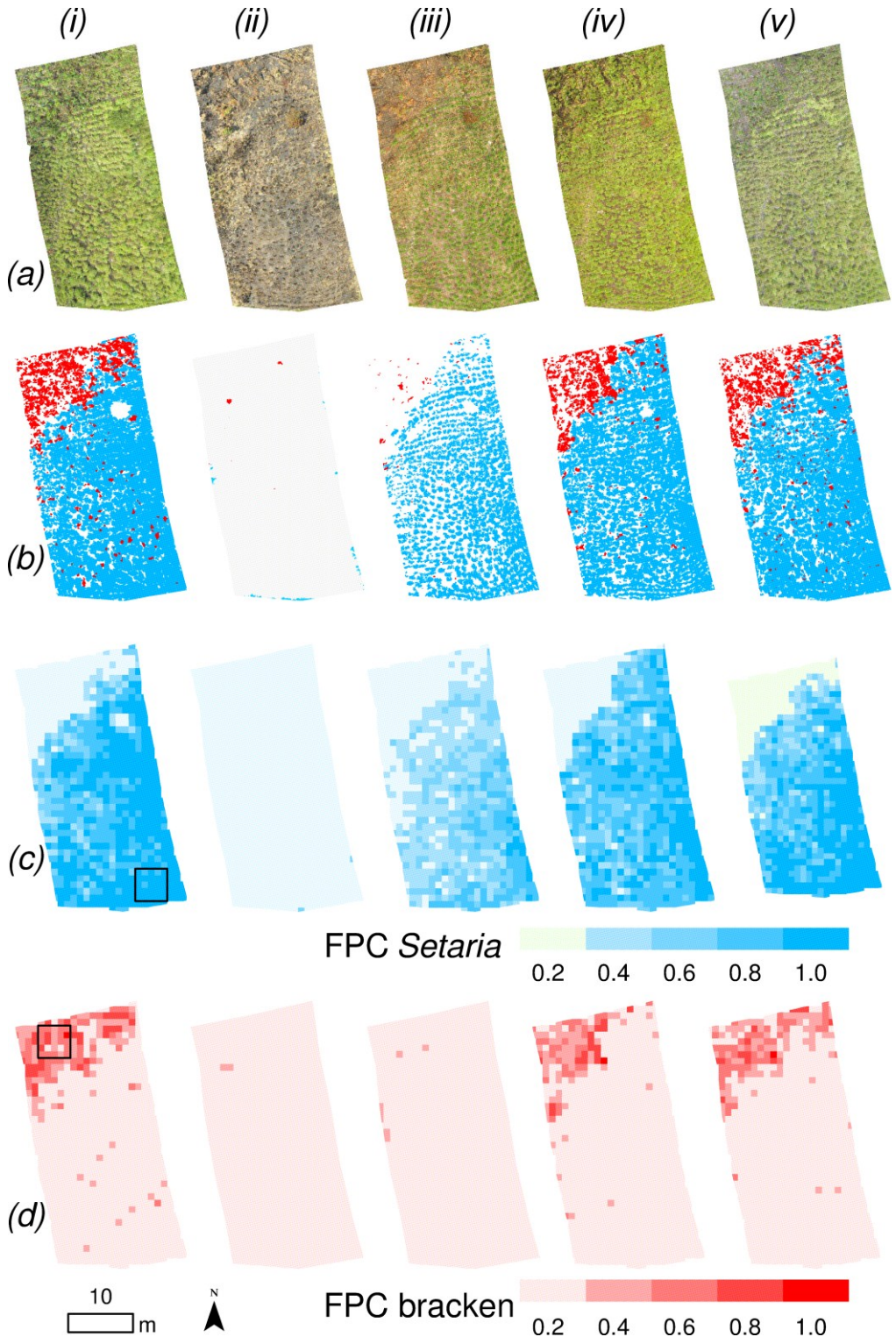

Figure 5-7. Time-series of five dates for the experimental plot. From left to right: time sequence corresponding to balloon flights. From top to bottom: image mosaics, cover maps, and foliage projective cover for *Setaria* (blue) and bracken (red). Areas of ground LAI measurements are depicted in the bottom left FPC maps.

5.5.7 Conversion of FPC to LAI

Fig. 5-8 shows the relationship between ground FPC and LAI data and the conversion function used to calculate the LAI values from FPC values. The more rapid exponential increase of *Setaria* LAI values is due to more vertical leaves in the developed foliage in comparison to bracken. Of great importance for simulation of vegetation productivity, the corresponding species-specific parameters (see Section 5.3.3) are shown in the same Fig. 5-8.

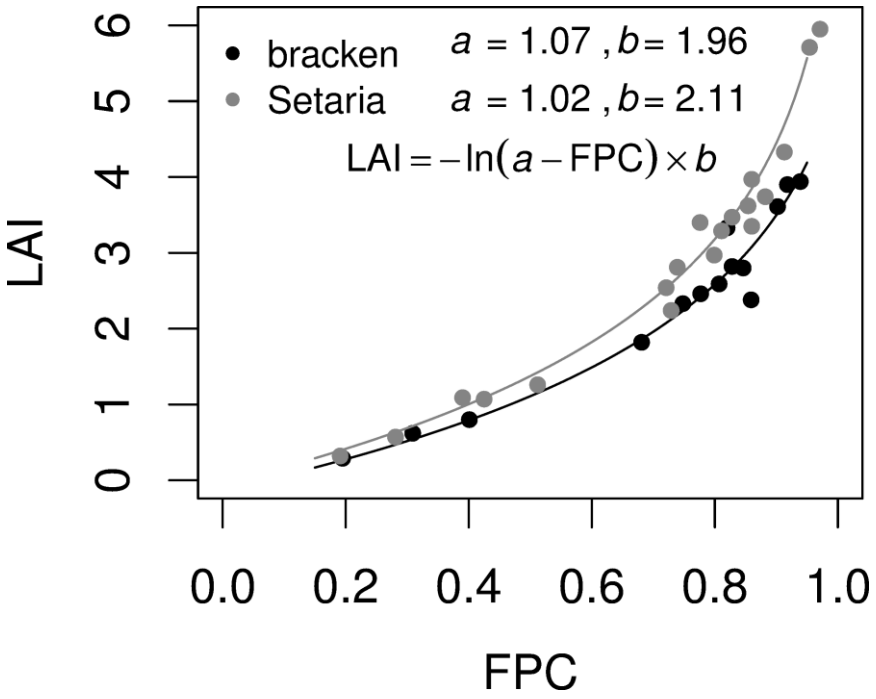

Figure 5-8. Relationship between ground FPC and LAI data; and conversion function calculated for bracken and *Setaria* foliages.

5.5.8 Validation of LAI data

Fig. 5-9 shows the observed LAI values through time, as derived from ground measurements (LAI ground) and FPC maps (LAI balloon). Time is normalised to months after the date of burning ("MAB" in Table 1). In general, LAI-values were underestimated with the species-cover maps derived from balloon photos. One reason is the overlapping of leaves, which is not completely resolved by the conversion function. This effect was stronger in the bracken canopy ((a) and (b) in Fig. 5-9) and was more pronounced in the first months (1 to 6). The presence of unfolded fronds (month 2) and sparse foliage (months 4 and 6) reduced the average area in the balloon-derived FPC and, thus, LAI. For instance, if the maximum FPC value is used, the RMSE decreases to 0.83 for bracken.

The rapid increase in *Setaria* foliage after burning was observed by both ground and balloon data. The variability observed in the averages of *Setaria* LAI ground data after burning is most likely due to non-confirmed assumptions made for LAI measurements (see Section 5.3). However, the deviation shows that the measurements from months 2, 4, and 6 can be considered at the same level, which means that the *Setaria* foliage is already developed after 2 months. To summarise, a better agreement was found for *Setaria* foliage in comparison to bracken, which is expressed by the lower RMSE ((b) and (d) in Fig. 5-9).

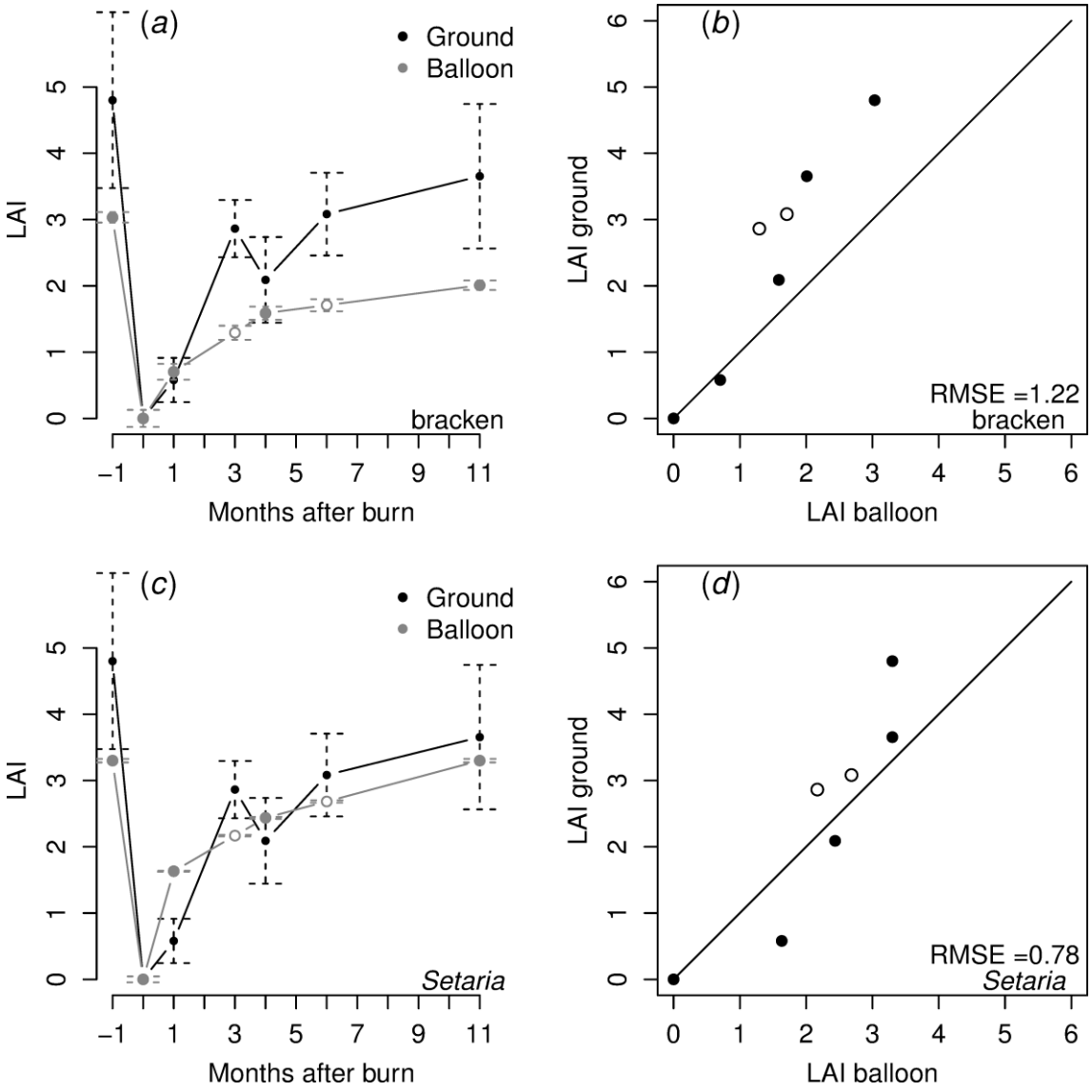

Figure 5-9. Comparison of LAI in time (left, (a) and (c)) and in dynamic range between ground measurement and LAI derived from balloon photography (right, (b) and (d)). Open circles are interpolated values.

5.6 Discussion

Compared to other approaches, the present methodology shows advances in using a cost-effective method to monitor an experimental plot, with the possibility of estimating species-specific LAI. Knowledge gained in the present approach can be used to overcome the influence of very high resolution phenomena, such as frond shading, deformations due to acquisition geometry, and the RGB-NIR displacement. For instance, leaves and fronds under partial shadowing could be categorised by the successive seeding and segmentation. This same procedure also helped to minimize the influence of the acquisition geometry, as well as illumination artefacts in the green canopy. Despite relative low spatial precision between RGB and NIR mosaics, these were fusioned in the attribute table based on the extracted segments of the green-enhanced RGB image. Grid-based statistics (e.g. NIR maximum value) maintained physical properties of the segments and were useful in the classification into bracken and *Setaria*. In the time-series, species cover maps were converted and analysed on a square meter basis, leading to promising results when compared to ground observations on cover and leaf area.

For the species of interest (bracken fern and *Setaria* pasture), differences were observed regarding image classification and canopy recovery. Due to horizontal-shaped fronds and homogeneously high infrared reflection, bracken fronds were relative easily detected in the *Setaria* pasture. Better performance was obtained in the time after burn, mainly due to different time of recovery in the first months. Nevertheless, sparse fronds of bracken also occur in the dense *Setaria* canopy. However, the well delineated segments by the successive seeding and region growing method could be used in a complementary visual interpretation, taking the automatic classification as a starting point. In the visual classification, the gain of the automatic classification can be measured in terms of time. An average of 4 hours of labour is required to construct a (25 m^2) species cover map by hand. With help of the automatic classification, a complete classification of the area (1000 m^2) would be achieved in the same 4 hours. Considering a future operational application, the present work pointed the good capability of detecting bracken canopy using a cost-effective system.

Adding the LAI functions to the projective cover maps (see Section 5.5.7), one can observe that the rapid recovery of *Setaria* means a higher increase in leaf area compared to bracken. One explanation for this observation is the availability of starch from subterranean plant matter. Because the area was fenced for about two years before the ecological fire experiment, the absence of grazing and trampling increased the rooting

system in the pasture. This information demonstrates the importance of combining the balloon-borne photos with field data for monitoring of species-specific canopy recovery. Although further ecological questions can be explored using the LAI and cover maps, this work summarises the data acquisition and processing, which can also be improved.

The present methodology can be easily adapted for other plot monitoring projects. We suggest five points for improvements: (i) simultaneous RGB-NIR imaging would considerably improve segmentation, since both spectral ranges could be fusioned in nominal resolution to the RGB and substitute the enhanced image; (ii) a more stable platform can be deployed to avoid wind-gust, which is a critical design issue for any hover flight platform; (iii) a digital surface model derived from laser altimetry (LiDAR) would enhance image rectification and reduce geometric distortions, and can also be used to estimate projected cover; (iv) the plant canopy analyser can be deployed to adjust the conversion function for other species, but the instrument operator should be aware of the effect of sparse canopies on the measurements; and (v) the automatic classification, especially of sparse fronds, can be improved by including metrics at the plot level and between time-steps in the time-series, such as distance to the next vegetation segment, or previously existent. With the exception of the latter two points, it is important to note that the deployment of the suggested tools would considerably increase the costs of the monitoring project, without necessarily leading to the same gain in information.

5.7 Conclusion

A methodology for recording and processing low-altitude balloon-borne photos was developed, focusing on the occurrence of species individuals (bracken fronds and grass bunches) on a plot scale. We showed that a cost-effective platform can be used to record quality image mosaics, which can be processed and used in automatic classification. Classification based on geometric and textural features of image segments showed promising results for monitoring invasive weeds and canopy recovery after fire. Regarding the given field conditions, *Setaria* pasture recovers more rapidly than bracken fern if fire is set to an undisturbed pasture (e.g. without cattle browsing). In combination with ground measurements, LAI can be estimated from projected cover at the species level, and the method can be easily extended for other grassland species. Consequently, we conclude that monitoring of the grassland canopy succession after burning should be considered at the species level. The same is valid for dynamic vegetation models, which consider plant

competition and make use of LAI to simulate vegetation succession on grasslands.

Acknowledgement

Thanks to Dr. D. Göttlicher and all students who support the flight operations.

Bibliography

[1]. N. Brummitt, E. N. Lughadha, "Biodiversity: Where's Hot and Where's Not", Conservation Biology, vol. 17, no. 5, pp. 1442-1448, 2003.

[2]. J. Bendix, E. Beck, "Spatial aspects of ecosystem research in a biodiversity hot spot of southern Ecuador – an introduction", Erdkunde, vol. 63, no. 4, pp. 305-308, 2009.

[3]. D. Göttlicher, A. Obregón, J. Homeier, R. Rollenbeck, T. Nauss, J. Bendix, "Land-cover classification in the Andes of southern Ecuador using Landsat ETM+ data as a basis for SVAT modelling", Int. J. of Remote Sensing, vol. 30, no. 8, pp. 1867-1886, 2009.

[4]. K. Roos, R. Rollenbeck, T. Peters, J. Bendix, E. Beck, "Growth of Tropical Bracken (*Pteridium arachnoideum*): Response to Weather Variations and Burning", Invasive Plant Sci. and Manage., vol. 3, no. 4, pp. 402-411, 2010.

[5]. J. Bendix, B. Silva, K. Roos, D. O. Göttlicher, R. Rollenbeck, T. Nauss, E. Beck, "Model parameterization to simulate and compare the PAR absorption potential of two competing plant species", Int. J. of Biometeorology, vol. 54, n. 3, pp. 283-295, 2010.

[6]. B. Silva, K. Roos, I. Voss, N. König, R. Rollenbeck, R. Scheibe, E. Beck, J. Bendix, "Simulating canopy photosynthesis for two competing species of an anthropogenic grassland community in the Andes of southern Ecuador", Ecological Modelling, vol. 239, pp. 14-26, 2012.

[7]. J. Bendix, R. Rollenbeck, D. Göttlicher, J. Cermak, "Cloud occurrence and cloud properties in Ecuador", J. of Climate Research, vol. 30, no. 2, pp. 133-147, 2006.

[8]. K. C. Swain and, H. P. W. Jayasuriya, "Low Altitude Remote Sensing applications for diversified farming conditions in developing countries: an overview", Asia-Pacific J. of Rural Develop., vol. 18, no. 2, pp. 81-98, 2008.

[9]. J. S. Aber, "Lighter-than-Air Platforms for Small-Format Aerial Photography", Trans. of the Kansas Academy of Sci., vol. 107, no. 1/2, pp. 39-44, 2004.

[10]. D. Wundram, J. Löffler, "High-resolution spatial analysis of mountain landscapes using a low-altitude remote sensing approach", Int. J. of Remote Sensing, vol. 29, no. 4, pp. 961-974, 2008.

[11]. M. Miyamoto, K. Yoshino, T. Nagano, T. Ishida, Y. Sato, "Use of balloon aerial photography for classification of Kushiro wetland vegetation, northeastern Japan", Wetlands, vol. 24, no. 3, pp. 701-710, 2004.

[12]. R. M. Lloveria, F. P-C., A. García-Martín, J. R. Fernández, "Combined Methodology Based on Field Spectrometry and Digital Photography for Estimating Fire Severity", IEEE Journal of selected topics in applied earth observations and remote sensing, vol. 1, no. 4, pp.226-274, 2008

[13]. F. Artigas, I. C. Pechman, "Balloon imagery verification of remotely sensed Phragmites australis expansion in an urban estuary of New Jersey, USA", Landscape and Urban Planning, vol. 95, no. 3, pp. 105-112, 2010.

[14]. X. Chen, L. Vierling, "Spectral mixture analyses of hyperspectral data acquired using a tethered balloon", Remote Sensing of Environment, vol. 103, no. 3, pp. 338-350, 2006.

[15]. Y. Inoue, S. Morinaga, A. Tomita, "A blimp-based remote sensing system for low-altitude monitoring of plant variables: A preliminary experiment for agricultural and ecological applications", Int. J. of Remote Sensing, vol. 21, no. 2, pp. 379-385, 2000.

[16]. L. A. Vierling, M. Fersdahl, X. Chen, Z. Li, P. Zimmerman, "The Short Wave Aerostat-Mounted Imager (SWAMI): A novel platform for acquiring remotely sensed data from a tethered balloon", Remote Sensing of Environment, vol. 103, no. 3, pp. 255-264, 2006.

[17]. B. P. Friedrich, J. Becker, B. Brimer, B. J. Merkel, "Low-cost aerial photography for high-resolution mapping of hydrothermal areas in Yellowstone National Park", Int. J. of Remote Sensing, vol. 29, no. 6, pp. 1781-1794, 2008.

[18]. D. G. Leckie, F. A. Gougeon, S. Tinis, T. Nelson, C. N. Burnett, D. Paradine, "Automated tree recognition in old growth conifer stands with high resolution digital imagery", Remote Sensing of Environment, vol. 94, no. 3, pp. 311-326, 2005.

[19]. L. T. Waser, C. Ginzler, M. Kuechler, E. Baltsavias, L. Hurni, "Semi-automatic classification of tree species in different forest ecosystems by spectral and geometric variables derived from Airborne Digital Sensor (ADS40) and RC30 data", Remote Sensing of Environment, vol. 115, no. 1, pp. 76-85, 2011.

[20]. A. B. Massada, O. Gabay, A. Perevolotsky, Y. Carmel, "Quantifying the effect of grazing and shrub-clearing on small scale spatial pattern of vegetation", Landscape Ecology, vol. 23, no. 3, pp. 327-339, 2008.

[21]. J. P. Lesschen, L. H. Cammeraat, A. M. Kooijman, B. van Wesemael, "Development of spatial heterogeneity in vegetation and soil properties after land abandonment in a semi-arid ecosystem", J. of Arid Environments, vol. 72, no. 11, pp. 2082-2092, 2008.

[22]. H. T. Søgaard, "Weed Classification by Active Shape Models", Biosystems Eng., vol. 91, no. 3, pp. 271-281, 2005.

[23]. M. D. Woebbecke, E. G. Meyer, K. Von Bargen, A. D. Mortensen, "Shape features for identifying young weeds using image analysis", Trans. of the ASAE, vol. 38, no. 1, pp. 271-281, 1995.

[24]. L. Tang, L. Tian, B. L. Steward, "Classification of broadleaf and grass weeds using gabor wavelets and an artificial neural network", Trans. of the ASAE, vol. 46, no. 4, pp. 1247-1254, 2003.

[25]. A. J. Perez, F. Lopez, J. V. Benlloch, S. Christensen, "Colour and shape analysis techniques for weed detection in cereal fields", Comput. and Electronics in Agriculture, vol. 25, no. 3, pp. 197-212, 2000.

[26]. G. A. Blackburn, J. I. Pitman, "Biophysical controls on the directional spectral reflectance properties of bracken (*Pteridium aquilinum*) canopies: Results of a field experiment", Int. J. of Remote Sensing, vol. 20, no. 11, pp. 2265-2282, 1999.

[27]. J. E. Taylor, "Factors Causing Variation in Reflectance Measurements from Bracken in Eastern Australia", Remote Sensing of Environment, vol. 43, no. 2, pp. 217-229, 1993.

[28]. G. A. Blackburn, C. M. Steele, "Towards the Remote Sensing of Matorral Vegetation Physiology: Relationships between Spectral Reflectance, Pigment, and Biophysical Characteristics of Semiarid Bushland Canopies", Remote Sensing of Environment, vol. 70, no. 3,pp. 278-292, 1999.

[29]. J. S. Aber, I. Marzolff, J. B. Ries, Small-Format Aerial Photography. Amsterdam: Elsevier Sci., 2010, pp. 85–87.

[30]. J. M. Welles, "Some indirect methods of estimating canopy structure", Remote Sensing Reviews, vol. 5, no. 1, pp. 31-43, 1990.

[31]. D. Göttlicher, J. Albert, T. Nauss, J. Bendix, "Optical properties of selected plants from a tropical mountain ecosystem – Traits for plant functional types to parametrize a land surface model", Ecological Modelling, vol. 222, no. 3, pp. 493-502, 2011.

[32]. J. A. Richards, X. Jia. Remote sensing digital image analysis: an introduction. Heidelberg: Springer, 2005.

[33]. Grass Development Team, Geographic Resources Analysis Support System (GRASS) Software. Open Source Geospatial Foundation Project. http://grass.osgeo.org, 2012.

[34]. D. Rocchini, M. Metz, A. Frigeri, L. Delucchi, M. Marcantonio, M. Neteler, "Robust rectification of aerial photographs in an open source environment", Comput. & Geosci., vol. 39, pp. 145-151, 2012.

[35]. John I. Pitman, "Absorption of photosynthetically active radiation, radiation use efficiency and spectral reflectance of bracken [*Pteridium aquilinum* (L .) Kuhnl] Canopies", vol. 85, no. 2, pp. 101-111, 2000.

[36]. Y. Wu, F. Y. Shih, J. Shi, Y. Wu, "A top-down region dividing approach for image segmentation", Pattern Recognition, vol. 41, no. 6, 1948-1960, 2008.

[37]. R. M. Haralick, K. Shanmugam, I. Dinstein, "Textural Features for Image Classification", IEEE Trans. on Syst., Man and Cybernetics, vol. SMC-3, no. 6, pp. 610-621, 1973.

[38]. R.T.T. Forman, Land mosaics: The ecology of landscapes and regions. Cambridge University Press, Cambridge, ch. 4, pp. 141-142.

[39]. J. H. Friedman, "Greedy Function Approximation: A Gradient Boosting Machine", The Ann. of Stat., vol. 29, no. 5, pp. 1189-1232, 2001.

[40]. G. Ridgeway. (2012, 12, 9). Generalized Boosted Models: A guide to the gbm package. Online]. Available: http://CRAN.R-project.org/package=gbm

[41]. J. Elith, J. R. Leathwick, T. Hastie, "A working guide to boosted regression trees", The J. of Animal Ecology, vol. 77, no. 4, pp. 802-813, 2008.

[42]. R Development Core Team (2012, 10, 26). R: A language and environment for statistical computing. [Online]. Available: http://www.R-project.org

[43]. J. A. Hanley, B. J. McNeil, “The meaning and use of the area under a Receiver Operating Characteristic (ROC) curve”, Radiology, vol. 143, pp. 29-36, 1982.

[44]. J. Pearce, S. Ferrier, “Evaluating the predictive performance of habitat models developed using logistic regression”, Ecological Modelling, vol. 133, pp. 225-245, 2000.

Chapter 6

6. Summary and outlook

6.1 Summary

Provisioning of ecosystems services and conservation of biodiversity strongly depend on sustainable land use. The present work contributes new knowledge to the hitherto scientifically unexplored problem of pasture invasion in southern Ecuador by bracken fern (*Pteridium arachnoideum*), which competes with cultivated pasture grass (*Setaria sphacelata*) for space. This work seeks to tests three hypotheses: first, under current climate conditions, net productivity of the bracken fern is higher than that of the undisturbed pasture grass *Setaria*; second, growth performance of the pasture grass *Setaria* will be favoured by global warming; third, bracken growth is stimulated by recurrent burning. Field observation shows that the bracken fern seems to overgrow and outcompete pasture grass under current pasture management practises, particularly recurrent burning, which is done to rejuvenate pasture grass.

To investigate the exact mechanisms that allow bracken fern to invade pasture land, this work pursues the following two objectives, both of which correlate to the hypothesis previously mentioned:

Objective 1 seeks to understand the response of the two competing species (bracken fern and *Setaria* pasture) to current and future climate conditions in a valley of the south-eastern Ecuadorian Andes. The Southern Bracken Competition Model (SoBraCoMo) was developed to investigate the competitive strength of bracken fern and *Setaria* pasture through model experiments. The modelling approach addressed three focal processes: (i) radiation absorption, (ii) net photosynthesis, and (iii) biomass productivity.

Objective 2 aims at understanding the post-fire canopy recovery of both species by monitoring an ecological burning experiment that was conducted in the study area of the Rio San Francisco Valley. A novel cost-effective method based on a balloon-borne monitoring system and entity-based image classification was developed and applied to monitor the vegetation before and after fire management at the field site. The experimental field site and the image acquisition and processing system were also established to support the validation of spatial SoBraCoMo runs (see section 6.2).

To achieve the two objectives, investigations in the present work were subdivided into four parts (i-iii for objective 1, iv for objective 2):

(i) Absorption of solar radiation is the most important factor in photosynthesis, and photosynthesis determines how much and how quickly plants grow. Either the canopy shape of the individual species itself or radiation interactions between species may contribute to the competitive strength of a single species. Thus, the potential radiation absorption of bracken and *Setaria* was the first factor to be investigated in detail. This potential was calculated in SoBraCoMo by considering the "two-big leaf" approach which requires diffuse and direct solar radiation, leaf and soil spectral traits, leaf area, and mean tilt angle for forcing and parameterization. Using long-term meteorological data from observations established by this thesis at the study site, bracken fern showed higher absorption than *Setaria* pasture only at daily photosynthetic active radiation (PAR) maximum above 615 W/m². Yearly sums of PAR absorption also suggested a slight advantage for *Setaria* (chapter 2). A novel formulation was thus proposed, including in the radiation partitioning the well-known dependency of the incoming radiation on solar geometry. In addition, newly calculated coefficients for radiation partitioning are available for the study area (chapter 3).

(ii) Net photosynthesis is the next factor contributing to competitive strength, because it depends not only on radiation absorption, but also, among others (e.g. autotrophic respiration), on the photosynthetic pathway which differs between the two species of interest. Net photosynthesis was calculated based on species-specific physiological parameters newly determined by field observations (e.g. quantum efficiency, carboxylation rate, and temperature regulation). Shade-adaption was innovatively included in the model formulations of C3- and C4-photosynthetic pathways and completely parameterized by porometry. The good agreement between SoBraCoMo net-photosynthesis simulations and independent porometry measurements at leaf scale are attributed to the species-specific parameterization and the realistic forcing of the model. At canopy scale, realistic simulations on productivity showed that *Setaria* pasture had a slight advantage throughout the year. This investigation revealed that, unlike in regards to radiation absorption (chapter 2), net productivity of bracken fern is favoured under diffuse radiation conditions (chapter 3). This is mainly due to the bracken's C3-pathway which is also more competitive than the *Setaria*'s C4-pathway under temperatures below average (ca. 14.8°C).

(iii) Finally, competitive strength is related to the speed at which a species can produce biomass. Thus, biomass productivity was simulated in diagnostic runs using the new Southern Bracken Competition Model (SoBraCoMo). Temperature regulation of net photosynthesis was validated using independent field and laboratory measurements. Coupling the SoBraCoMo with climate predictions scenarios for the study area a considerable growth advantage of *Setaria* was observed, particularly under conditions of global warming. This growth advantage is mainly due to the C4-pathway becoming more efficient as temperatures rise (chapter 4).

(iv) For growth and re-growth monitoring of both species under the current pasture management practise of burning, a novel cost-effective balloon-borne VIS/NIR photography method was developed (chapter 5). The acquired digital images were used to differentiate individual plants in a stepwise segmentation and a subsequent classification of species cover. Ground validation indicated a feasible and operational remote-sensing method for species cover monitoring in the harsh and remote mountain environment of South Ecuador. Although bracken fronds were more numerous one year after fire-treatment than before, a rapid recovery of *Setaria* pasture and no significant invasion of bracken were observed. These results suggest that other disturbances, such as grazing and trampling, may reduce the competitive strength of *Setaria* stands, and thus might be responsible for the competitive advantage of bracken in pasture systems of southern Ecuador.

The outcomes of the current work allowed the initial hypotheses (refer to introduction) to be tested. To review: the first hypothesis, related to objective 1, states that under current climate conditions, net productivity of the bracken fern is higher than that of the undisturbed pasture grass *Setaria*. This hypothesis is not supported by the results. Despite the moderate annual average temperature at the study site (ca. 14.8°C), the C4-*Setaria* pasture is slightly more productive than the C3-bracken under current climate conditions. The second hypothesis, also related to objective 1, states that growth performance of the pasture grass *Setaria* will be boosted by global warming. This hypothesis is confirmed by the simulations which have shown that biomass productivity of pasture grass tends to increase with temperature. Objective 2 provides the answer to the third hypothesis, which is that recurrent burning alone stimulates bracken growth. This hypothesis must be rejected as well. Observations made with balloon-borne photography showed no significant increase of bracken cover after fire-treatment. This contradicts the observations in the field which shows clear bracken invasion under

recurrent burning and cattle browsing. In this context, however, it should be stressed that on the experimental plot, only fire-recovery and otherwise undisturbed vegetation have been investigated thus far.

The present work has shown by means of simulations with a properly validated model that, under natural environmental conditions and fire-treatment on undisturbed pasture, *Setaria* will probably slightly outperform bracken fern and be aided by global warming. Here no shading of the grass by bracken fronds is presumed, although this scenario might only become crucial in very dense bracken canopies (LAI > 3). In addition, no pasture invasion was detected after one year of canopy-recovery from fire-treatment. These are striking results that aid our understanding of the problem of pasture invasion by bracken fern in the Rio San Francisco Valley, South Ecuador. However, since bracken invasion might be triggered by other mechanisms, such as grazing and trampling by livestock, new hypotheses should be tested in the future (e.g. biomass removal by grazing and trampling favours bracken in competition with *Setaria* pasture). Future research will profit from the new Southern Bracken Competition Model (SoBraCoMo) developed in this thesis, which provides realistic calculations on biomass productivity of bracken and *Setaria*.

6.2 Outlook

The current work has produced a tool to model and monitor bracken and *Setaria* growth competition under realistic current and probable future environmental conditions. The approach supports both research and management on bracken occurring pastures in the tropical Andes of southern Ecuador. The results of the study also provide new insights which require further investigation. The following three paragraphs are thus dedicated respectively to useful future model extension, improvement of the monitoring method, and the combined use of the model and monitoring approaches.

Future developments of the model (SoBraCoMo) should aim a complete prognostic model with mechanisms for direct competition for light, and also account for the combined effects of grazing and trampling on pasture (disturbance module). The first model extension would aid investigation of the hypothesized negative effect of bracken fern's frond shadow on the productivity of shaded grass bunches normally growing below the taller fern plants. The inclusion of light competition should take into account the horizontal fraction of shaded cover and the vertical intensity of shading which are connected to the canopy radiation transfer module. The second improvement would help explain the competitive strength of bracken

observed in the field, where pasture is intensively used for grazing. The inclusion of grazing and trampling should take into account the removal of aboveground biomass and the impact on ground permeability, both connected to the modules for net photosynthesis, biomass allocation and soil hydrology. The modularity of SoBraCoMo also warrants coupling with other existing models, to include, for instance, dynamics in the substrate (e.g. soil water using the Catchment Modelling Framework, or CMF). Competition for soil water is relevant to bracken fern and *Setaria*, since roots (and rhizomes) developed by bracken are deeper than roots of ungrazed *Setaria* pastures. A more advanced approach can include species dispersion, soil chemistry and effects of nutrient limitation on biomass productivity. However, it is important to note that extensions like these require a longer investigation than was possible given the restricted time span of this work, as well as a restructured experimental design.

The novel monitoring method using balloon-borne photography is easily replicable and can be used for species detection worldwide. The basic concept of the technique is the successive thresholding of an enhanced image prior to classification. The successive thresholding can be adapted to different segmentation algorithms (e.g. semi-variogram based region growing). The classification of the resulting individual plant crown entities is based on the geometric and radiometric data available, which depend on the type of sensor used. The detection of bracken fern and *Setaria* by means of passive remote sensing is highly dependent on cover, illumination and camera angle (chapter 5). To overcome this problem, the segmentation and classification method can be applied using LiDAR data. Figure 6-1 shows preliminary results on detecting tree-species, considering similar patterns used to detect bracken fern and *Setaria*. Palm-trees have ramified long leaves, like bracken fronds, whereas most other tree canopies are circular in shape, like *Setaria* grass bunches. In Figure 6-1 palm-trees were classified and separated from other tree-families based on the point-cloud recorded on a mountain forest experimental site. If the point density is high enough to depict the species of concern, LiDAR data reduce dependence on geometry, thereby considerably enhancing the classification.

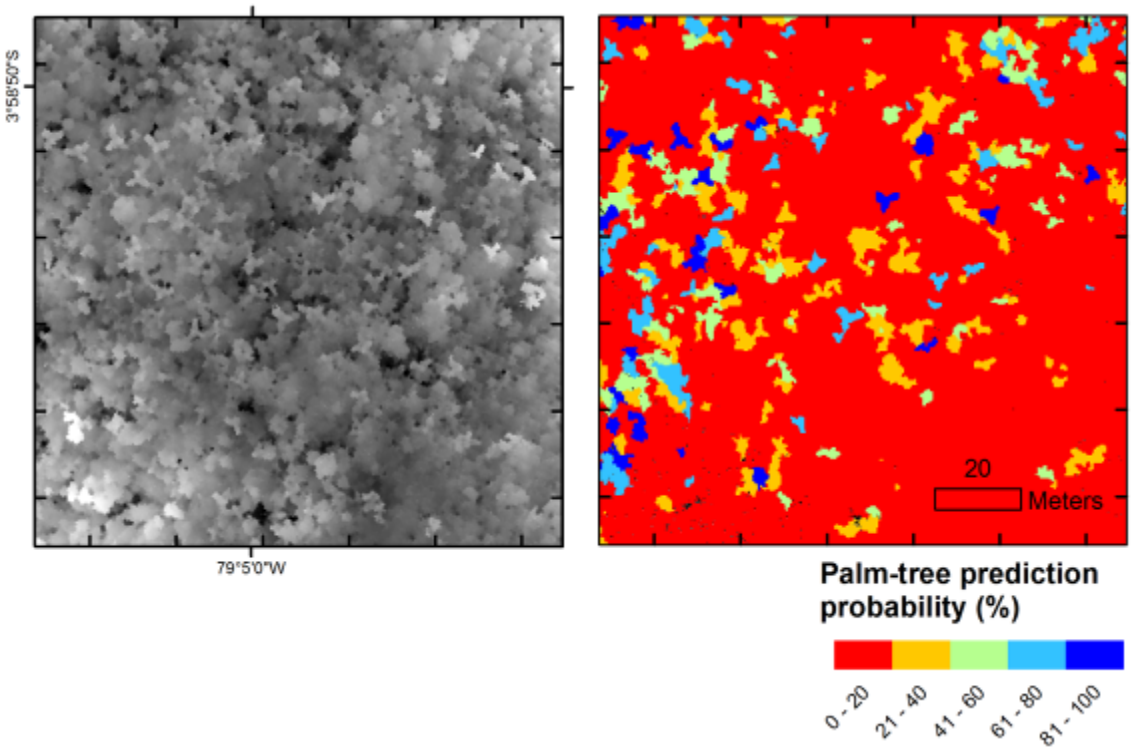

Figure 6-1. Palm-tree detection using LiDAR data and the method developed for bracken and *Setaria* classification.

Finally, species-cover monitoring and biomass productivity modelling can be combined in a long-term research project based on the present study. In such a case, prognostic short-term simulations should corroborate with operational monitoring which can then be used to reduce model uncertainties in a subsequent time step of the model output. The balloon-borne photography provides species cover data for direct application to the problem of pastures invaded by bracken fern. In light of different conditions within the Rio San Francisco valley, the model can be tested using area-wide remote sensing data. Since grid-based model runs are initialized with fractions of projected cover (FPC), the species-specific FPC to LAI conversion (chapter 5) can be used as a scaling function. In using area-wide optical remote sensing data, FPC is assumed equal to cover abundance, as obtained with the mixture model technique applied on broadband high-resolution or hyper-spectral data. The basin-wide model and monitoring system is especially applicable to bracken fern, which is spectrally more distinguished from co-occurring species.

Executive Summary

The megadiverse tropical mountain forests in the southeastern Andes of Ecuador, including their biodiversity and ecosystem services, are severely threatened due to climate warming and the clearing of forests to produce pasture land. The common local practice of recurrent burning for pasture rejuvenation has proven to be non-sustainable, since it enables bracken fern to invade pastures, causing farmers to abandon heavily infested pastures and instead clear new tracts of natural forest. No quantitative information on the growth potential of pasture grass and bracken fern under current and future environmental conditions has yet been available for the Andes of Ecuador. The scientific basis required to understand bracken invasion has yet to be established. This scientific basis would enable the development of sustainable pasture management strategies. Such strategies would, in turn, help protect the remnants of natural forest. Consequently, the present work aims at investigating the growth potential of two competing species under current and future climate conditions. Outcomes provide new knowledge and methodological developments concerning pasture invasion by bracken fern in southern Ecuador. The method entails the development of a new model, the Southern Bracken Competition Model (SoBraCoMo), realistically parameterized and validated. The model code is based on existing Soil Vegetation Atmosphere Transfer (SVAT) and vegetation dynamic models to calculate the potential growth of two main competitors, the southern bracken fern (*Pteridium arachnoideum*) and the pasture grass (*Setaria sphacelata*). Extensive field measurements and proper meteorological forcing delivered new site and species-specific parameters for realistic productivity simulations of both species. An experimental site was established to observe pasture and bracken fern development under the practice of recurrent burning, and to provide atmospheric data for a realistic forcing of the developed model. A novel balloon-borne monitoring system was developed to detect species cover and provided new insights into post-fire canopy recovery. The main results demonstrate that, under current environmental conditions, *Setaria* has a slightly higher competitive growth potential under undisturbed conditions (no grazing, trampling, or light competition). Furthermore, this growth advantage of *Setaria* should most likely increase due to global warming. Because field observations show bracken infestation, however, other factors than those investigated should be responsible for the bracken fern's current success. The most likely cause of bracken success to be investigated in the future is cattle browsing; although browsing continuously removes aboveground biomass, this disruption of the upper soil does not affect deep

roots and rhizomes of bracken plants. The newly developed SoBraCoMo can now provide an excellent basis to implement new mechanisms like browsing for future simulations.

Zusammenfassung

Der Bergregenwald in den südöstlichen Anden von Ecuador mit seiner außergewöhnlich hohen Artenvielfalt und seinen wichtigen Ökosystemleistungen ist stark bedroht. Dies ist vor allem eine Folge von Klimaerwärmung und Landnutzungsänderungen. Auf Weideflächen erweist sich das landesübliche Abbrennen als nicht nachhaltige Pflegemaßnahme. Abbrennen begünstigt die Verbreitung von für die Weidewirtschaft kontraproduktiven Pflanzenarten. Dies führt zum Verlassen der stark verunkrauteten Weideflächen und zur weiteren Abholzung von natürlichen Waldgebieten. Bislang waren keine quantitativen Angaben über das Wachstumspotenzial der in Südecuador vorkommenden Nutzpflanzen und deren Konkurrenten unter lokalen Umweltbedingungen verfügbar. Damit fehlten wissenschaftliche Grundlagen zur Entwicklung Strategien, welche nachhaltige Weidewirtschaft und Waldschutz gleichzeitig ermöglichen. Daher war Ziel dieser Arbeit die Untersuchung des Wachstumspotenzials zwei konkurrierenden Pflanzenarten - der südliche Adlerfarn (*Pteridium arachnoideum*) und das Weidegras (*Setaria sphacelata*) - unter aktuellen und zukünftigen klimatischen Bedingungen. Die Ergebnisse sind Erkenntnisse und methodische Entwicklungen zu der bisher wissenschaftlich unerforschten Verunkrautung von Weideflächen durch den Adlerfarn in Südecuador. Im Rahmen der Arbeit wurde das Southern Bracken Competition Model (SoBraCoMo) entwickelt, auf die zu untersuchenden Pflanzenarten parametrisiert und validiert. Der Quellcode des Modells basiert auf state-of-the-art SVAT- (Soil Vegetation Atmosphere Transfer) und Vegetationsdynamik-Modellen. Verschiedene Feldmessungen und die Erhebung von meteorologischen Daten liefern neue standort- und pflanzenartspezifische Parameter für eine realitätsnahe Simulation. Zur Beobachtung des Wachstums nach Bränden und zur Erhebung meteorologischer Daten wurde ein experimentelles Untersuchungsgebiet eingerichtet. Um unter anderen artspezifischen Bodenbedeckungen zu erkunden, konnte ein Monitoringsystem mit Installation von Standard- und Infrarotkameras an einem Heliumballon entwickelt und eingesetzt werden. Die Ergebnisse weisen für aktuelle Klimawerte und ungestörte lokale Bedingungen (keine Beweidung / Trampeln, keine Beschattung) eine geringfügig höhere Wettbewerbsfähigkeit des Weidegrases aus. Es wird gezeigt, dass sich dieser Wachstumsvorteil bei einer weiteren Klimaerwärmung noch erhöhen würde. Da Feldbeobachtungen dennoch auf eine Verdrängung des Weidegrases hindeuten, müssen andere Faktoren für den Erfolg des Adlerfarns verantwortlich sein. Wahrscheinlichster Faktor hierfür ist die Beweidung selbst. Diese beeinträchtigt das Weidegras stärker

als den Adlerfarn. Das Modell SoBraCoMo kann als hervorragende Grundlage für zukünftige wissenschaftliche Arbeiten auf diesem Gebiet eingesetzt werden.

Curriculum Vitae

Brenner Silva
Laboratory for Climatology
and Remote Sensing
University of Marburg
FB19 – AG Bendix
Deutschhausstr. 12
Marburg D-35037

Phone: +49 6421 28 25951
Fax: +49 6421 28 28950
E-mail: silvab@geo.uni-marburg.de

Education

1988- 1994	High school at ”Major Joao Pereira“ (Landesschule) Itajubá, Brazil
January 1995	Admission to University by national “Vestibular“ examination
1996-1999	Studies of Computer Science (BSc.) at Federal University of Sao Carlos, UFSCar, Brazil
January 2000	Bachelor degree in Computer Science
1999-2000	Five months trainee program with Geographic Information System at HTW-Zittau, Germany
April 2001	Admission to Master studies at National Institute for Space Research, INPE, Brazil
April 2004	Master degree in Remote Sensing
2004-2005	Scientific assistant at INPE with image processing and technical reports
2007	Scientific assistant at INPE with vegetation mapping for conservation planning in Amazon (Geoma project).
2007-2008	German courses at Goethe Institut Mannheim (DSH Certificate)
March 2008	Start of PhD-research at University of Marburg, Admission in November 2007

Work Experience

2005	Interpretation and audit in the PRODES (Amazonian Forest Monitoring by Satellite) program, Sao Jose dos Campos, Brazil.
2004	Consultant at "Fortification of Management Council in the Serra da Mantiqueira, Atlantic Forest Protected Area"
2000-2001	System analyst at PROGEO (LLC), Pantanal, Brazil, with land survey and planning.

Language skills

German, English, and Spanish (native Portuguese speaker)

Personal Bibliography

Peer-reviewed publications:

Silva, B., Roos, K., Voss, I., König, N., Rollenbeck, R., Scheibe, R., Beck, E., Bendix, J. 2012. Simulating canopy photosynthesis for two competing species of an anthropogenic grassland community in the Andes of southern Ecuador. Ecological Modelling, doi:10.1016/j.ecolmodel.2012.01.016.

Bendix, J., Silva, B., Roos K., Göttlicher D., Rollenbeck R., Nauß T., Beck E. 2010. Model parameterization to simulate and compare the PAR absorption potential of two competing plant species. International Journal of Biometeorology, doi:10.1007/s00484-009-0279-3

Master thesis:

Silva, B.S.G. Permanent Plot Selection in Mountainous Ecosystems (translation of "Seleção de Parcelas Permanentes em Ecossistemas Montanhosos". M. Sc. Thesis on Remote Sensing. Publication of INPE, National Institute for Spatial Research) São José dos Campos, Brazil.

Book chapter:

Lopes, P.M.O.; Silva, B.S.G.; Bottino, M.J.; Valeriano, D.M. Irradiância solar incidente modelada a partir de dados do sensor MODIS. In: Rudorff, B.F.T.; Shimabukuro, Y.E.; Ceballos. J.C. (Eds.). *O Sensor MODIS e suas aplicações ambientais no Brasil*. 1 ed. São José dos Campos: Bookimage, 2006, p. 1-448.

Selected publications on events:

Silva, B. and Bendix, J. 2012, Monitoring and modelling competing grassland species using very-high and high-resolution remote sensing in the Andes of Ecuador. Geoscience and Remote Sensing Symposium (IGARSS), 2012 IEEE International , vol., no., pp.5376-5378, 22-27 July 2012. doi:10.1109/IGARSS.2012.6352392

Silva, B. and Bendix J. 2011. Modelling and monitoring of vegetation growth from leaf to plot scale. Proceedings 3rd iLEAPS Science Conference, Garmisch-Partenkirchen, 20. Sep 2011. ESA Special Publications SP-688.

Silva, B., Lehnert, L., and Bendix J. 2011. Balloon aerial photography applied to the investigation of the southern bracken. GTÖ - Society for Tropical Ecology - Conference, Frankfurt, Feb. 2011

Silva, B. and Bendix J. 2010. Atmosphere-vegetation modelling and assessment of photosynthesis for two grassland competing species. European Geoscience Union - Conference, Vienna, Austria, 02 – 07 May 2010

Silva, B. et al. 2008. Some aspects of climate and radiation into a grassland competition model, AKKlima Symposium, Nov. 2008, Aachen, Germany

Silva, B. S. G.; Valeriano, D. M.; Correção atmosférica e topográfica de imagens de satélite em terrenos montanhosos. Proceedings. XII *Simp. Brasileiro de Sensoriamento Remoto*, 2005, INPE, p. 3587-3594.

Valeriano, D.M.; Silva, B.S.G., Clear sky irradiance simulation in a mountainous region in Brazil, Geoscience and Remote Sensing Symposium, 2003. IGARSS '03. Proceedings. 2003 IEEE International , vol.5, no., pp. 3216- 3218 vol.5, 2003, doi:10.1109/IGARSS.2003.1294734

Espírito-Santo. F.D.B; Silva, B.S.G.; Shimabukuro, Y.E. Detecção da dinâmica da floresta de bambu no sudeste do Acre com o uso de técnicas de processamento de imagens de satélite. In: Proceedings. XI *Simp. Brasileiro de Sensoriamento Remoto*. p.649-656. CD-ROM.